Studies on the regulatory domain of the yeast Methylene tetrahydrofolate reductase (MTHFR), a key enzyme in one-carbon metabolism

MUSKAN BHATIA

A thesis submitted for the partial fulfillment of
the degree of the Doctor of Philosophy

Department of Biological Sciences
Indian Institute of Science Education and Research Mohali
Knowledge city, Sector 81, SAS Nagar, Manauli PO, Mohali 140306, Punjab, India.

September 2020

Dedicated to Science and my Family

Acknowledgments

My life at IISER culminates with my PhD thesis and this study would have been incomplete without the mention of the efforts put in by many people, to whom I would be forever indebted for helping and supporting me on this emotional and enlightening journey. First and foremost, I would like to express my heartfelt gratitude to my Ph.D. supervisor, Prof. Anand K. Bachhawat, who doesn't believe in hand holding method of training and gives complete freedom to each of his student to design and execute their experiments as per their scientific acumen and understanding. He is a visionary who believes in nurturing his graduate students as soon as they embark on their scientific careers as independent researchers, an essential trait required for becoming future scientists. Besides being a supportive mentor, he is a brilliant researcher intrigued by challenging research problems. Also, he is the most humble, generous, considerate and patient person I have come across. Lest I forget – his narrative skills and dedication; he is a charming storyteller, with an exceptional ability to understand, organize and explain any scientific problem in the simplest possible manner. He is not only an experimentalist in the boundaries of his research lab but also in the classrooms where he researches, experiments and analyzes newer methods of teaching the undergrad and grad students. Here only, I would also like to thank Dr. Nandita Bachhawat for her care and concern throughout these years. I personally treasure all my meetings with her at various events, be it after some scientific lectures, or a lab get together or during my visits to their home.

I am sincerely thankful to my doctoral committee members, Dr. Rachna Chaba and Dr. Shravan Kumar Mishra, for their critical suggestions and motivation during our regular committee meetings. A special thanks to Dr. Rachna Chaba for having long discussions regarding my project beyond the doctoral committee meetings which expanded by scientific knowledge and way of thinking. I whole-heartedly thank her for providing the emotional

support and professional guidance throughout this tenure. Her encouraging words helped me sail through this rather intense journey.

I express my sincere gratitude to IISER Mohali directors, Prof. N. Sathyamurthy, Prof. Debi P. Sarkar, and Dr. J. Gowrishankar, for providing with an excellent academic environment- vibrant, enthusiastic, heterogeneous yet cooperative IISER community, and the remarkable lab facilities throughout the years of my study.

I would also take this opportunity to thank my numerous collaborator, without their help I would not have been able to complete this thesis. Dr. Shyam Kumar Masakpalli and his student Jyotika for helping us with stable isotope labelling studies. His insights using flux based analysis enabled us to reach a logical conclusion in our studies. Many thanks to Jyotika for calmly handling all my queries and acquainting me with required knowledge of the subject which was quite new to me. I would like to thank Dr. Sunil laxman for not only helping me in the metabolite estimations for this project but also for training me to perform metabolite extractions from yeast during my visit to Bengaluru in the starting years of my PhD study. His enthusiasm for science is quite inspiring. A special thanks to all his lab members- Hemanth, Meghana, Shuili, Dr. Adish, Dr. Ritu, Rudra, Dr. Shambhavi, Amit, Zeenat and Pranoy for providing a supportive environment in their lab at InStem. During my stay at the NCBS, the transit campus of inStem, there were many other people who made my stay comfortable and cheerful- Shuili, Amit, Oliver, Dr. Ramya, Dilawar, Anu, and Shweta. Thank you everyone! Dr. Shantanu Sen Gupta and his students Rahul and Shalini for their efforts in helping me with folic acid and lipid estimations. His lab members Rahul, Shalini and Praveen helped me a great deal in not only performing the experiments but also taught me the analysis part. I am also grateful to Dr. Monika Sharma for persistently helping us with the modeling and docking studies in our project. Working with each one of them was quite an enriching experience.

Help also came from several colleagues at different labs in IISER, Mohali who helped me to learn different techniques and provided assistance at several levels. I duly thank Dr. Purnananda Guptasarma for taking out time to hear my work and give critical suggestions in improving it. Due credit also goes to his lab members Bhishem, Arpita Mrigwani, Dr. Prince, and Rachit in helping me with ITC and size exclusion chromatography experiments. I am also thankful to Dr. Kaushik Chattopadhyay and his lab members- Dr. Nidhi Kundu and Pratima for helping me with AUC experimentation and analysis. I also offer special thanks to Dr. Hema, Dr. Anupa, Priyanka Madhu, Aishwarya, and Sayanta from Dr. Samrat's lab for helping me with CD spectroscopy and Fluorescence based experiments. I would also like to acknowledge by Dr. Prashant, Dr. Kiran, and Poulami from Dr Shravan's Lab for sharing their lab resources with me. Dr. Gayathri and Jagdish from Sabyasachi's lab aided me in some of the biophysical studies. I cannot thank enough the lab members of Dr. Rachna, Dr. Bhupinder, Kanchan, and Garima for discussions regarding important experiments. I would also like to thank Dr. Andrew D Hanson (University of Florida, USA), and Dr. Rima Rozen (McGill University, Quebec, Canada) for providing plasmid constructs which were used in this study.

I duly acknowledge Indian Council of Medical Research and Department of Science and technology, India for the financial support.

Completing my Ph.D. was fun and adventurous, and I owe this to the members of the Bachhawat lab, lovingly called as AKB lab. I am grateful to all my seniors, Dr. Shailesh, Dr. Anup, Dr. Zulkifli, Dr. Aman, Dr. Avinash, and Dr. Manisha for sharing their knowledge and lab space with me. Dr. Shailesh was the one who initially gave me guidance in all the experimentation part and mindful recording of experiments. I was fortunate to have such generous and kind seniors. My heartfelt thanks to all the current lab members Banani mam, Harsha, Prarthna, Shradha, Pratiksha, and Nikita for the interesting scientific discussions and the fun play times we have shared in the lab. I would also like to thank some of the previous

lab members Anuj and Shambhu for providing emotional support during my initial years in the lab. A heartfelt thanks to the previous BS-MS students, Bindia, Varsha and Swati. A special mention to Bindia for her comical nature, Aakanksha for her happy go lucky attiude, Chirag for his carefree and caring approach, Aarushi for cheerful presence, Archi for her brilliant teaching skills and Ashwin for his scientific acumen and enterprising nature, and Vibhu for his frankness. It was great sharing lab space with you all throughout these years. Mentioning about lab without Vidya would be incomplete. His arduous effort in keeping our lab in perfect condition at all times is commendable.

During my PhD. years, I have been lucky enough to form some endearing friendships which I would keep for life. Special thanks to Kanchan, Gayathri, Manpreet, Anuj and Nitin (Dhamu) for their unconditional support and care throughout all these years. I am grateful that our friendship only grew exponentially since the day we met. I thank Deepinder, Mukund, Neeraj, Megha and Swati for many memorable times within and outside IISER. I would also like to take this moment to thank my friends Shourya and Shweta who always encouraged me when things went downhill. I will always be thankful to Nisha, Surbhi, Sai, Sayan, Kiran, Bhishem, Prince, Aakanksha, Krishna, and Vinay for their precious time during my journey at IISER Mohali.

This entire journey would not have been possible without the unconditional support of my family members. I was fortunate to have a loving father (whom I lost before I could complete this journey) and an extremely supportive and strong-willed mother who believed in me and gave me the freedom to be who I am today. I draw my inspiration and strength from my brothers, Amit and Jatin, who like my parents are the most hardworking souls. A huge credit for the successful completion of my PhD goes to my Husband, Aman. Despite being from a non-biological background he heard me very patiently almost every day while I was writing my thesis and helped me organize my thoughts. I also express my gratitude to my adorable in-

laws (Mumma, Papa, Manas di, Karthik, Trina di and Anirudh) for their continued support, guidance and encouraging words during all these years.

Muskan Bhatia

Publications

Bhatia M, Thakur J, Suyal S, Oniel R, Chakraborty R, Pradhan S, Sharma M, Sengupta S, Laxman S, Masakapalli SK, Bachhawat AK. Allosteric inhibition of MTHFR prevents futile SAM cycling and maintains nucleotide pools in one carbon metabolism. **Journal of Biological Chemistry. 295(47), 16037-16057**

Deshpande, A. A., **Bhatia, M.***, Laxman, S., & Bachhawat, A. K. (2017). Thiol trapping and metabolic redistribution of sulfur metabolites enable cells to overcome cysteine overload. ***Microbial Cell***, *4*(4), 112.

*co-first author

Abstract

Methylenetetrahydrofolate reductase (MTHFR), is an enzyme that links the folate cycle to the methionine cycle in one-carbon metabolism. Previous studies with the purified eukaryotic MTHFR have revealed that the enzyme is under allosteric inhibition by S-Adenosyl methionine (SAM). Although this allosteric regulation has been known for decades, the importance of this regulatory control to one-carbon metabolism has never been adequately understood, as mutants defective in this regulation have never been obtained.

We describe in this thesis the identification of amino acid residues within the regulatory region of MTHFR critical for its regulation by SAM and the creation of mutations within this region to yield feedback insensitive, deregulated MTHFR. These mutants were exploited to investigate the effects of defective allosteric regulation. Genetic analysis revealed a strong growth defect in the presence of methionine.

To understand the metabolic consequences we carried out biochemical and metabolite analysis. We observed that both the folate and methionine cycles were affected in these mutants, as was the transsulfuration pathway leading to decreased formation of glutathione and its precursors critical for redox homeostasis. The major consequences, however, appeared to be in the depletion of nucleotides. Folates are precursors to nucleotides, but folate supplementation led to only partial recovery. ^{13}C isotope labelling and metabolic studies revealed that the deregulated MTHFR cells undergo continuous transmethylation of homocysteine by CH_3THF to form methionine, which drives SAM formation accentuating ATP depletion. SAM was also cycled back, leading to futile cycles of SAM synthesis and recycling. This also explains the need for MTHFR to be regulated by SAM, and the study has yielded valuable insights into one-carbon metabolism. Furthermore, these mutants would be powerful tools both in yeasts and in humans (which have a similar domain) to further dissect the regulation of one-carbon metabolism and its intersections with various pathways.

Thesis Synopsis

Studies on the regulatory domain of the yeast Methylene tetrahydrofolate reductase (MTHFR), a key enzyme in one-carbon metabolism

Introduction

One-carbon metabolism is a universal metabolic process, where single-carbon methyl groups are transferred to enable the synthesis of several essential metabolites serving important cellular functions. These include DNA synthesis (thymidine and purines), amino acid homeostasis (serine, glycine, and methionine), redox balance, and epigenetic maintenance. This carbon partitioning across various cellular outputs involves three different pathways, namely, the folate cycle, the methionine cycle, and the transulphuration pathways (Locasale, 2013). While the centrality of one-carbon metabolism has always been recognized, recent studies reveal the immense importance of its homeostasis for health and disease (Ducker & Rabinowitz, 2017). Due to the role of one-carbon metabolism in such varied cellular processes, the flux of one-carbon units among these different pathways requires tight regulation. Despite the critical role of regulation of one-carbon metabolism, it has not yet been extensively studied.

Methylene tetrahydrofolate reductase (MTHFR) is an enzyme that straddles the folate and methionine cycles of one-carbon metabolism. It is a flavoprotein that catalyses the reduction of methylene tetrahydrofolate (CH_2THF) to methyl tetrahydrofolate (CH_3THF) using NADPH as the reducing equivalent. The methyl tetrahydrofolate that is formed is then utilized in the methylation of homocysteine to methionine. MTHFR is thus found at a critical branch point of one-carbon metabolism and is one of the key regulatory nodes being under allosteric feedback inhibition by SAM.

Typical eukaryotic MTHFR enzymes have two domains: a catalytic domain of approximately 300 amino acids and an equally large regulatory domain for feedback regulation by SAM. The catalytic domain of the enzyme has been extensively studied, and the catalytic

mechanism as well as the NADPH, FAD and substrate binding sites have been clearly delineated (Trimmer, 2013). The role of the regulatory domain of MTHFR, however, in contrast, has not been rigorously investigated. Indeed, the consequences of an absence of regulation by SAM of an otherwise functional MTHFR has been unclear till now. Although the allosteric regulation has been known for decades (Kutzbach & Stokstad, 1967, 1971), the importance of this regulatory control to one carbon metabolism has never been adequately understood. In fact, the SAM binding regions on the MTHFR regulatory domain are still not unequivocally recognized (Froese et al., 2018; Goyette et al., 1994).

This thesis investigates the regulation of MTHFR in light of one-carbon metabolism. Using yeast as a model system, we have examined two different aspects concerning MTHFR regulation, based on our two objectives below:

(1) To investigate the regulatory domain and to identify the amino acid residues within the regulatory domain of MTHFR protein, which are critical for regulation by MTHFR. Further, to create a feedback insensitive deregulated mutant of yeast MTHFR.

(2) To understand the basis and importance of MTHFR regulation by SAM for one-carbon metabolism.

The work described under these two objectives has been described in Chapter 3 and Chapter 4, respectively. This work is summarized Chapter-wise below.

Chapter 3: To investigate the regulatory domain of MTHFR and to isolate and characterize deregulated mutants of Met13p, yeast MTHFR

In this chapter, I have described our attempts to isolate, create, and characterize a feedback insensitive deregulated yeast MTHFR mutant.

An analysis of the regulatory region of yeast MTHFR protein (Met13p) was first carried out to identify residues that would be involved in the binding of SAM. The sequence-based analysis revealed the presence of three short blocks of high conservation in the regulatory

domain, which we defined as conserved region 1 (CR1), conserved region 2 (CR2), and conserved region 3 (CR3). Structural analysis indicated residues (Tyr404 and Glu422) crucial for SAM binding which were present in entirely different regions of the regulatory domain.

We evaluated these residues of MTHFR for potential SAM-mediated repression. Mutational analysis showed that all the mutants of Met13p were functional as these enzymes were capable of complementing the methionine auxotrophy of the *met13Δ* strain. However, two of the mutants- MET13_E422A and MET13_M2 (R357A.S361A, a mutant of CR1 region) exhibited defective growth on methionine, where the former displayed a mild defect on methionine media and the latter demonstrated a more severe growth defect. The wild-type and mutant recombinant protein revealed that the inhibition by SAM was lost partially in the mutant MET13_E422A and completely in the MET13_M2.

Further mutational analysis within the CR1 region revealed that a short stretch of amino acids (F353, P354, N355, G356, R357, and G359) within the CR1 is critical for regulation of MTHFR protein by SAM. We also confirmed the SAM insensitive behaviour of two representative mutants of the CR1 region (MET13_R357A and MET13_P354A) using *in-vitro* enzyme assays.

The deregulated mutants displayed a methionine specific growth defect. This was shown to be due to the deregulated property of MTHFR since, in the background of a catalytically inactive mutant of MTHFR, this phenotype of the deregulated mutant was not seen.

These results clearly demonstrate the successful isolation and characterization of deregulated mutants of MTHFR that lack feedback inhibition by SAM. Importantly, we have also discovered a growth phenotype of such mutants in methionine medium, which has been exploited to investigate the impact of defective allosteric regulation on one-carbon metabolism.

Chapter 4: To understand the metabolic consequences of MTHFR deregulation on one-carbon metabolism

In this chapter, I describe our attempts to understand the importance of the SAM mediated feedback inhibition of MTHFR in the maintenance of one-carbon metabolism. The growth defect seen in the feedback-insensitive deregulated MTHFR mutant on methionine medium provided an opportunity to understand the metabolic reasons behind the regulation of MTHFR by SAM.

We first examined whether the deficiency of folate pools was the chief cause of defective growth of the deregulated MTHFR enzyme by supplementing cells with folic acid and obtained a significant rescue only at higher folic acid concentrations (1mM). To further define which folate pools were deficient, we examined the steady-state levels of the different folate pools and observed a decrease in the levels of the substrate of MTHFR, CH_2THF in the deregulated mutant, whereas the pools of the product of MTHFR, CH_3THF, appeared to be higher in the mutant.

As CH_2THF, the substrate of MTHFR, is essential for the synthesis of nucleotides (purines and thymidine), depleted CH_2THF pools would be reflected in depleted nucleotide pools. Therefore, we determined the nucleotide levels in the MTHFR deregulated mutant strains. We observed a striking, 10-fold depletion of the cellular AMP, GMP, and CMP pools in the cells transformed with the mutant protein (MET13_R357A). While these observations are consistent with the depletion of CH_2THF, which is a precursor in nucleotide biosynthesis, the much steeper decreases in the nucleotide levels suggested that folate depletion might be only one of the causative factors.

The MTHFR enzyme uses NADPH as the reducing equivalent for its catalytic activity. Additionally, it has a FAD moiety non-covalently bound to it, which is also essential for the oxidoreductase activity. Both NADPH/NADP and FAD/$FADH_2$ derive from adenine pools.

Therefore, we were interested in examining the depletion of these cofactor pools due to unregulated MTHFR activity as the additional contributing factors for the defective growth phenotype. We observed that both NADPH and FAD pools were deficient in the deregulated mutant.

Metabolite estimations of sulphur metabolites were subsequently carried out to investigate the impact of MTHFR deregulation on the methionine cycle and transsulfuration pathway. Methionine levels, surprisingly, remained almost unchanged. SAM levels were, however, increased, whereas SAH showed decreased levels in the deregulated mutant. The metabolites of the reverse transsulfuration pathway, homocysteine, cystathionine, and cysteine, showed decreased levels, the most striking decrease being in the levels of cystathionine. We also observed lower levels of both the oxidized and reduced forms of glutathione (GSH and GSSG), suggestive of redox imbalance. Further studies revealed that glutathione was indeed depleted in these strains.

The surprisingly unchanged levels of methionine suggested that in the presence of exogenous methionine, the homeostasis of cellular methionine might be maintained by repression of synthesis since in the presence of exogenous methionine, methionine biosynthesis is repressed. However, genetic experiments exploiting the knockouts of the high affinity methionine transporter (MUP1) and methionine synthase (MET6) seemed to indicate that both endogenous biosynthesis and the transport of exogenous methionine were essential factors in the growth defect on methionine.

To confirm the suggestions from the genetic experiments, we needed more rigorous confirmation as to whether methionine biosynthesis by CH_3THF, the substrate of MTHFR, was required. To evaluate this aspect, we resorted to ^{13}C metabolic studies where we observed significantly higher m+1 isotopomer for all fragments of methionine in the case of deregulated MTHFR bearing cells compared to the WT in [1-^{13}C-glucose] fed cells. The results revealed a

continuous biosynthesis of methionine in yeast (with significantly higher rates in the mutants) through the substrates of ^{13}C-labelled CH_3 and homocysteine.

To examine alterations in pathway preferences in these deregulated mutants, we further analysed the ^{13}C isotope labelling data to analyse the fluxes of central metabolism pathways (glycolysis, tricarboxylic acid cycle, and pentose phosphate pathway) under pseudo-steady state conditions. The ^{13}C redistribution in the amino acids retro-biosynthetically reporting on the central precursors of different pathways of central metabolism shows that the relative fluxes in the WT and mutant are predominantly stable with only minor but appreciably significant readjustments in glycolysis pathway as supported by the extent of ^{13}C incorporations in the mass isotopomers of serine and alanine.

The absence of any major metabolic readjustments in the deregulated mutant as compared to the WT suggested that pathways downstream of methionine were responsible for the methionine-dependant growth defect in the MTHFR deregulated mutants. Methionine formation drives the ATP dependant enzymatic synthesis of S-adenosyl methionine (SAM). The metabolite analysis had indicated an increase in SAM, which can meet two distinct fates. In the first case, SAM is involved in the methylation of a variety of cellular substrates such as nucleic acids, proteins, and lipids. Phosphatidylethanolamine (PE) methylation appears as the major SAM consumer. Therefore, we quantified the relative abundance of phospholipids [phosphotidyl ethanolamine (PE), and phosphatidylcholine (PC)] in the deregulated MTHFR mutant and observed a noticeable increase (≈1.6 fold) in the total PC levels along with a marginal decline in cellular abundance of PE in the mutant harbouring cells. However, a concomitant increase in SAH, a side product of PE methylation and other methylation, was not observed. Rather, SAH, in turn, is hydrolysed to homocysteine and adenosine, both of which are in increased requirements in the mutant. Adenosine is required because of the depleted

adenine pools, while homocysteine is required owing to the continuous unregulated formation of CH_3THF.

The second route of SAM metabolism is through the methionine salvage pathway. In this pathway, the methionine, which converts to SAM, is converted back to methionine with the release of adenine and polyamine following the decarboxylation of SAM. In the polyamine pathway, the decarboxylated-SAM can be used in the synthesis of spermidine from putrescine or in the formation of spermine, which eventually releases methyl-thioadenosine (MTA), subsequently yielding methionine and adenine. We observed a significant increase of 2.5 fold in the amount of spermine for the deregulated mutant (MET13_R357A) with no change in spermidine levels. This clearly suggested a significant conversion of SAM back to methionine and adenine, with the concomitant formation of spermine. The methionine so formed would again drive the ATP-dependant formation of SAM.

Thus, the major consequence of the deregulated mutants was a severe nucleotide depletion that was accentuated by futile cycles of SAM synthesis and recycling.

References

Ducker, G. S., & Rabinowitz, J. D. (2017). One-Carbon Metabolism in Health and Disease. *Cell Metab, 25*(1), 27-42. doi:10.1016/j.cmet.2016.08.009

Froese, D. S., Kopec, J., Rembeza, E., Bezerra, G. A., Oberholzer, A. E., Suormala, T., . . . Yue, W. W. (2018). Structural basis for the regulation of human 5,10-methylenetetrahydrofolate reductase by phosphorylation and S-adenosylmethionine inhibition. *Nat Commun, 9*(1), 2261. doi:10.1038/s41467-018-04735-2

Goyette, P., Sumner, J. S., Milos, R., Duncan, A. M., Rosenblatt, D. S., Matthews, R. G., & Rozen, R. (1994). Human methylenetetrahydrofolate reductase: isolation of cDNA mapping and mutation identification. *Nat Genet, 7*(4), 551.

Kutzbach, C., & Stokstad, E. L. (1967). Feedback inhibition of methylene-tetrahydrofolate reductase in rat liver by S-adenosylmethionine. *Biochim Biophys Acta, 139*(1), 217-220. doi:10.1016/0005-2744(67)90140-4

Kutzbach, C., & Stokstad, E. L. (1971). Mammalian methylenetetrahydrofolate reductase. Partial purification, properties, and inhibition by S-adenosylmethionine. *Biochim Biophys Acta, 250*(3), 459-477. doi:10.1016/0005-2744(71)90247-6

Locasale, J. W. (2013). Serine, glycine and one-carbon units: cancer metabolism in full circle. *Nat Rev Cancer, 13*(8), 572-583. doi:10.1038/nrc3557

Trimmer, E. E. (2013). Methylenetetrahydrofolate reductase: biochemical characterization and medical significance. *Curr Pharm Des, 19*(14), 2574-2593. doi:10.2174/1381612811319140008

Table of Contents

Chapter 1 Review of literature

Chapter 3 Isolation and characterization of deregulated mutants of yeast MTHFR, MET13

List of Figures

Chapter 1 Review of Literature

Chapter 3 Isolation and characterization of deregulated mutants of yeast MTHFR, MET13

List of tables

Chapter 2 Materials and Methods

Chapter 3 Isolation and characterization of deregulated mutants of yeast MTHFR, MET13

Chapter 4 Deregulation of MTHFR disrupts the redox and metabolic homeostasis in S. cerevisiae

Abbreviations

°C	Degree celsius
AHCY	S-adenosyl homocysteine hydrolase
AICART	Amino imidazole carboxamide ribonucleotide formyl transferase
APS	Ammonium persulphate
ATP	Adenosine triphosphate
BDMCS	t-butyl-dimethylchlorosilane
BSA	Albumin, Fraction V, Sigma
CBL	Cystathionine beta lyase
CBS	Cystathionine beta synthase
$CD_{A/B}$	Catalytic domain A and B
CIP	Calf intestinal phosphate
CGL	Cystathionine gamma lyase
CGS	Cystathionine gamma synthase
Cm	Centimeter
CoA	Co-enzyme A
CR1/2/3	Conserved region 1/2/3
C-terminal	Carboxyl-terminal
CTH	Cystathionase
Cys	Cysteine
dcSAM	Decarboxylated S-adenosyl methionine
DHF	Dihydrofolate
DHFR	Dihydrofolate reductase
DHK-MTPene	1,2-dihydroxy 3-ketomethiopentene
DK-MTP-1P	2,3-Diketomethiopentane-1-phosphate
DMSO	Dimethyl sulfoxide
DNA	Deoxyribonucleic acid
dNTPs	Deoxynucleotide triphosphates
DOPE	Discrete optimized protein energy
DTT	Dithiothreitol
dTMP	Deoxythymidine monophosphate
dUMP	Deoxyuridine monophosphate
EDTA	Ethylenediaminetetraacetic acid
ESR	Envelope stress response
ETC	Electron transport chain
eV	Electron volt
FAD	Flavin adenine dinucleotide
FMN	Flavin mononucleotide
GART	Glycinamide ribonucleotide transformylase
GCL	Glutamate cysteine ligase
GC/MS	Gas chromatography/Mass spectrometry

GDC	Glycine decarboxylase
GNMT	Glycine N-methyl transferase
GSH	Glutathione reduced
GSSG	Glutathione oxidised
H^+	Proton
HHcy	Hyperhomocysteinemia
H_2O_2	Hydrogen peroxide
HPLC	High-performance liquid chromatography
IPTG	Isopropyl β- d-1-thiogalactopyranoside
kDa	Kilodalton
LB	Lysogeny broth
LC/MS	Liquid chromatography/ mass spectrometry
LiAc	Lithium acetate
LiAcTE	Lithium acetate tris EDTA
MtBSTFA	N-methyl-N-(t-butyldimethylsilyl) trifluoroacetamide
Min	Minutes
Ml	Milliliter
mM	Millimolar
N- terminal	Amino-terminal
NADH	Nicotinamide adenine dinucleotide
NADP	Nicotinamide adenine dinucleotide phosphate
MAT	Methionine aminotransferase
MCT	Microcentrifuge tube
MRM	Multiple reaction monitoring
MID	Mass isotopomer distributions
MTA	Methyl thioadenosine
MS	Mass spectrometer
MTHFR	Methylene tetrahydrofolate reductase
MTOB	4-Methylthio-2-oxobutyrate
MTR	Methyl ribose
MTs	Methyl transferases
MTRu1P	methylthioribulose-1-phosphate
nM	Nanomolar
NIST	National institute of standards and technology
OD	Optical density
OMPs	Outer membrane porins
PAGE	Polyacrylamide gel electrophoresis
PC	Phosphatidyl choline
PCI	Phenol-chloroform-isoamyl alcohol
PCR	Polymerase chain reaction
PE	Phosphatidyl ethanolamine
PEG	Polyethylene glycol
PL	Phospholipids
PMSF	Phenyl methyl sulphonyl fluoride

PS	Phosphatidyl serine
RNA	Ribonucleic acids
RT	Room temperature
SAH	S-adenosyl homocysteine
SAM	S-adenosyl methionine
SD	Standard deviation
SDS	Sodium dodecyl sulphate
ssDNA	Single stranded deoxyribonucleic acid
SHMT	Serine hydroxyl methyl transferase
SOB	Super optimal broth
SOC	Super optimal broth with catabolite repression
STEM	Scanning tunneling electron microscope
TAE	Tris-Acetate-EDTA
TCA	Tri-carboxylic acid
TEMED	N, N, N', N'-Tetramethyl ethylene diamine
THF	Tetrahydrofolate
TYMS	Thymidine synthase
UHPLC	Ultra high performance liquid chromatography
WT	Wild-type
YNB	Yeast nitrogen base
YPD	Yeast extract peptone dextrose
α-KG	α-ketoglutarate
µl	Microliter
µM	Micromolar
µmol	Micromoles
1C	One-carbon
5-CH_3THF	5-Methyl tetrahydrofolate
5,10-CH_2THF	5,10-Methylene tetrahydrofolate
10-CHO-THF	10-Formyl tetrahydrofolate

Chapter 1

Review of Literature

1. Chapter 1

1.1. Introduction: One-carbon metabolism

One-carbon (1C) metabolism is a core metabolic process of all living cells. It involves the methionine and folate cycles that are central to cellular function. These pathways provide 1C units (methyl groups) for the synthesis of DNA, certain amino acids, SAM, phospholipids, polyamines, and creatinine. Due to the distribution of its 1C units to varied acceptor compounds, one-carbon metabolism serves as a regulator and sensor for the cellular nutrient status (Figure 1.1). Moreover, it can contribute to the maintenance of the energy balance in the cell by providing molecules of ATP and NADPH. It not only allocates 1C units for the biosynthesis but also tunes the nutrient status of the cell with epigenetic and redox statuses (Reviewed by Shuvalov et al., 2017).

Due to the integration of numerous metabolic processes within one-carbon metabolism, disturbances in this pathway have been associated with a wide array of diseases (Ducker & Rabinowitz, 2017). These might occur either due to dietary deficiencies, genetic enzyme polymorphisms, or enzymatic blocks resulting from loss of function mutations at one or multiple steps. Besides chronic nutritional deficiencies, lack of supplements such as folates, vitamin B_6 and B_{12}, omega-3, and minerals may also disturb normal one-carbon metabolism (Seth et al., 2015).

In adults, dietary folate deficiency leads to anemia. In addition, disruption of folate arm in the metabolic network of one-carbon metabolism has also been known to cause neural tube defects, involving failure in neural tube closure early in pregnancy, in the offspring of mother's suffering from folate deficiency. In the developing fetus, the outcomes might range from severe to mild. In a more severe form, neural tube defects cause anencephaly causing fetal loss to a milder form, i.e., spina bifida with partial leg paralysis (Copp et al., 2015).

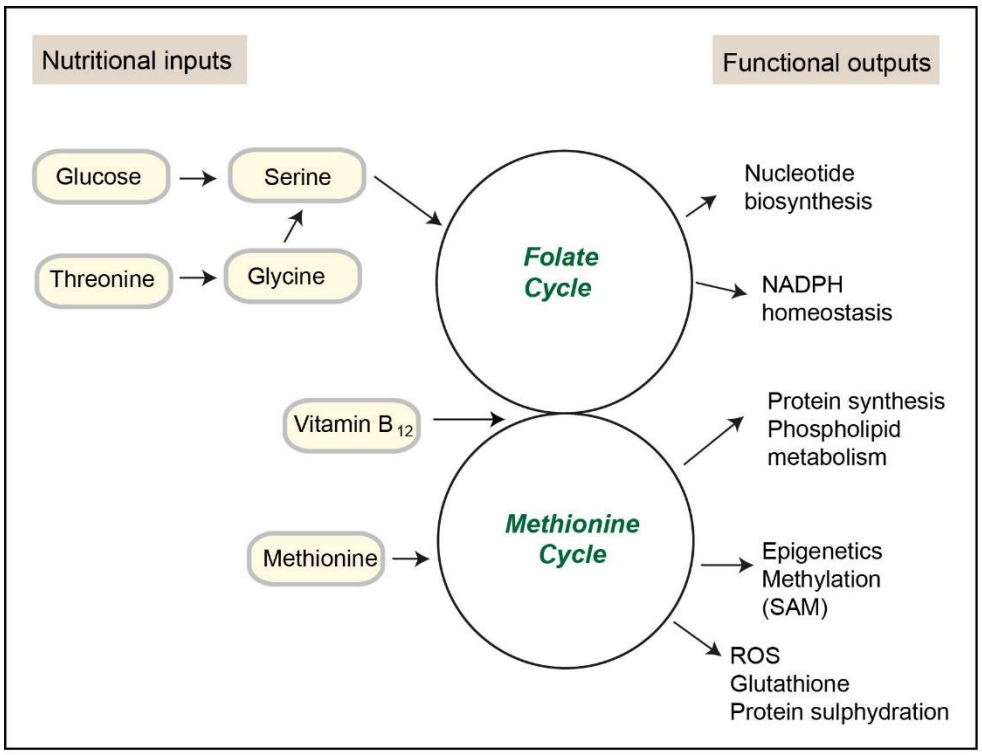

Figure 1.1 One-carbon metabolism as a nutrient sensor and regulator.
Several nutrient sources (amino acids, glucose, and/or vitamin) which are either imported or synthesized *de novo* enter one-carbon metabolism either through folate cycle or methionine cycle. These nutrients are processed through these metabolic routes depending on the nutritional state of the cell. Integration of such diverse signals generates a variety of outputs like nucleotide synthesis, protein synthesis (methionine), reducing power (NADPH), antioxidant (GSH), methylation power (SAM), and substrates for methylation.

Disturbances of the methionine cycle lead to a condition called hyperhomocysteinemia (HHcy). Elevated homocysteine levels have been associated with an increase in disorders such as autoimmune disorders, neuropsychiatric disorders, cardiovascular and neurodegenerative diseases, diabetes, renal disease, osteoporosis, and cancer (Brustolin et al., 2010). In addition to HHcy, altered one-carbon metabolism, including both folate and methionine metabolism, has also been associated with genome maintenance, and epigenetic alterations primarily change in DNA methylation. Recently, the modification of cellular epigenetic status has been linked to the hyperactivation of this pathway, which is considered as one of the driving factors for oncogenesis (Locasale, 2013).

Within eukaryotes, 1C metabolism has been demonstrated to occur in different subcellular compartments, i.e., cytoplasm, mitochondria, and nucleus (Barlowe & Appling, 1988; Thomas et al., 1991; Tibbetts & Appling, 2010). Several factors influence the flow of 1C units through these compartments: metabolite concentration, enzyme expression, the genotype of the organism (Christensen & MacKenzie, 2006; Ducker et al., 2016), and cell or tissue type for a multicellular organism.

1.2. One-carbon metabolism and its different modules

The different modules of one-carbon metabolism and their intermediates are described below (Figure 1.2).

1.2.1. Folate cycle

One of the constituent pathways of 1C metabolism is the folate cycle. The primary function of folate metabolism is to produce activated 1C units. These activated 1C units, via a series of steps, are utilized either in the *denovo* biosynthesis of nucleotides (purines and thymidine), methionine, or consumed for the generation of the major methylation power of the cell, i.e., SAM. Most bacteria, yeast, and plants can synthesize folates, whereas animals need dietary folate intake. Due to its indispensable role in DNA synthesis that is critical for cellular proliferation, folate metabolism has long been a critical target for several antibiotics and chemotherapeutics (Chattopadhyay et al., 2007). As mentioned previously, eukaryotic folate metabolism is compartmentalized and can occur in cytoplasm, mitochondria, nucleus, and also in plastids in the case of plants. However, here we would focus and describe mainly the yeast cytosolic folate pathway and its intermediates.

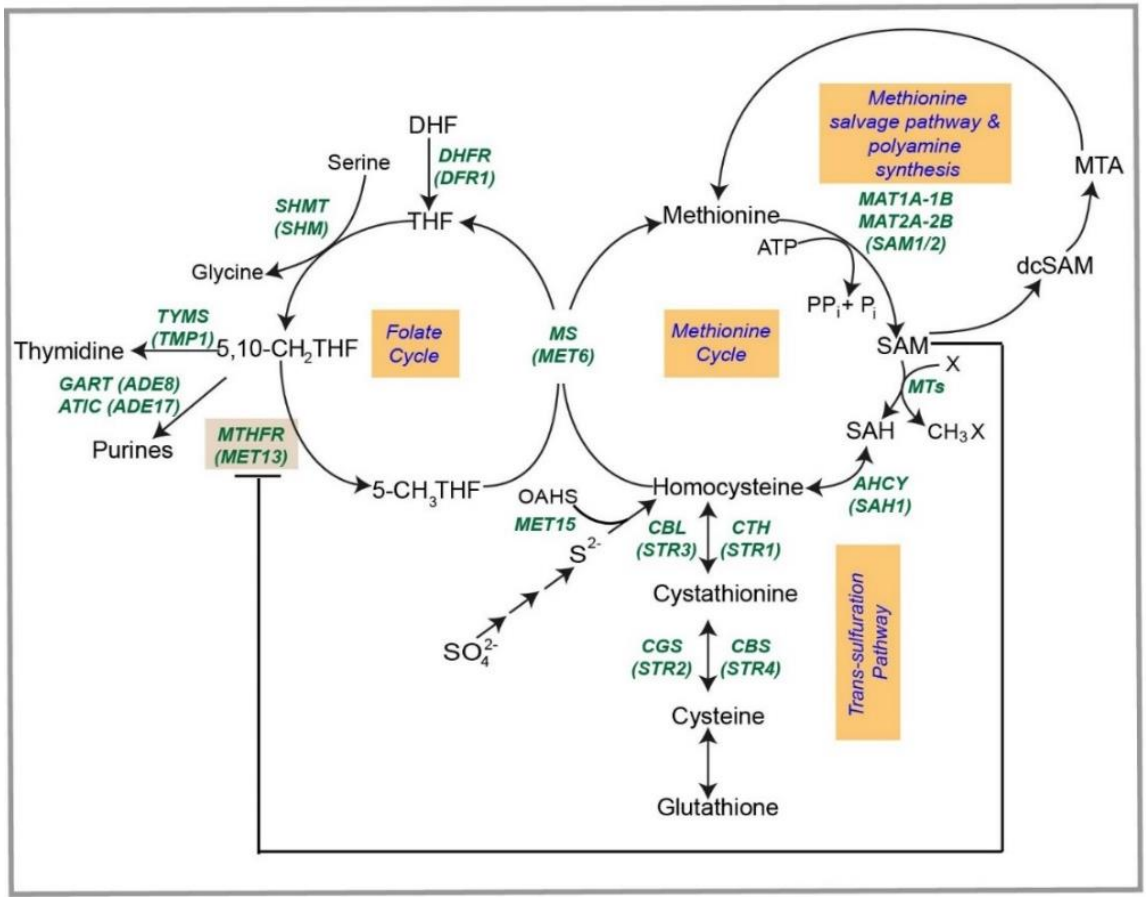

Figure 1.2 An overview of one-carbon (1C) metabolism and its importance.
1C metabolism encompasses the folate cycle**,** methionine cycle, and trans-sulfuration pathway. The folate cycle plays a crucial role in nucleotide biosynthesis (Purines and thymidine), redox balance (by utilization and production of NADPH at various steps) and amino acid homeostasis (serine, glycine, and methionine) Folate metabolism is linked to the methionine cycle via 5-methyl tetrahydrofolate (5-CH_3THF), a folate intermediate synthesized by the activity of the MTHFR enzyme. Methionine synthase remethylates homocysteine to methionine by expending 5-CH_3THF, which has entered the methionine cycle. The methionine cycle besides providing methionine for protein translation, is the major source of S-adenosyl methionine (SAM), the cellular methylation currency. SAM also yields polyamines via the methionine salvage pathway or it enters the trans-sulfuration pathway via hydrolysis of S-adenosyl homocysteine (SAH) to homocysteine. The trans-sulfuration pathway synthesizes GSH via a series of steps. Reduced glutathione (GSH) is the major anti-oxidant moiety in the cell. DHFR-Dihydrofolate reductase; SHMT-Serine hydroxyl methyltransferase; TYMS-Thymidine synthase; GART-Glycinamide ribonucleotide transformylase; AICART-Aminoimidazole carboxamide ribonucleotide formyltransferase; MTHFR-Methylene tetrahydrofolate reductase; MS-Methionine synthase; MAT-Methionine adenosyl transferase; MTs-Methyl transferases, AHCY-Adenosyl homocysteinase; CTH-Cystathioninase; CBS-Cystathionine-β-synthase; CGS-Cystathionine-γ-synthase, CBL- Cystathionine-β-lyase. of polyglutamate tails to the folates by isoforms of folylpolyglutamate gamma glutamate synthase activity (MET7).

1.2.1.1. Tetrahydrofolate

Tetrahydrofolate (THF) is the biologically active form of the vitamin folic acid and the primary carrier of 1C units within the cell. Its chemical structure comprises three elements: a pteridine ring, a para-aminobenzoic acid moiety, and a polyglutamate tail (Figure 1.3A). Carbon units, such as methyl, methylene, methenyl, and formyl, are added at positions N5 and N10 of the pteridine ring as per the cellular requirements through the involvement of folate interconverting enzymes (Figure 1.3B). THF and its derivatives are restricted to the compartments in which they are formed (Pasternack et al., 1994) as a consequence of the addition of polyglutamate tails to the folates by isoforms of folylpolyglutamate gamma glutamate synthase activity (MET7). Therefore, the transfer of 1C units between the compartments requires 1C donors, i.e., serine, glycine, or formate.

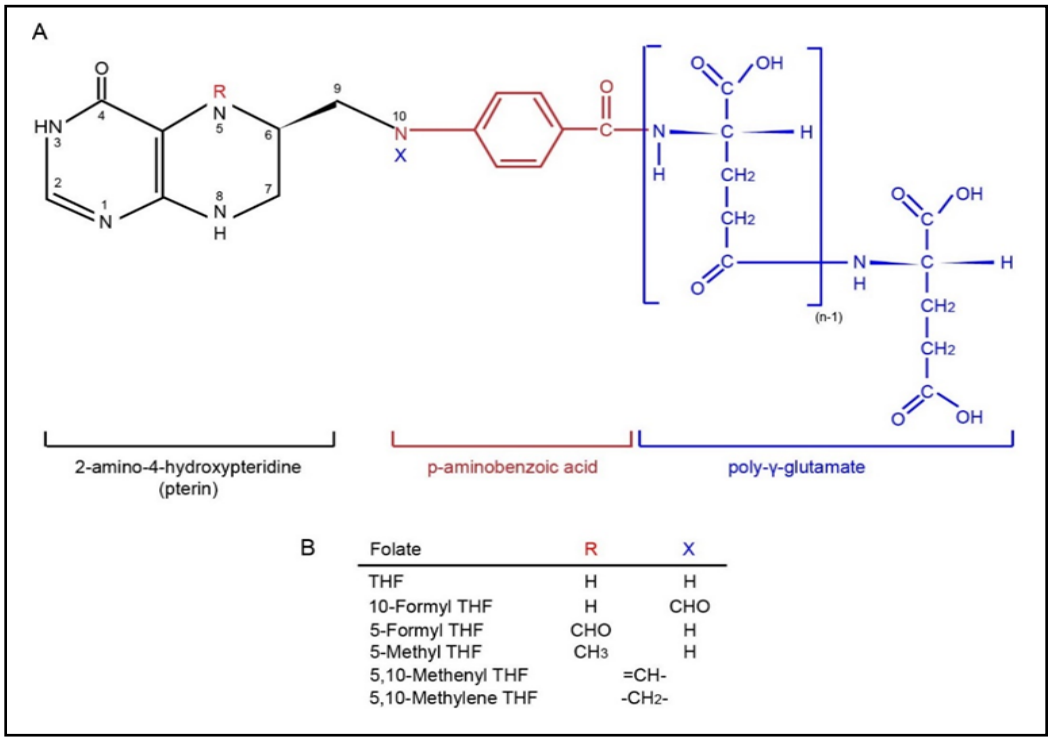

Figure 1.3 Structure of folates.
Chemical structure of folic acid. (B) Various one carbon substituents of THF.

In yeast, THF is obtained either from *denovo* synthesis from dihydrofolate (DHF), or as a by-product of homocysteine remethylation. *Denovo* synthesis of folate consists of multiple steps involving a range of enzymes (Figure 1.4A), whereas homocysteine remethylation is catalysed by methionine synthase, a vitamin B12 dependent enzyme encoded by MET6 (Figure 1.2). Another route of THF synthesis in the cell is through regeneration from DHF. Thymidine synthase (TMP1) converts deoxyuridine monophosphate (dUMP) to deoxythymidine monophosphate (dTMP) in 5,10-CH_2THF dependent manner and regenerates DHF as a side product, which can now serve as a source of THF (Figure 1.4B).

THF in the cytoplasm accepts a one-carbon unit from serine and gets converted to 5,10-CH_2THF (Figure 1.2). This reaction is reversible and is catalysed by serine hydroxymethyltransferase (SHMT). Cells can use SHMT to make serine in one compartment and catabolize it in another. The direction of flow depends on the demand and supply of 1C units within a given compartment (Ducker et al., 2016).

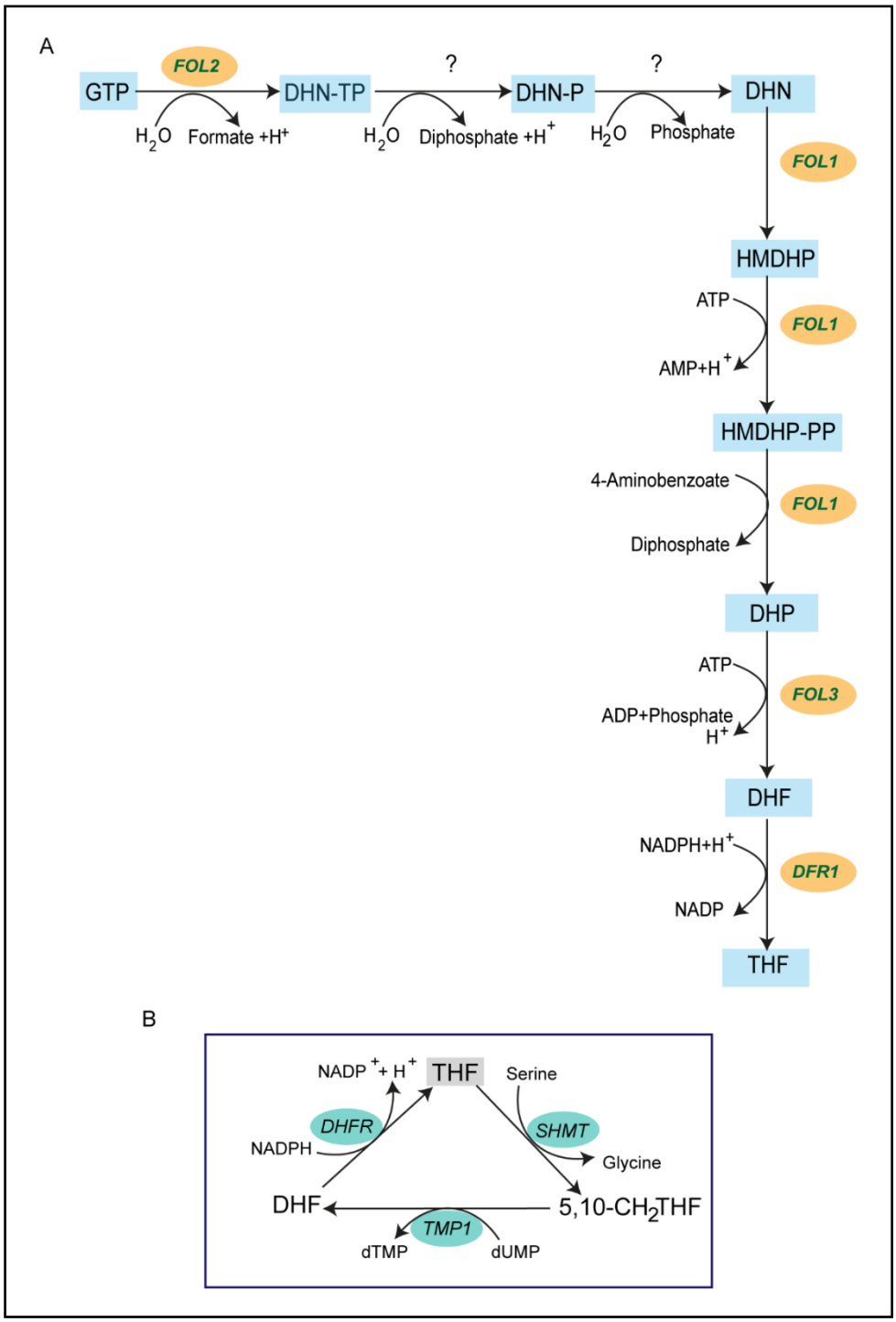

Figure 1.4 Biosynthesis pathways of THF.

(A) *De novo* synthesis. (B) Salvage pathway. FOL2-GTP cyclohydrolase 1; FOL1-Folic acid synthesis protein; FOL3-Dihydrofolate synthetase; DFR1-Dihydrofolatereductase; DHN-TP-7,8-Dihydroneopterin-3'-triphosphate; DHN-P-7,8-Dihydroneopterin-3'-phosphate; DHN-7,8-Dihydroneopterin; HMDHP-6(hydroxyl)-7,8-Dihydroneopterin; HMDHP-PP-(7,8-Dihydroneopterin-6-yl) methyl diphosphate; DHP-7,8-Dihydropteroate; DHF-Dihydrofolate; THF-Tetrahydrofolate.

1.2.1.2. 5,10-methylene THF

5,10-methylene THF (5,10-CH_2THF), a key form of folates, can be generated from the cleavage of L-serine to glycine by the activity of serine hydroxymethyltransferase either in the cytoplasm or the mitochondria (Schirch, 1984) (Figure 1.5A). Glycine cleavage system, prevalent exclusively in mitochondria, can also generate 5,10-CH_2THF by utilizing glycine decarboxylase enzyme complex (GDC) (Ogur et al., 1977) (Figure 1.5B). GDC complex of *S. cerevisiae* is composed of four subunits- GCV1, GCV2, GCV3, and LPD1 (McNeil et al., 1997; Nagarajan & Storms, 1997; D. A. Sinclair et al., 1996). Another source of 5,10-CH_2THF is formate both in mitochondria as well as cytoplasm. 10-formyltetrahydrofolate synthetase activity of C1-tetrahydrofolate synthases in either the cytoplasm (ADE3) or mitochondria (MIS1) (McKenzie & Jones, 1977; Pirkov et al., 2008) contributes to the synthesis of 5,10-CH_2THF from formate (Figure 1.5C).

5,10-CH_2THF can be used in three different ways (Figure 1.2). First, it can serve as 1C-donor for the initial step of thymidylate biosynthesis, a reaction catalysed by thymidylate synthase (TMP1). In this reaction, 5,10-CH_2THF is oxidized into dihydrofolate (DHF), where the one-carbon group released is used for the pyrimidine biosynthesis (as shown in Figure 1.2 and 1.4B). In the next reaction, dihydrofolate reductase (DHFR) reduces DHF to THF, closing this metabolic loop (Figure 1.4B). 10-HCO-THF is a 1C-donor for the two reactions of purine biosynthesis catalysed by the trifunctional enzyme Phosphoribosylglycinamide Formyl transferase/ Synthetase/ Phosphoribosylaminoimidazole Synthetase (GART) and Bifunctional 5-Aminoimidazole-4-Carboxamide Ribonucleotide Formyltransferase/IMP cyclohydrolase (ATIC), both of which also generate THF (Figure 1.2). Third, 5,10-CH_2THF is used by methylene tetrahydrofolate reductase (MTHFR) to generate 5-methylTHF (5-CH_3THF) (as illustrated in Figure 1.2). The latter donates a methyl group to homocysteine resulting in the formation of methionine and THF. In this way, the folate cycle is coupled with the methionine

cycle. Finally, THF is converted by serine hydroxymethyl transferases to yield 5,10-CH_2THF once again, closing the cycle.

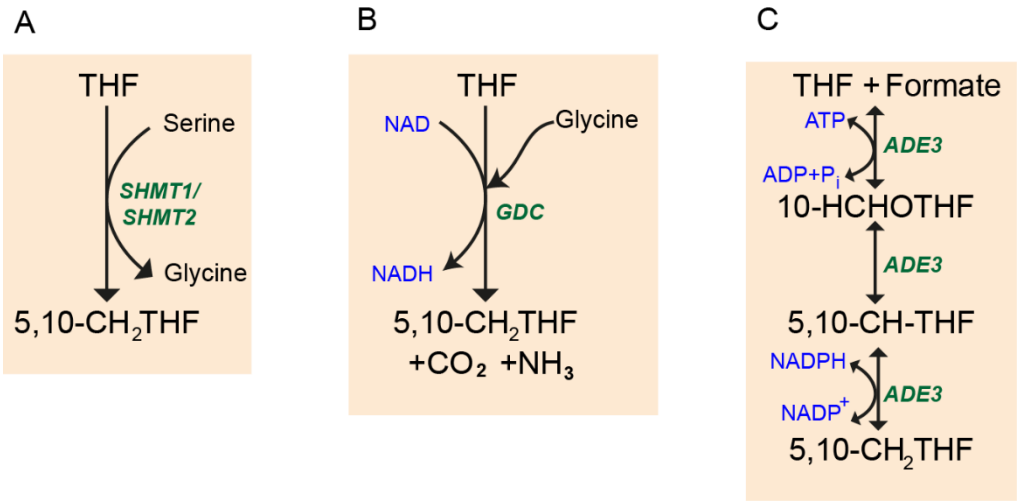

Figure 1.5 Biosynthesis pathways of CH_2THF.
(A) CH_2THF synthesis from serine can occur either in the cytoplasm or in mitochondria by serine hydroxymethyl transferases. (B) Glycine cleavage system in mitochondria also generates CH_2THF with the help of glycine decarboxylase enzyme complex. (C) CH_2THF synthesis from formate catalysed by ADE3, a trifunctional enzyme present in the cytoplasm and mitochondria. SHMT-Serine hydroxyl methyl transferase; GDC-Glycine decarboxylase complex; ADE3-C_1-THF synthase (trifunctional enzyme: methylenetetrahydrofolate dehydrogenase/ methylene tetrahydrofolate cyclohydrolase, formyl tetrahydrofolate synthetase).

1.2.1.3. 5-Methyl tetrahydrofolate

5-Methyl tetrahydrofolate (5-CH_3THF) is the most abundant folate derivative in the cytoplasm of both yeast and mammals (Roje et al., 2002; Tibbetts & Appling, 2010). Besides being the most abundant, it is also one of the most stable forms of folates (Tibbetts & Appling, 2010). As per the current knowledge, 5-CH_3THF is exclusive to the cytoplasm within a living cell. Therefore, both its synthesis and degradation is brought about by enzymes localized in the cytosol. The generation of 5-CH_3THF is a single-step reduction reaction. MTHFR, an oxidoreductase, catalyses the reduction of 5,10-CH_2THF to 5-CH_3THF and uses NADPH as a reducing equivalent for this conversion.

5-CH_3THF transfers the 1C to homocysteine to form methionine, which then enters the methionine cycle. The folate group is regenerated as THF and re-enters the folate cycle. The conversion of homocysteine to methionine reaction is catalysed by the methionine synthase enzyme encoded by the MET6 gene in the case of yeast (Figure 1.2).

1.2.2. Methionine cycle

The methionine cycle (activated methyl cycle or methyl cycle) involves the formation of S-adenosyl methionine (SAM), an activated form of methionine that is followed by its recycling in a series of reactions back to methionine. The first evidence of the methyl cycle in *S. cerevisiae* was reported by Duerre, who demonstrated the incorporation of radioactivity in the intracellular homocysteine, cysteine, methionine, and SAM upon feeding yeast cells with radioactive SAH. In the methionine cycle, SAM can serve as a methyl donor for a variety of substrates, and itself get converted to SAH. SAH is hydrolyzed to homocysteine in a single step, catalysed by *S*-adenosylhomocysteine hydrolase. The cycle continues with the methylation of homocysteine to methionine using a methyl group from methylated folate (CH_3THF). Finally, the cycle is completed with the regeneration of SAM by *S*-adenosylmethionine synthetase (Thomas & Surdin-Kerjan, 1997) (Figure 1.2). In contrast to the folate cycle, the methionine cycle in yeast occurs exclusively in the cytoplasm.

1.2.2.1. Methionine

Methionine is an essential sulfur-containing amino acid catabolized and recycled through a series of metabolic reactions termed the methionine cycle (Gao et al., 2019). About 20% of the cellular methionine pools contribute towards protein synthesis, and the remaining is converted into SAM, the major methyl donor in the cell.

Methionine synthesis takes place both by *de novo* and salvage pathways (Figure 1.2). As discussed previously, the methionine synthase enzyme encoded by MET6 gene in yeast is responsible for the *de novo* synthesis of methionine. This enzyme accepts the methyl group

from CH_3THF, methylating homocysteine to methionine. Methionine also converts to S-Adenosyl methionine (SAM), the cellular methyl donor. In addition, methionine can also be generated from the polyamine biosynthesis by-product methylthioadenosine (MTA) via the methionine salvage pathway (Pirkov et al., 2008). Methionine synthesis via the salvage pathway is a multi-step process catalysed by several different enzymes (Figure 1.6). Firstly, methionine gets activated by an adenosyl moiety producing the universal methyl donor, SAM. SAM then undergoes decarboxylation to synthesize decarboxylated SAM (dcSAM) before it condenses with putrescine, an arginine derived polyamine obtained by the decarboxylation of ornithine. SAM and ornithine decarboxylation are catalysed by SAM decarboxylase (SPE2) and Ornithine decarboxylase (SPE1), respectively. Spermidine synthase encoded by SPE3 generates a molecule of MTA as a side product by the reaction of putrescine with dcSAM to form spermidine. Another molecule of MTA is released during spermine synthesis by condensation of spermidine with dcSAM in the presence of spermine synthase (SPE4). MTA molecule further releases the adenine and methionine molecule to be cycled back to purine synthesis and methionine cycle, respectively. This recycling itself takes place in a series of six steps. In the first step, the phosphate group of an inorganic phosphate gets incorporated into MTA with the help of MTA phosphorylase (MEU1), resulting in the production of methylthioribose-1-phosphate (MTR). In the successive step, methylthioribose-1-phosphate isomerase (MRI1) carries out isomerisation of MTR and forms methylthioribulose-1-phosphate (MTRu-1P). Isomerisation is followed by a dehydration step catalysed by methylthioribulose-1-phosphate dehydratase (MDE1), which yields 2,3-Diketomethiopentane-1-phosphate (DK-MTP-1P). UTR4p, encoding an enolase/phosphatase, facilitates the de-phosphorylation and an alkene formation from DK-MTP-1P, which produces 1,2-dihydroxy 3-ketomethiopentene (DHK-MTPene). In the penultimate step of the MTA pathway, a dioxygenase (ADI1) catalyses the transfer of an oxygen molecule to DHK-MTPene and

generates 4-methylthio-2-oxobutyrate (MTOB). In the final step, methionine is regenerated from MTOB by transfer of amino group to a variety of amino acids (branched chain amino acid and/or aromatic amino acid). Based on the substrate involved, different enzymes might catalyse these transamination reactions.

1.2.2.2. SAM

SAM is one of the critical metabolite of the methionine cycle. It is one of the most abundant cofactors used in metabolic reactions (second only to ATP). It serves as the primary methyl donor for various substrate-specific methyltransferases that enables the methylation of DNA, RNA, and proteins, and these can have profound metabolic consequences in the cell.

The sulphur atom of methionine is activated by the transfer of an ATP molecule resulting in the formation of SAM (Figure 1.2). This is an irreversible reaction and is catalysed by S-adenosyl methionine synthetase. In yeast, there are two isoforms of S-adenosyl methionine synthetases, SAM1 and SAM2. The specific function of these two isoforms has not been assigned in yeast. However, the SAM2 gene has been reported to exhibit increased expression during the exponential phase of growth, resulting in increased SAM production (Thomas et al., 1991).

Transmethylation reactions are the major consumer of SAM. Recent studies in yeast have reported phosphatidylethanolamine (PE) methylation and histone modifications as the major SAM consumer (Ye et al., 2017). SAM is also metabolized through the methionine salvage pathway, wherein SAM is first decarboxylated and then recycled with the release of methionine, adenosine, and polyamines (Figure 1.2) (Murin et al., 2017).

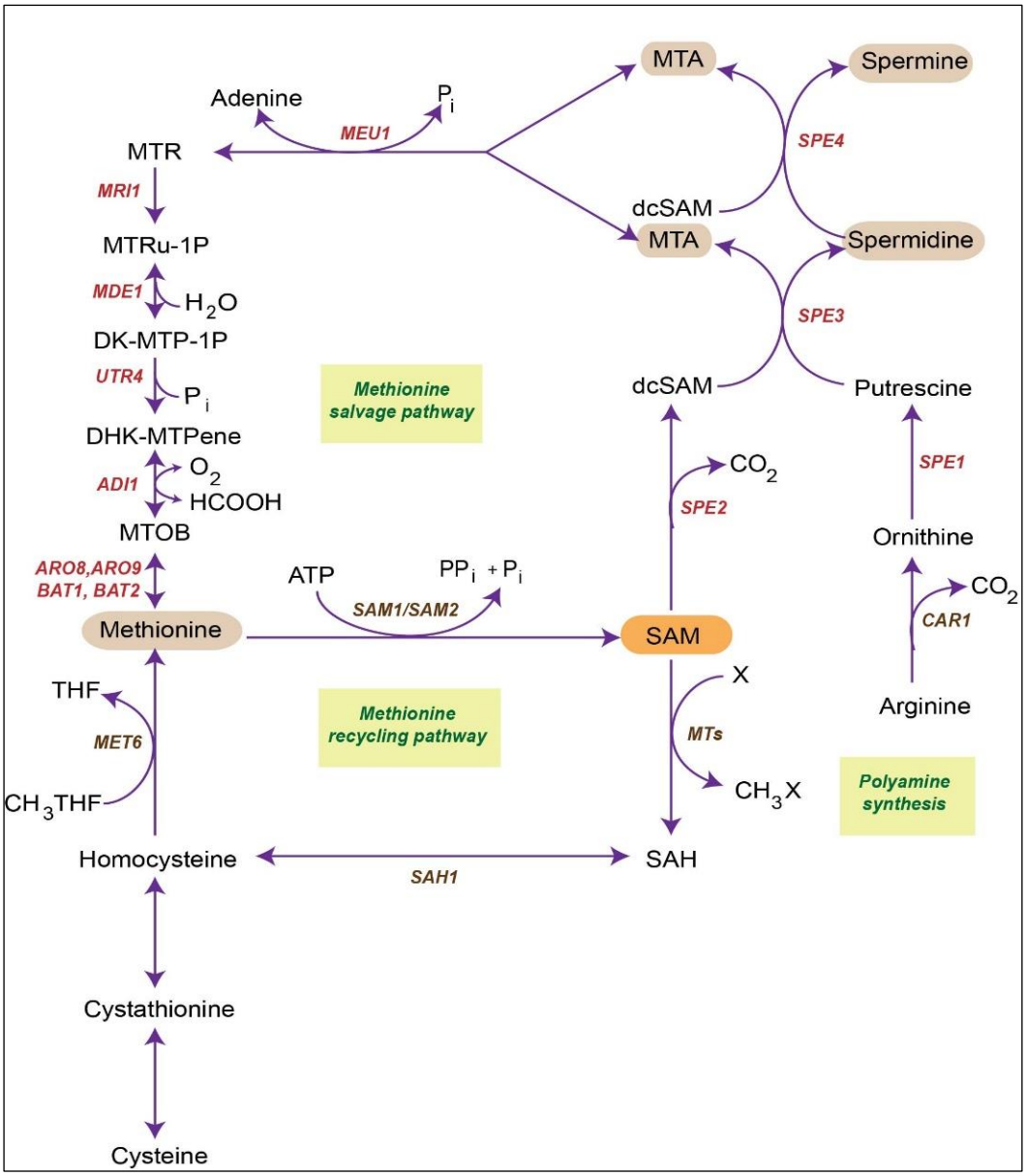

Figure 1.6 Metabolic fate of SAM.

SAM can be catabolized through two alternative routes- methionine cycle or methionine salvage pathway. In both cases, methionine is recycled as a by-product. MET6-Methionine synthase; SAM1/2-S-adenosyl methionine synthetase; MTs-Methyl transferase; SAH1-S-adenosylhomocysteine hydrolase; CAR1-Arginase; SPE1-Ornithine decarboxylase; SPE2-S-adenosyl methionine decarboxylase; SPE3-Spermidine synthase; SPE4-Spermine synthase; MEU1-S-methyl-5'-thioadenosine phosphorylase; MRI1-Methylthioribose-1-phosphate isomerase; MDE1-Methyl thioribulose-1-phosphate dehydratase; UTR4-Enolase phosphatase E1; ADI1-1,2-dihydroxy-3-keto-5-methylthiopentene dioxygenase; ARO8/9-Aromatic aminotransferase 1/2; BAT1/2-Branched chain amino acid transferase 1/2.

1.2.2.3. SAH

S-Adenosyl homocysteine (SAH) is the metabolic precursor of homocysteine and a potent inhibitor of cellular methylation reactions. It is formed by demethylation of SAM, a reaction catalysed by several different types of methyltransferases. SAH gets hydrolyzed to homocysteine and adenosine by the enzyme S-adenosyl homocysteine hydrolase encoded by SAH1. While the reaction catalysed by this enzyme is reversible, the equilibrium favors the synthesis of SAH (Figure 1.2). As a result, the removal of the hydrolysis product homocysteine is crucial for the continuous operation of the cycle. This is achieved by the efficient conversion of homocysteine to methionine via methionine synthase.

1.2.2.4. Homocysteine

Yeast, unlike mammals, can carry out de novo synthesis of homocysteine from inorganic sulphate (Figure 1.2). The majority of the homocysteine pool in a yeast cell is the product of the O-acetyl homoserine sulfhydrylase reaction. This is the only reaction that allows the incorporation of inorganic sulfur (S^{2-}) in *S. cerevisiae* and is catalysed by O-acetyl homoserine sulfhydrylase enzyme encoded by the product of MET15 (Figure 1.2). Besides this *denovo* synthesis, homocysteine can also be formed by the hydrolysis of SAH. The transsulfuration pathway is another source for homocysteine synthesis. This is the pathway from cysteine to homocysteine. The hydrolysis of the intermediate, cystathionine, is carried out by the gene product of STR3, i.e., Cystathionine β lyase, to yield homocysteine (Figure 1.7D).

Homocysteine is present at the junction of the folate cycle, methionine cycle, and transsulfuration pathway. It has three alternative metabolic fates (Figure 1.2). It can be re-methylated to form methionine, or it can get condensed with serine to form cystathionine with the help of cystathionine β synthase (STR4) (Figure 1.7A), or it can revert back to SAH via SAH hydrolase reaction (Finkelstein & Martin, 1986).

1.2.3. Transsulfuration pathway

The transsulfuration pathway consists of reactions that involve the interconversion of homocysteine to cysteine (reverse transsulfuration) and cysteine to homocysteine (forward transsulfuration) via the intermediate formation of cystathionine (Figure 1.7) (Steegborn et al., 1999; Thomas & Surdin-Kerjan, 1997). In enteric bacteria, cysteine to homocysteine conversions is the only means of the transsulfuration pathway. In contrast, mammals possess only homocysteine to cysteine conversions. However, in yeast, both the transsulfuration pathways are present and involve two different sets of enzymes. In prokaryotes, fungi, and plants, the pathway can operate in the reverse orientation to synthesize methionine from cysteine and was initially termed as transsulfuration pathway, whereas in mammals, it was designated as reverse transsulfuration pathway (Steegborn et al., 1999). Here, for convenience sake, I would use the term transsulfuration pathway to describe the conversion of homocysteine to cysteine.

1.2.3.1. Cystathionine to Homocysteine conversion & Homocysteine to Cystathionine conversion

Cystathionine is a modified sulfur-based amino-acid that plays a key role in the synthesis of cysteine. It is a lesser reactive thiol due to the absence of a free thiol group. Previous reports have indicated increased levels of cystathionine in yeast cells upon exposure to cysteine overload (Deshpande et al., 2017).

In *S. cerevisiae*, cystathionine-β-synthase (CBS; STR4) and cystathionine-γ-synthase (CGS; STR2) are the enzymes that are responsible for cystathionine synthesis (Figure 1.7C). STR4 catalyses cystathionine synthesis by β-addition reaction, which involves the condensation of homocysteine and serine moiety. On the other hand, STR2 catalyses the formation of cystathionine from O-succinyl-homoserine and cysteine via a γ-replacement reaction.

Similar to cystathionine anabolism, its breakdown is also an enzyme driven process which is performed by another set of enzymes participating in transsulfuration reactions (Figure 1.7B&D). STR1 encoding cystathionine-γ-lyase (CGL) catalyses the hydrolysis of cystathionine resulting in the release of a cysteine molecule. Additionally, cystathionine can also be hydrolysed by cystathionine-β-lyase (CBL; STR3), which recycles a homocysteine molecule.

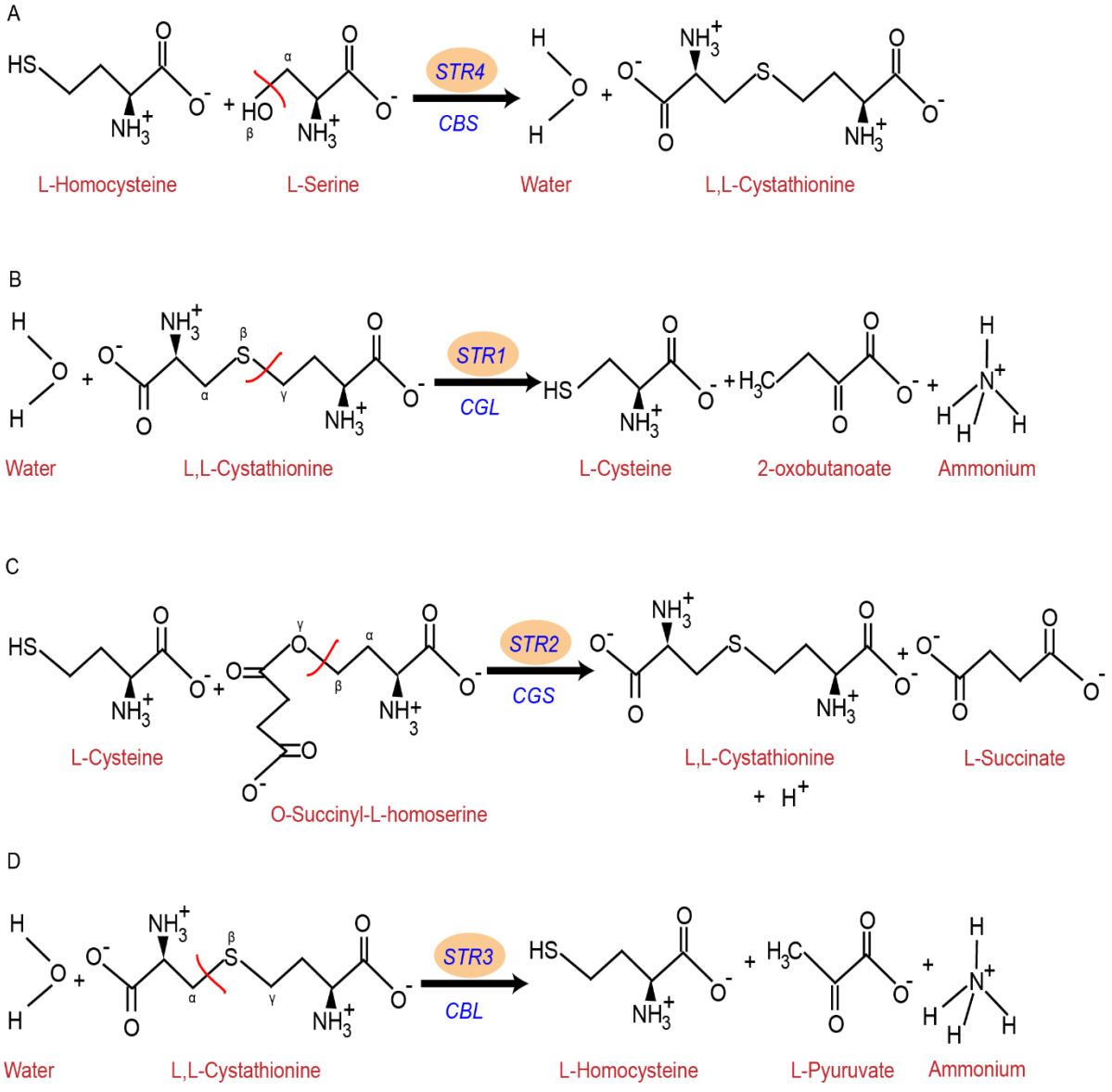

Figure 1.7 Transsulfuration pathways in yeast.
Transsulfuration pathways involve interconversion of homocysteine to cysteine and vice-versa via the formation of an intermediate, cystathionine. CBS (STR4)-Cystathionine-β-synthase; CGL (STR1)-Cystathionine-γ-lyase; CGS (STR2)-Cystathionine-γ-synthase; CBL (STR3)-Cystathionine-β-lyase.

1.2.3.2. Cysteine to Cystathionine conversion & Cystathionine to cysteine conversion

Cysteine is a highly reactive thiol-containing amino acid. At steady-state intracellular pools of cysteine are maintained at a lower concentration than other amino acids (Laxman et al., 2013). Cysteine is synthesized from homocysteine via the formation of cystathionine, and the final step is catalysed by STR1 (Figure 1.7B). While *S. cerevisiae* assimilates inorganic sulfate with homocysteine formation, some fungi can also assimilate sulfate to form cysteine.

Cysteine degradative mechanism present in yeast is shared among bacteria and other eukaryotes, including mammals. Cysteine desulfidase (IRC7) acts on cysteine, which gets converted to 2-aminoprop-2-enoate, releasing hydrogen sulphide as a by-product. In the final step of cysteine degradation, 2-aminoprop-2-enoate spontaneously forms pyruvate and ammonium. Glutathione biosynthesis is where the bulk of cysteine is utilized (in addition to protein synthesis).

1.2.3.3. Glutathione

Glutathione, a tripeptide composed of glutamate, cysteine, and glycine is one of the major redox regulating system in yeast. It is a highly abundant thiol in yeast cells with concentrations up to 10mM. Although glutathione is not truly a part of the transsulfuration pathway yet, we would discuss it as a part of this thesis being a critical sulfur metabolite.

Two ATP dependant enzymes, glutamate cysteine ligase (GCL; GSH1) and glutathione synthase (GS; GSH2) are involved in the cytosolic, non-ribosomal synthesis of this unusual tripeptide. In the first step, GCL catalyses the formation of γ-glutamylcysteine from glutamate and cysteine, and it is the rate-determining step of glutathione biosynthesis. The second step includes the ligation of γ-glutamylcysteine to glycine in another ATP dependent reaction to yield γ-glutamylcysteineglycine or glutathione. These two reactions (Figure 1.8A) are a part of γ-glutamyl cycle, which was proposed by Meister.

After the formation of glutathione, it can be degraded into 5-oxoproline and cysteinyl glycine by the action of cytoplasmic ChaC family of γ-Glutamate cyclotransferases (γ-GCTs; GCG1). The products, 5-oxoproline, and cysteinyl glycine can be further broken down to yield glutamate, and cysteine and glycine, respectively (Kumar et al., 2012). For these cleavages to take place, 5-oxoprolinase must react with 5-oxoproline and cysteinyl glycine with cys-gly peptidases. Additionally, glutathione is also acted upon by a second yeast glutathione degrading enzyme, Dug2p/Dug3p. This pathway is exclusive to yeast and fungi. The enzyme is found in the cytosol, which belongs to the N-terminal nucleophilic hydrolases, and it cleaves glutathione to give glutamate and cys-gly (Ganguli et al., 2007; Kaur et al., 2012). In yeast, cytoplasmic Dug1p that belongs to the M20A family, is the chief cys-gly peptidase (Kaur et al., 2009).

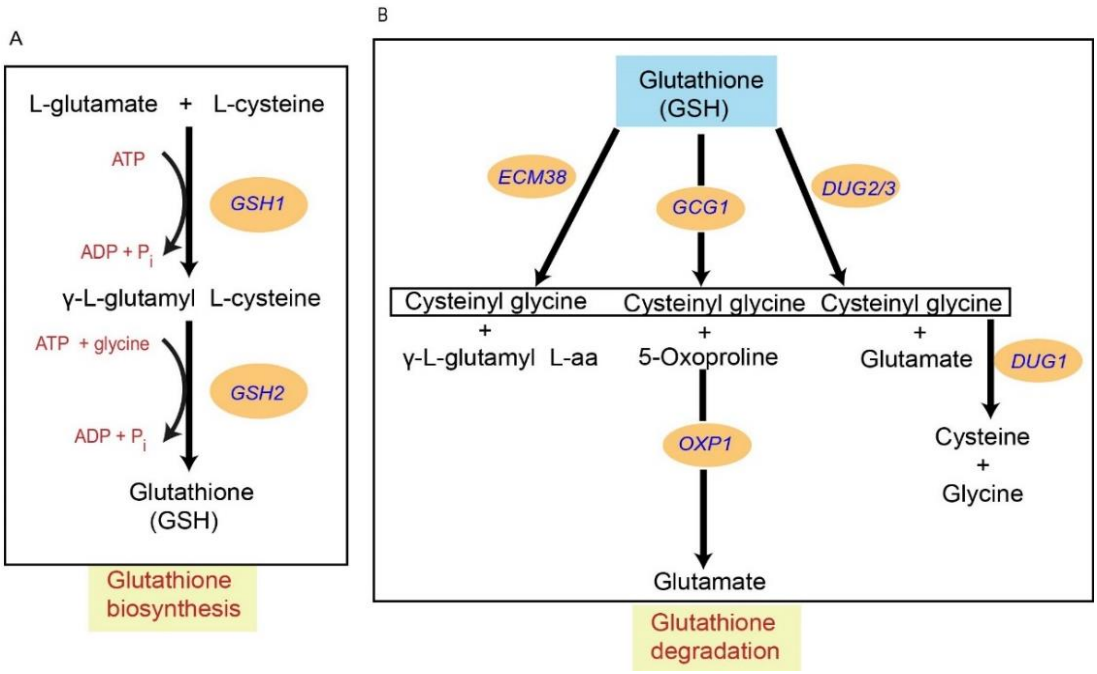

Figure 1.8 Metabolism of GSH in yeast.
(A) Anabolism of GSH is an energy-intensive process catalysed enzymatically and occurs in two steps. (B) GSH degradation pathways. GSH1-Glutamate cysteine ligase; GSH2-Glutathione synthetase; ECM38-Glutathione hydrolase proenzyme; GCG1-Glutathione specific-γ-glutamyl cyclotransferase; OXP1-5-Oxoprolinase; DUG1-Cys-gly metallodipeptidase; DUG2-Probable di-tripeptidase; DUG3-Probable glutamine amidotransferase.

1.3. Physiological role of one-carbon metabolism

The redistribution of 1C-groups through folate and methionine cycles of one-carbon metabolism results in the biosynthesis of numerous compounds of importance, including nucleotides, several amino acids, SAM and GSH molecules. The cofactors generated through one-carbon metabolism pathways produce both purine and pyrimidine (thymidylate) nucleotides. An abundant supply of nucleotides is required for the maintenance of cellular growth, replication of the genome, and transcription of genetic material. Apart from their function as an energy source, nucleotides are also important for cell transduction pathways and as the donor of the phosphate group in phosphorylation reactions.

Due to the integration of several critical metabolic pathways, one-carbon metabolism serves as an important cellular nutrient sensor. Hence, the nutritional status of the cell differentially affects the fate of these metabolic pathways in order to maintain the overall metabolic homeostasis. However, in several diseased conditions, the amino acid homeostasis gets disturbed (DeBerardinis, 2011; Hoffman & Erbe, 1976; Locasale, 2013; Yang & Vousden, 2016). Studies investigating cross-talk between metabolism and epigenome highlights the specific contribution of one-carbon metabolism dependant DNA methylation towards the long term development of individuals (Clare et al., 2019; Dominguez-Salas et al., 2014; Mentch et al., 2015; K. D. Sinclair et al., 2007; Waterland et al., 2010). In addition to alteration of epigenetic status of the cell, SAM generated during the methionine cycle has been reported to have biosynthetic roles in the generation of phospholipids as a result of methylation reactions. More recently, epigenetic mechanisms have been suggested to affect embryonic development in animal models (Wu et al., 2019).

1.4. Regulation of one-carbon metabolism

One carbon group performs several essential functions by providing critical metabolic intermediates involved in the synthesis of DNA, certain amino acids, SAM, phospholipids,

polyamines, and creatinine. Due to its role in such varied cellular processes, the flux of one-carbon units among these different pathways requires tight regulation. Depending on the nutritional state of the cell or the abundance of any one of the intermediates of one-carbon metabolism, the methyl group of one-carbon units is distributed among its canonical pathways: purine synthesis, thymidylate synthesis, and methylation reactions. In addition to this canonical role, one-carbon units are also required for maintaining the amino acid homeostasis. Despite the critical role of regulation of one-carbon metabolism, it has not yet been extensively studied.

The earliest report regarding the regulation of folate and methionine metabolism dates back to the 1970s, where Tyler et al. suggest an indirect increase in formyltetrahydrofolate dehydrogenase (a key enzyme of one-carbon metabolism) activity by cellular methionine concentrations (Krebs et al., 1976). Another study regarding the regulation of the balance of one-carbon metabolism conducted in yeast has indicated the role of glycine or folate limitation in controlling the partitioning of one-carbon units among the purine synthesis or methylation reactions (Piper et al., 2000). In plants (*Arabidopsis thaliana*), cleavage of the N-terminal regulatory domain of Cystathionine-γ-synthase (CGS) has been implicated to play a role in the regulation of one-carbon metabolism under folate starvation conditions (Loizeau et al., 2007). Additionally, one-carbon metabolism is also known to be allosterically controlled by SAM. SAM and 5-CH_3THF, the product of MTHFR, have been well established as an allosteric inhibitor of mammalian Methylenetetrahydrofolate reductase (MTHFR) (Kutzbach & Stokstad, 1971) and Glycine-N-Methyl transferase (GNMT), respectively (Luka et al., 2009). Inhibition of both these enzymes prevents the flux of folates towards the methylation reactions. The regulation of the former enzyme has been discussed extensively in the sections below.

1.5. MTHFR a key enzyme of one-carbon metabolism

Methylenetetrahydrofolate reductase (MTHFR), a cytosolic flavoenzyme, is found at a critical branch point in one-carbon metabolism (Figure 1.2). As a part of the folate cycle, MTHFR

catalyses the physiologically irreversible reduction of 5,10-methylenetetrahydrofolate (5,10-CH_2THF) to 5-methyl tetrahydrofolate (5-CH_3THF). This is a two-step reaction in which reducing equivalents are transferred from NADPH to the cofactor FAD, which is non-covalently bound to the enzyme (Sheppard et al., 1999), and then passed on to 5,10-CH_2THF forming 5-CH_3THF (Figure 1.9). In contrast to certain eukaryotes (yeast and mammals) (Matthews & Daubner, 1982; Roje et al., 2002) which utilize NADPH as the reducing source, prokaryotes (Sheppard et al., 1999) and plants (Roje et al., 1999) use NADH as the reducing equivalent in the first step of reduction. CH_3THF, the product of the MTHFR reaction, is exclusively used by methionine synthase, and the demethylated form of folate (THF) gets recycled back to the folate cycle (Figure 1.2). Hence, MTHFR commits THF-bound one-carbon units to the methionine cycle. Within the methionine cycle, the methylation of homocysteine to methionine yields an essential amino acid. MTHFR competes for tetrahydrofolate bound one-carbon units with thymidylate synthase (TMP1) and with the AICAR/ATIC (ADE17) and GAR (ADE8) transformylases, which catalyse the incorporation of one-carbon units into uridine monophosphate and the nascent purine ring system, respectively (Matthews & Daubner, 1982). Therefore, it forms a key regulatory node of the one-carbon metabolism, controlling the folates' entry into the methionine cycle. This flux of folates towards the methionine cycle is regulated by allosteric inhibition of MTHFR by S-adenosyl methionine (SAM). As a result of this, MTHFR allows the maintenance of the balance between folates utilized for DNA synthesis and methionine biosynthesis.

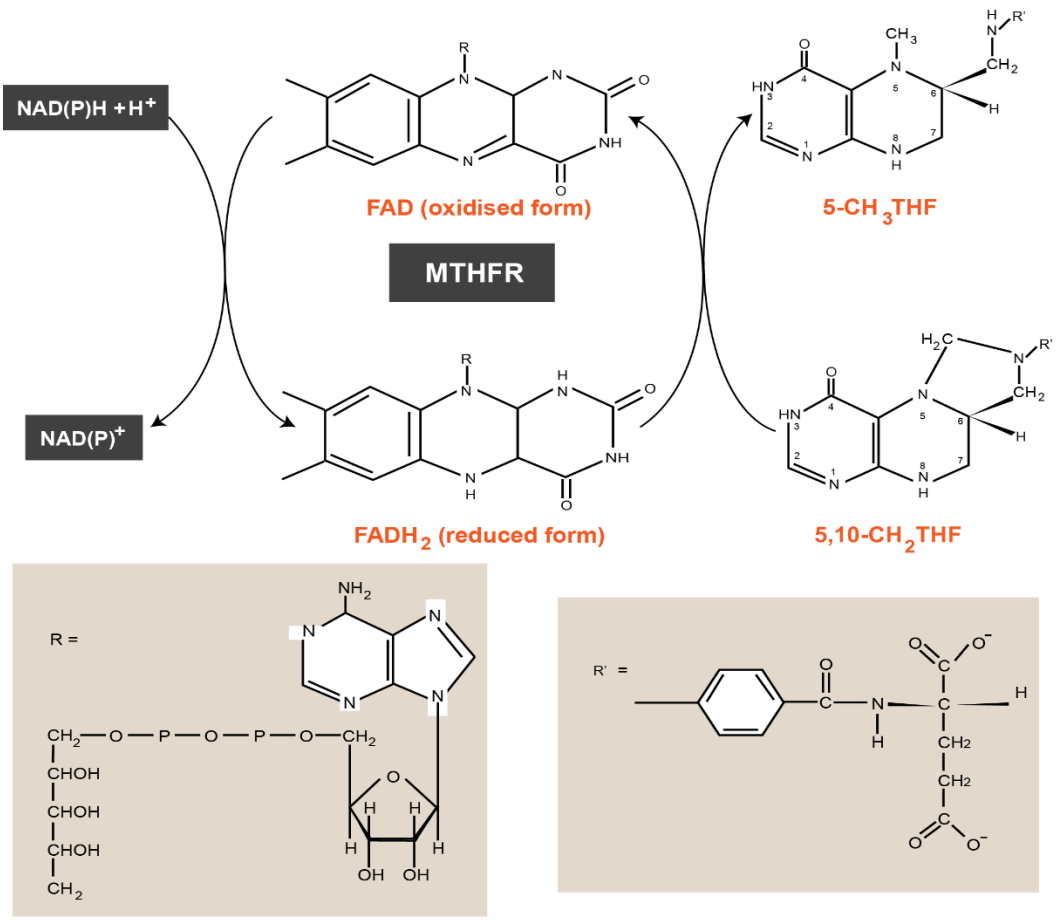

Figure 1.9 Biochemical reaction of MTHFR.
MTHFR is a flavoprotein that obtains reducing equivalents from NADPH. FAD bound to the enzyme then transfers the protons and electrons to the substrate- CH_2THF to synthesize CH_3THF.

1.5.1. Role of MTHFR in folate and methionine metabolism

Besides controlling the partitioning of folates between nucleotide biosynthesis and methionine synthesis, MTHFR in humans plays a critical role in maintaining the plasma homocysteine levels. Even though homocysteine is not a substrate for MTHFR, yet through its product, i.e., CH_3THF, the levels of homocysteine are significantly determined in the cell by the action of methionine synthase, which transfers a methyl group to homocysteine to produce methionine. Even a mild deficiency of MTHFR activity results in an elevated concentration of homocysteine in the blood, causing the condition hyperhomocysteinemia. Elevated levels of homocysteine have been implicated as an independent risk factor for cardiovascular diseases. Increased homocysteine levels have also been associated with several diseases and clinical

conditions like fetal neural tube defects (Mills et al., 1995), Alzheimer's disease (McCaddon et al., 1998), end-stage renal disease (van Guldener & Stehouwer, 2003), schizophrenia (Applebaum et al., 2004), and non-insulin-dependent diabetes (de Luis et al., 2005). Therefore, MTHFR is one of the crucial enzymes influencing homocysteine levels.

MTHFR generates methionine, which is an essential amino acid in humans. It can be used either in protein synthesis or converted to S-adenosyl methionine (SAM), the major methyl donor in the cell. SAM methylates various substrates like DNA, RNA, proteins, lipids, and several small molecule metabolites and itself gets converted to S-adenosyl homocysteine (SAH). Intracellular SAM/SAH ratios also have a regulatory role in controlling the activities of several SAM-dependent methyltransferases. SAM, other than being a methyl donor, is also involved in the production of spermine and spermidine, polyamines that affect cell division and proliferation (Figure 1.1, 1.2 & 1.6) (Fontecave et al., 2004). Clearly, due to its role in methionine synthesis, MTHFR is indispensable for all these critical metabolic processes in the cell.

1.5.2. Domain organization and structural differences of MTHFR among prokaryotes and eukaryotes

Yeast MTHFR, encoded by the MET13 gene, is a 600 amino-acid protein bearing two domains, catalytic domain, and regulatory domain, which are separated by a small linker region (Figure 1.10). The N-terminal catalytic domain, which is roughly 300 amino-acid long, is conserved across evolution. However, an equally large regulatory domain exists only in the eukaryotic MTHFR enzyme (Figure 1.10). The negative feedback regulation of the MTHFR is known to occur by binding of SAM to this C-terminal regulatory domain (Goyette et al., 1994; Matthews & Daubner, 1982; Sumner, Jencks, Khani, & Matthews, 1986). Besides these two domains, mammalian MTHFR protein has been shown to have an additional 35 amino acid serine-rich region at the very N-terminal end, which is not found in MTHFR orthologs of bacteria, yeast,

and even lower animals (Figure 1.10) (Yamada et al., 2005). This region has been reported to be involved in another level of regulation of this protein via substrate-level phosphorylation. A detailed account of the regulation of MTHFR is provided in the next section. Additionally, mammalian MTHFR (human) exists in two isoforms- 70kDa and 77kDa. However, the functional significance of these two distinct isoforms is not clear.

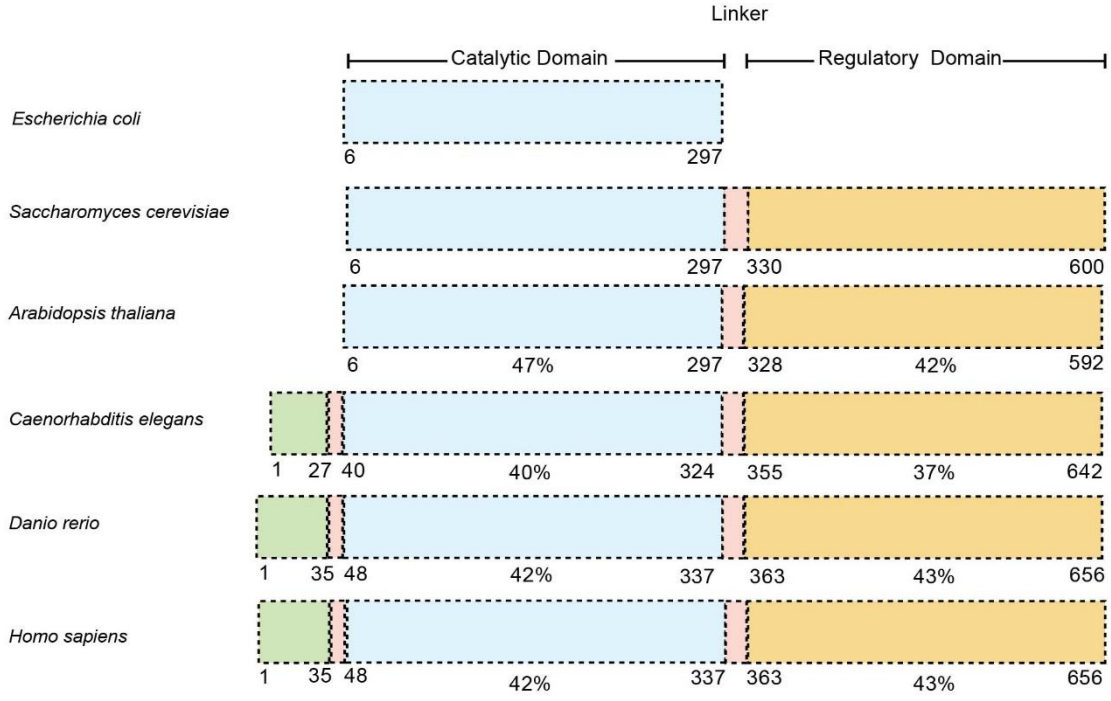

Figure 1.10 Schematic representation of MTHFR domain organization across evolution. Prokaryotic MTHFR is composed of the only single catalytic domain represented here in blue, whereas eukaryotic MTHFR consists of two domains: N-terminal catalytic domain and C-terminal regulatory domain represented in yellow separated by a small linker region (shown here in pink). Higher eukaryotes contain an additional serine-rich stretch of approximately 40 amino acids.

The catalytic domain of MTHFR adopts a TIM-barrel ($\beta_8\alpha_8$) structure, which has been evolutionarily conserved across all kingdoms (Figure 1.11). These structures have revealed residues critical for the binding of cofactor FAD (Guenther et al., 1999), the electron donor NADPH (NADH (Pejchal et al., 2005) in bacteria), and the product CH_3THF (M. N. Lee et al., 2009; Pejchal et al., 2005). In the case of humans, the catalytic domain has three additional helices apart from the TIM-barrel (Figure 1.12) (Froese et al., 2018). The insights regarding

the crystal structure of the regulatory domain have been recently reported from studies performed with a slightly truncated version (37 residues at the N-terminal end and 12 residues at the C-terminal end were truncated) of human MTHFR protein (Figure 1.12 and 1.13) (Froese et al., 2018). The regulatory domain at the C-terminal end forms a novel fold that consists of two-five stranded β-sheets arranged side-by-side in the core, surrounded by several α-helices. There is no direct contact between the two domains in the crystal structure, and rather they are simply connected by an extended linker region (Figure 1.13). The linker region, composed of three β-turns, makes multiple contacts with both catalytic and regulatory domains by taking turns twice.

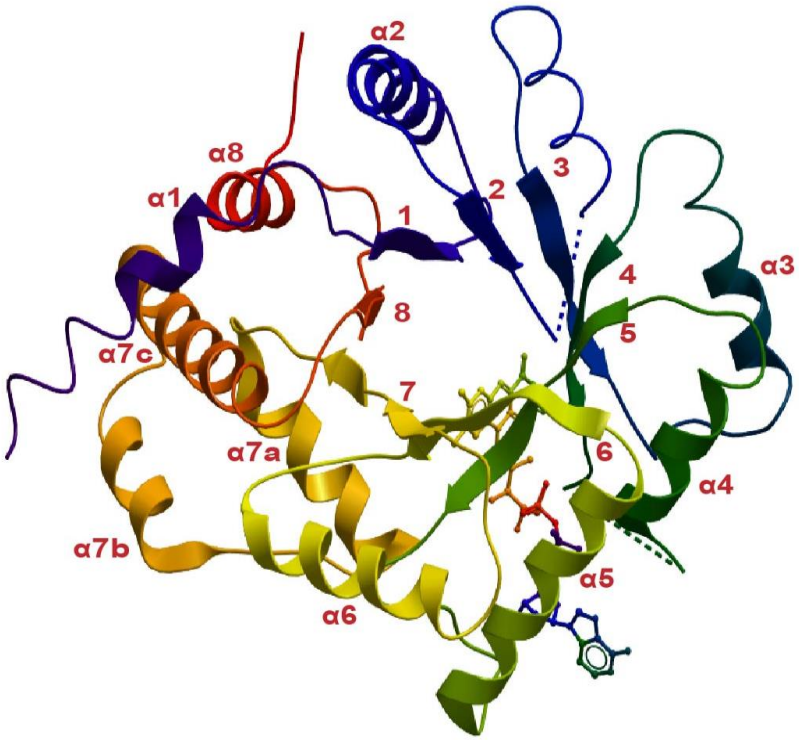

Figure 1.11 Structure of *E. coli* MTHFR.

TIM barrel structure of the catalytic domain of *E. coli* MTHFR (PDB ID: 1zpt). View along the axis of the $\beta_8\alpha_8$ barrel looking toward the N-terminal ends of the β–strands. FAD is drawn in ball-and-stick mode. The image was created using the ICM browser (www.molsoft.com).

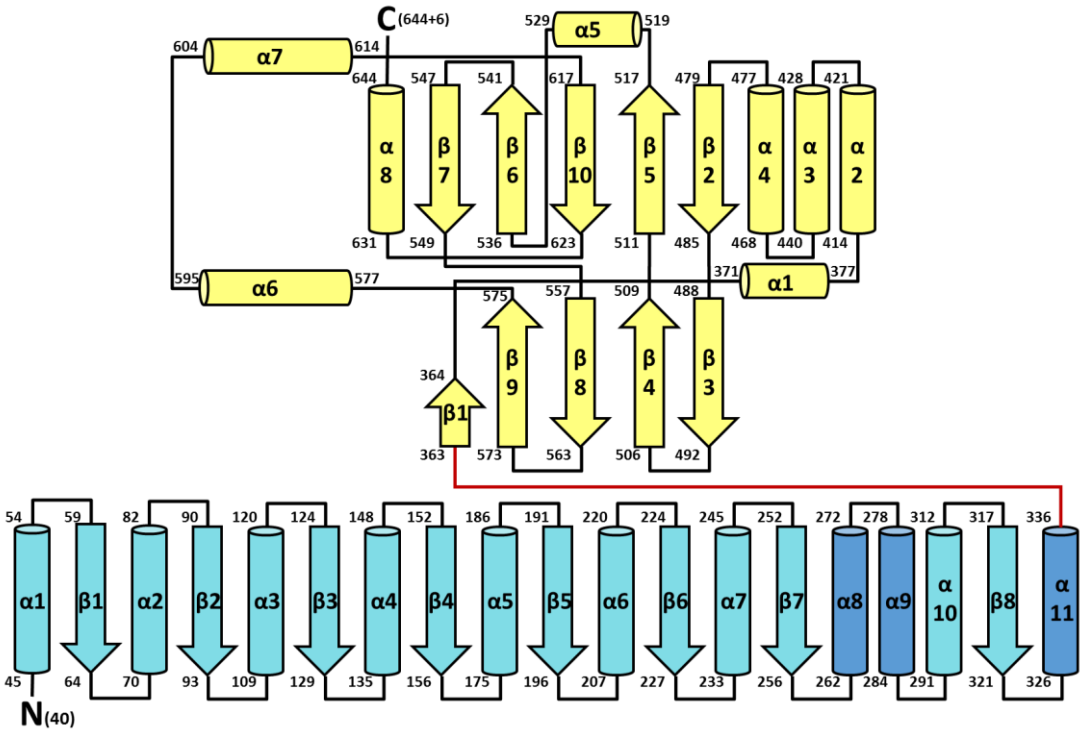

Figure 1.12 Topology diagram of Human MTHFR (HsMTHFR)

Schematic representation of the secondary structures present in the catalytic and regulatory domain of HsMTHFR. Numbers are given to indicate amino acids at the N-terminus (40) and C-terminus (644+6 – including six residues incorporated from the vector) of the structure, as well as the beginning and end of each secondary structure element. Catalytic domain in cyan, the linker in red, and the regulatory domain in yellow. α-helices are shown as cylinders and β-sheets as arrows. α8, α9, and α11 are coloured a darker blue to indicate that they are not part of the $(\alpha/\beta)_8$ barrel. (Figure adapted from Yue et al., Nature Metabolism 2018)

E. coli MTHFR forms a tetramer of the four catalytic subunits (Guenther et al., 1999), whereas *Thermus thermophilus*, another MTHFR protein of bacterial origin, adapts a dimeric configuration composed of catalytic domain only (Figure 1.14A-B) (Igari et al., 2011).

Human MTHFR exists as a homodimer, and within these homodimers, each of the two catalytic domains is presented away from the interface of the dimer (Figure 1.14C) (Froese et al., 2018). Moreover, the active sites are also at the opposite ends of the overall elongated shape and face away from each other. In this arrangement, catalytic domains are not involved in forming the higher oligomer, unlike the bacterial MTHFR proteins. Rather, the regulatory domains of each protomer mediate dimerization for human MTHFR (Figure 1.13 & 1.14C).

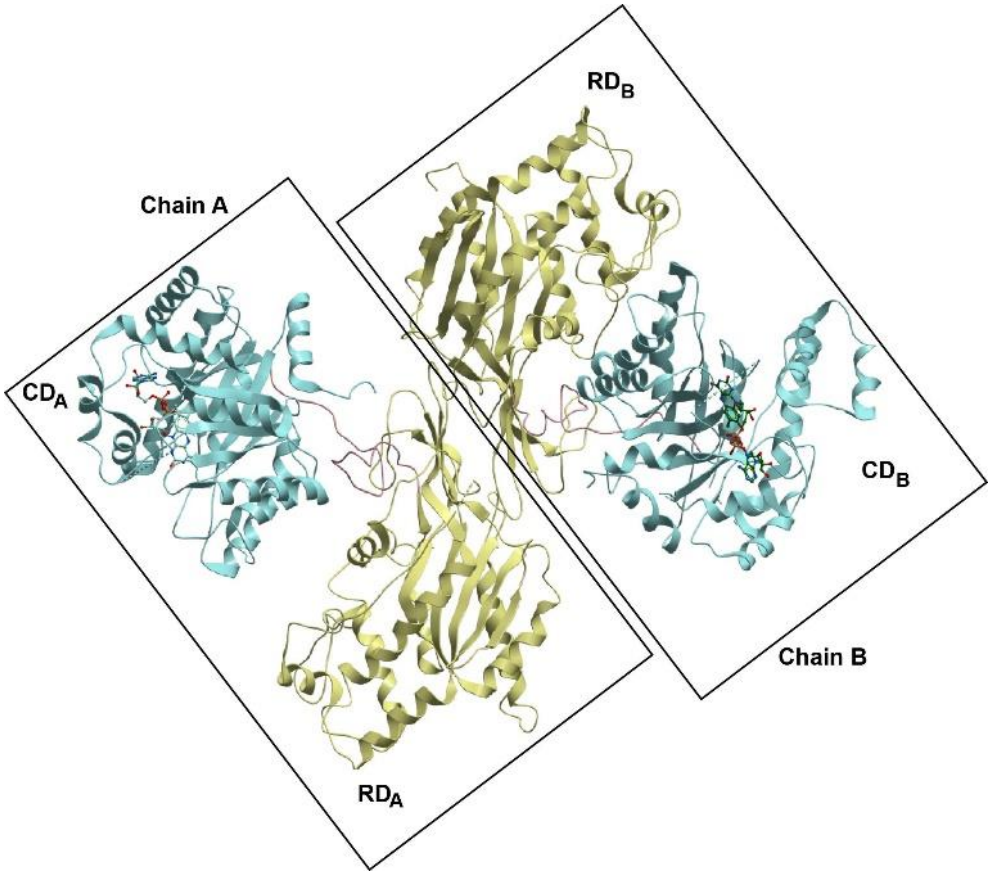

Figure 1.13 Structural Overview of HsMTHFR

Homodimer of HsMTHFR as seen in the crystal. Chain A and Chain B represent the two monomers. The catalytic domain (shown in cyan) and regulatory domain (shown in yellow) of each monomer lacks direct contact with each other; rather, they are connected by a small linker region (shown in pink). FAD required for catalysis (shown in ball and sticks) is present at the far, opposing end in the catalytic domain of each monomer. Two monomers are held together by interactions through the regulatory domain. CD_A and $CD_{B:}$ Catalytic domain of chain A and B; RD_A and $RD_{B:}$ Regulatory domain of chain A and B. The image was created using the ICM browser (www.molsoft.com).

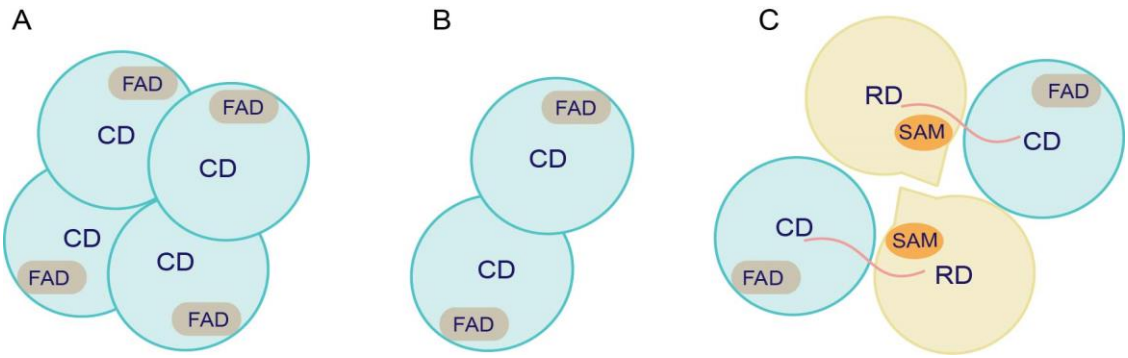

Figure 1.14 Schematic comparison of oligomer arrangement of MTHFR orthologs.

Higher oligomer states of different MTHFR orthologs (A) *E. coli* MTHFR (PDB ID: 1ZPT) forms a homotetramer (B) *T. thermophilus* MTHFR (PDB ID: 3APY) adopts a homodimer configuration (C) *H. sapiens* MTHFR (PDB ID: 6FCX) also arranges as a homodimer. Oligomers of prokaryotic MTHFR (*E.coli* and *T. thermophilus*) comprises exclusively of the catalytic domain, whereas in eukaryotes (humans), each protomer is composed of a catalytic domain and a regulatory domain. FAD is present at the far, opposing end in the catalytic domain of each monomer. SAM binds at the N-terminal end of the regulatory domain. Two monomers of HsMTHFR are held together by interactions through the regulatory domain. The catalytic domain (shown in cyan), regulatory domain (shown in yellow) of each monomer, and a small linker region (shown in pink). CD: Catalytic domain; RD: Regulatory domain.

1.5.3. Regulation of MTHFR

Despite the occurrence of differences in the structure and domain organization of prokaryotic and eukaryotic MTHFR, they seem to share similarities in their mode of regulation. Both bacterial and eukaryotic MTHFR exhibit SAM mediated repression; however, there are variations in these mechanisms of regulation. These changes in regulatory mechanisms are highlighted in the section below.

1.5.3.1. Transcriptional regulation of MTHFR in prokaryotes

Bacterial MTHFR encoded by *metF* gene in *E. coli* is a member of the methionine regulon. Methionine regulon proteins have been shown to exhibit repression in the presence of methionine with the help of a regulatory protein-MetJ. Being a part of methionine regulon, *metF* is under the negative transcriptional regulation of MetJ, a repressor protein. There are two known mechanisms of *metJ* mediated transcriptional repression, one that takes place in the presence of SAM in the medium (Greene et al., 1973; Greene et al., 1970) and another one

resulting from the occurrence of the vitamin B_{12} in the growth medium (Kung et al., 1972). Biochemical and genetic studies have discovered a significant reduction in *metF* expression at higher levels of MetJ protein alone (Shoeman et al., 1985). However, SAM at concentrations greater than 10µM acts as a co-repressor at lower cellular MetJ concentrations (Shoeman et al., 1985). Additionally, studies with *Salmonella typhimurium metF* protein have revealed the role of another protein MetR, an activator protein, in the transcriptional regulation of *metF* gene product. Mutational analysis of strains lacking metR protein have suggested MetR antagonizes MetJ mediated transcriptional repression (Cowan et al., 1993).

1.5.3.2. Transcriptional regulation of eukaryotic MTHFR

Transcriptional regulation of eukaryotic sulphur metabolic network genes has been extensively studied in budding yeast, *S. cerevisiae*. In yeast, proteins involved in the synthesis of sulphur-containing amino acids are encoded by genes belonging to MET regulon. Transcription of the MET regulon member proteins is either repressed or induced depending on the sulphur status of the cell. The identity of the metabolite that senses and controls the MET regulon remains elusive majorly due to the lack of explanation regarding the role of SAM and other metabolites in this regulation. However, recent reports have suggested intracellular cysteine as the major regulatory signal for the MET gene expression (Hansen & Johannesen, 2000).

Sulphur metabolism genes are transcriptionally regulated by Met4 (T. A. Lee et al., 2010; Thomas & Surdin-Kerjan, 1997). Met4 despite having the DNA binding domain of basic leucine zipper family at the C-terminal end, lacks DNA binding activity. Hence, it relies on interactions with proteins called Met4 cofactors for transcriptional activation of specific genes. Met4 cofactors can be divided into two categories based on their function: (1) DNA binding cofactors (Met31/Met32 and Cbf1) that aid in recruiting Met4 protein on the appropriate promoters and (2) Stabilizing cofactor (Met28), which plays a role in stabilizing the DNA-bound Met4 complex (Blaiseau & Thomas, 1998; Kuras et al., 1997). Met31 and Met32 are

highly similar zinc-finger proteins that can individually bind to Met31/ Met32 cis-regulatory element (with the consensus sequence of AAACTGTGGC), whereas Cbf1 is a basic helix-loop-helix protein that homodimerizes to bind a Cbf1 cis-regulatory element which comprises of a CACGTGA motif (Blaiseau et al., 1997; Blaiseau & Thomas, 1998; Kuras et al., 1997; T. A. Lee et al., 2010; Thomas et al., 1989). Many MET regulon genes have binding sites for both Met31/Met32 and Cbf1 in their promoters, while several genes have binding site(s) for only one or the other. In a recent study, 45 core Met4-dependent promoters were identified, each containing a Met31/Met32-binding site. Furthermore, in 24 of these 45 core Met4-dependent promoters, a Cbf1 motif was present (T. A. Lee et al., 2010). In another independent study, MET13 has been shown to be transcriptionally regulated by Met4 by the use of Met32 as a cofactor (Carrillo et al., 2012).

The transcriptional activation or repression of MET regulon by Met4 depends on the cellular cysteine concentrations and SCF^{Met30}. Met4 is negatively controlled by SCF^{Met30}, a ubiquitin ligase complex composed of Skp1/Cdcd53/F-box protein and Met30. Under cysteine limiting conditions, MET30 dissociates itself from the SCF^{Met30} complex resulting in loss of Met4 ubiquitination, which prevents the proteasomal degradation of Met4 and its cofactors (Barbey et al., 2005; Kuras et al., 2002; Leroy et al., 2006). As a consequence, there is an induction of MET gene expression.

Conversely, during non-repressive conditions, i.e., when cysteine is in abundant supply, SCF^{Met30} ubiquitylates MET4. Polyubiquitylation stabilizes the interaction of MET4 with its cofactors. Furthermore, the Met4-SCF^{Met30}-associated cofactors are polyubiquitylated, which causes their degradation (Ouni et al., 2010), resulting in repression of MET regulon.

1.5.3.3. Post-translational regulation of eukaryotic MTHFR

Allosteric inhibition of the mammalian enzyme by SAM has been suggested by studies of Kutzbach and Stokstad (Kutzbach & Stokstad, 1971). They showed that reactions of MTHFR

are inhibited by SAM, and the addition of SAH along with SAM could partially reverse this inhibition. Besides SAH, heat treatment could also desensitize MTHFR to the inhibitory effect of SAM with only partial loss of catalytic activity (Kutzbach & Stokstad, 1971; Matthews & Baugh, 1980).

Scanning Tunnelling Electron Microscopy (STEM) analysis, limited proteolysis, and photoaffinity labeling experiments have been performed with the porcine MTHFR to investigate the SAM binding region. STEM analysis showed the existence of MTHFR protein as a homodimer with a molecular weight of 77 kDa for each monomer (Matthews et al., 1984). It also demonstrated that an individual monomer is further composed of two subunits containing two globular domains of approximately equal size arranged in a planar rosette. In agreement with these results, limited proteolysis of this protein with trypsin cleaved the 77 kDa fragment into an N-terminal fragment of 40 kDa and a C-terminal fragment of 37 kDa. The catalytic activity of the enzyme was observed despite the proteolysis; however, it was desensitized to inhibition by SAM (Matthews et al., 1984). Further, when this SAM insensitive and partially digested MTHFR was subjected to photolabeling with 8-azido-SAM, the label was incorporated into the C-terminal fragment of 37 kDa. These labelling experiments pointed out the location of the SAM binding site to the C-terminal end of the protein (Jencks & Mathews, 1987). Therefore, these three studies together suggested that the MTHFR protein is made up of two domains – an N terminal domain, which plays a role in catalysis, and a C-terminal domain, responsible for SAM binding and regulation. However, the molecular details of the allosteric regulation were not clearly understood. Early observations by Matthews and co-workers had suggested that MTHFR could exist in active and inactive forms, even in the absence of SAM (Vanoni et al., 1983). Based on these studies, later researchers proposed loss of SAM sensitivity as a consequence of the inability to sufficiently stabilize the inactive state of the enzyme upon breaking it into its constituent domains. SAM mediated inhibition, thus,

seems to require specific interaction between the two domains of the enzyme (Sumner, Jencks, Khani, & Matthews, 1986).

Later photo-affinity labeling of SAM was carried out to find out the SAM binding regions of porcine and human MTHFR (Goyette et al., 1994). These studies had indicated a completely different region of the MTHFR regulatory domain, i.e., within a stretch of about 30 amino acids starting 30 residues after the junction between the two domains (Goyette et al., 1994; Raymond et al., 1999; Roje et al., 2002; Sumner, Jencks, Khani, Matthews, et al., 1986). In particular, a 6kDa region of the protein located at the N-terminal end of the regulatory domain was suggested in these studies to be important for SAM binding (Goyette et al., 1994). More recently, the crystal structure of human MTHFR has been solved, which has provided the first insights into the eukaryotic MTHFR with its large regulatory region (Froese et al., 2018). This structure was obtained using a truncated protein which has deletions, both, at the N and C-terminal ends. Moreover, the crystal structure could be attained only with SAH and not with SAM, the known inhibitor of the MTHFR enzyme. Although SAH is not an inhibitor of MTHFR, the similarity in structure to SAM was used to extract insights regarding residues involved in SAM binding. However, the SAM binding regions on the MTHFR regulatory domain are still not unequivocally recognized. While photo-affinity labelling identified a shorter region in the N-terminal region of the regulatory domain (Goyette et al., 1994), the recent structure of the human MTHFR has suggested a slightly different part of the regulatory region (Froese et al., 2018).

The hypothesis of the existence of the active and inactive state of the enzyme was also supported by the model proposed by Jencks and Matthews (Jencks & Mathews, 1987). This model was used to explain the interactions of MTHFR both with the inhibitor molecule, SAM, as well as the reducing equivalent, NADPH, which is essential for the enzymatic activity (Jencks and Matthews., 1987). According to this model, there are two quaternary states for the

dimeric enzyme, an active R form and an inactive T form, to which the ligands, SAM and NADPH, bind with opposing affinities. The binding of SAM to the R state drastically reduces the latter's affinity for NADPH and marginally increases the rate of interconversion between R and T states. On the other hand, the binding of the R form to NADPH decreases the affinity of the former for SAM (Jencks & Mathews, 1987). In conclusion, this study indicated the alterations in the fractions of active (R) and inactive (T) states as a result of SAM binding to exert an inhibitory effect.

A dual-mode of regulation has been demonstrated for the mammalian MTHFR protein-allosteric inhibition and phosphorylation (Yamada et al., 2005). The earliest studies reporting phosphorylation of the MTHFR enzyme revealed threonine residue at position 34 within the extended N-terminal region of the protein participating in the phosphorylation event (Yamada et al., 2005). However, recently another group has shown multisite phosphorylation (16 in total), increasing the SAM sensitivity and inhibition (Froese et al., 2018). DYRK1A/2 and GSK3A/B have been identified among the kinases as being responsible for the phosphorylation of serine and threonine residues of the MTHFR enzyme (Zheng et al., 2019). Moreover, structural, biophysical, and biochemical data of human MTHFR protein have provided molecular insights into the enzyme regulation by SAM binding and phosphorylation. Structural data of full-length human protein has revealed that the catalytic inhibitory signal is transmitted to the catalytic domain by a long-range conformational change of the linker region, which occurs upon binding of SAH/SAM to the unique fold of regulatory domain (Froese et al., 2018).

1.6. Polymorphisms in human MTHFR and their functional and phenotypic consequences

Mudd et al. were the first who identified a patient with homocystinuria due to a severe deficiency of the MTHFR enzyme (Mudd et al., 1972). In 1988, a thermolabile variant of MTHFR, i.e., C677T, was identified in patients with cardiovascular disease (Kang et al., 1988).

MTHFR polymorphism was the most common inborn error of folate metabolism and has been since then investigated for its association with several multifactorial disorders. The occurrence of MTHFR deficiency is still relatively rare. A little over 100 patients have been estimated to be affected by MTHFR deficiency (Schiff et al., 2011; Watkins & Rosenblatt, 2012). Most of the disease-causing mutations of the MTHFR enzyme are private mutations, i.e., they occur in less than five patients. Besides the disease-causing mutations, there are several SNPs and one/two nucleotide deletion/insertion that are known to occur in the human MTHFR gene (Marini et al., 2008; Martin et al., 2006; Pavlikova et al., 2012). Two of the most common polymorphisms that have been investigated thoroughly are C677T and A1298C, with allele frequency ranging between 24-40% for the former and approximately 33% for the latter (Brattstrom et al., 1998; Hanson et al., 2001; Pavlikova et al., 2012; Winkelmayer et al., 2004). The frequency of these polymorphisms varies depending on the population being studied. Both these polymorphisms result in active enzyme with 45% and 68% residual MTHFR activity as compared to the WT protein. Indeed, some level of correlation has been shown to exist between the severity of symptoms, residual enzyme activity, and the genotype of MTHFR.

1.7. Motivation and objective of the present study

When one looks at the current state of knowledge regarding MTHFR and one-carbon metabolism, one finds that despite the immense importance of both one-carbon metabolism and MTHFR to cellular physiology and metabolism, there are several gaps in our knowledge that stand out:

MTHFR is an extensively studied enzyme, but the focus has been almost on the catalytic domain. We know virtually nothing about the large C-terminal regulatory domain, and this part of MTHFR has almost completely un-investigated.

SAM is known to bind MTHFR and allosterically inhibit the enzyme. It is also established that SAM binds MTHFR in the regulatory domain. However, the exact region is

unclear, and in fact, controversial. The photoaffinity mapping data and the structural data point to quite different regions of MTHFR to which SAM is expected to bind.

MTHFR is present at an important node in one-carbon metabolism. MTHFR regulation by SAM is therefore expected to be critical for one-carbon metabolism. However, the exact consequences that might result in case the regulation is lost are unknown and have never been explored.

Based on the above lacunae, I have accordingly formed the following objective of my thesis:

1. Investigation of the regulatory domain of MTHFR with an attempt to identify the SAM binding domain more precisely.
2. Create mutations in the SAM-binding domain of MTHFR to generate a deregulated, SAM-insensitive MTHFR.
3. Investigate the metabolic consequences of a SAM-insensitive deregulated MTHFR in terms of the effects on various cycles that are part of one-carbon metabolism: the folate cycle, the methionine cycle, and the transsulfuration pathway, and also the impact on the overall metabolic homeostasis.

Chapter 2

Materials and Methods

2.1. Materials

2.1.1. Chemicals and reagents

All the chemicals used were obtained from commercial sources and were of analytical grade. Fine chemicals, media components, HPLC grade solvents, and reagents were purchased from Sigma Aldrich, HiMedia, Merck Millipore India Ltd., USB, and Difco. Folic acid was purchased from Schircks Laboratories (Jona, Switzerland). Enzymes: restriction enzymes, Calf Intestinal Phosphatase (CIP), T4 DNA ligase, T4 polynucleotide kinase, and dNTPs were purchased from New England Biolabs (Beverly, MA, USA). Standard Taq DNA polymerase, Vent DNA polymerase, Phusion polymerase, their buffers, and dNTPs were obtained from New England Biolabs (Beverly, MA, USA). DNA/Protein molecular ladders were obtained from New England Biolabs or Thermo Fisher Scientific, or Gold Biotech (Olivette, MO, USA). Gel extraction kits and plasmid miniprep columns were obtained from Bioneer Inc. (Daejeon, South Korea) or Promega Corporation (Wisconsin, USA), and the Ni-NTA agarose resin was obtained from Qiagen (Germany). NADP/NADPH-Glo™ assay kit for NADPH estimation was procured from Promega Corporation (Wisconsin, USA). Oligonucleotides (primers) were designed using Snap gene software and were purchased from IDT, India, or Sigma (Bangalore, India). Sequencing services were obtained from 1st Base (Malaysia) or Eurofins (Bangalore, India), or AgriGenome Labs Pvt. Ltd. (Kochi, Kerala). Softwares used in this study are Agilent Chemstation, MassHunter, IsoCorr, Metalign, MATLAB, Amdis (NIST).

2.1.2. Strains

Table 2.1 provides a list of yeast strains used in the study. Various deletion strains of *Saccharomyces cerevisiae* in BY4742 and BY4741 background were used for dilution spotting experiments, growth curve assays, targeted metabolite analysis, and ^{13}C stable isotope labelling analysis. *Escherichia coli* strain DH5-α and Rosetta™ (DE3) was used as a cloning host and expression host for protein expression and purification, respectively.

Table 2.1 List of bacterial and yeast strains used in the study

Strains	Genotype	Source
Yeast Strains		
ABC 734	MATα *his3Δ leu2Δ 0 lys2Δ0 ura3Δ0*	Euroscarf
ABC 2614	BY4742, *ygl125wΔ*::*KanMX*	Euroscarf
ABC 733	MATa *his3Δ leu2Δ 0 met15Δ0 ura3Δ0*	Euroscarf
ABC 2613	BY4741, *met13Δ*::*KanMX*	Euroscarf
ABC 5609	BY4742, *met6Δ*::*KanMX, met13Δ*:: *LEU2Δ*	This study
ABC 5611	BY4742, *mup1Δ*::*KanMX, met13Δ*:: *LEU2Δ*	This study
Bacterial Strains		
ABE 460 DH5α	*F+gyrA(Na1) recA1 endA1 thi-1 hsdR17 (rk mk) GlnV44 deoR Δ (lacZYA-argF) U169*	Novagen
ABE 2085 Rosetta™ (DE3)	*F⁻ ompT hsdSB(rB- mB-) gal dcm (DE3) pRARE (Cam^R)*	Novagen

2.1.3. Plasmids

Strain DH5α was used for cloning in plasmids p416TEF and pET21(d).

Table 2.2 List of plasmids used in the study

Plasmid name	Clone No	Description	Source
p416TEF	ABE 443	Centromeric shuttle vector bearing URA3 marker, TEF promoter, MCS region and CYC terminator for yeast expression and Amp^r marker for selection in *E. coli*	Dr. Martin Funk
p315TEF	ABE 3488	TEF promoter and terminator region including MCS, was evicted from p416TEF (ABE 443) plasmid and cloned in pRS315 plasmid at *SacI* and *XbaI* sites and cloned by Shailesh Kumar.	Lab stock
p313TEF	ABE 3569	pRS313 vector digested with *SacI* and *ApaI* was ligated with *SacI* and *ApaI* digested fragment (1941bp) from p416 TEF (ABE 443). Cloned by Manisha Wadhwa.	Lab stock

p313TEFZWF1	ABE 5287	Complete ZWF1 gene cloned in 313TEF vector at *BamHI* and *EcoRI* sites and cloned by Manisha Wadhwa.	Lab stock
p416TEFMET13	ABE 4934	Complete MET13 gene cloned in 416TEF vector at *XbaI* and *ClaI* sites	This study
p416TEFMET13 HIS C1	ABE 5347	Complete MET13 gene with C-terminal His tag cloned in 416TEF at *XbaI* and *ClaI* sites (Clone 1)	This study
p416TEFMET13 HIS C2	ABE 5348	Complete MET13 gene with C-terminal His tag cloned in 416TEF at *XbaI* and *ClaI* sites (Clone 2)	This study
p416TEFMET13_M1 HIS C1	ABE 5379	MET13 gene mutated at S340A.R344A.T345A with C terminal His tag cloned in 416TEF at *XbaI* and *ClaI* sites (Clone 1)	This study
p416TEFMET13_M1 HIS C1	ABE 5380	MET13 gene mutated at S340A.R344A.T345A with C terminal His tag cloned in 416TEF at *XbaI* and *ClaI* sites (Clone 2)	This study
p416TEFMET13_M2 HIS C1	ABE 5381	MET13 gene mutated at R357A.S361A with C terminal His tag cloned in 416TEF at *XbaI* and *ClaI* sites (Clone 1)	This study
p416TEFMET13_M2 HIS C2	ABE 5382	MET13 gene mutated at R357A.S361A with C terminal His tag cloned in 416TEF at *XbaI* and *ClaI* sites (Clone 2)	This study
p416TEFMET13_M3 HIS C1	ABE 5383	MET13 gene mutated at S340A.R344A.T345A.R357A.S361A with C terminal His tag cloned in 416TEF at *XbaI* and *ClaI* sites (Clone 1)	This study
p416TEFMET13_M3 HIS C2	ABE 5384	MET13 gene mutated at S340A.R344A.T345A.R357A.S361A with C terminal His tag cloned in 416TEF at *XbaI* and *ClaI* sites (Clone 2)	This study
p416TEFMET13_M4 HIS C1	ABE 5385	MET13 gene mutated at T440A.N442A.S443A.Q444A.P445A with C terminal His tag cloned in 416TEF at *XbaI* and *ClaI* sites (Clone 1)	This study

p416TEFMET13_M5 HIS C1	ABE 5386	MET13 gene mutated at T519A.W520A with C terminal His tag cloned in 416TEF at *XbaI* and *ClaI* sites (Clone 1)	This study
p416TEFMET13_M5 HIS C2	ABE 5387	MET13 gene mutated at T519A.W520A with C terminal His tag cloned in 416TEF vector at *XbaI* and *ClaI* sites (Clone 2)	This study
p416TEFMET13_M6 HIS C1	ABE 5388	MET13 gene mutated at Q468A.K469A with C terminal His tag cloned in 416TEF at *XbaI* and *ClaI* sites (Clone 1)	This study
pET21(d)MET13 HIS C1	ABE 4246	Complete MET13 gene cloned in pET21(d) at *NheI* and *SacI* sites. (Clone 1)	This study
pET21(d)MET13 HIS C2	ABE 4247	Complete MET13 gene cloned in pET21(d) at *NheI* and *SacI* sites. (Clone 2)	This study
pET21(d)MET13_M1 HIS C1	ABE 5389	MET13_M1 (ABE 5379) clone with C terminal His tag subcloned in pET21(d)MET13 HIS (ABE 4246) at *BamHI* and *SalI* sites. (Clone 1)	This study
pET21(d)MET13_M1 HIS C2	ABE 5390	MET13_M1 (ABE 5379) clone with C terminal His tag subcloned in pET21(d)MET13 HIS (ABE 4246) at *BamHI* and *SalI* sites. (Clone 2)	This study
pET21(d)MET13_M2 HIS C1	ABE 5424	MET13_M2 (ABE 5381) clone with C terminal His tag subcloned in pET21(d)MET13 HIS (ABE 4246) at *BamHI* and *SalI* sites (Clone 1)	This study
p416TEFMET13_R357A HIS C1	ABE 5507	MET13 gene mutated at R357A with C terminal His tag cloned in 416TEF at *XbaI* and *ClaI* sites (Clone 1)	This study
p416TEFMET13_R357A HIS C2	ABE 5508	MET13 gene mutated at R357A with C terminal His tag cloned in 416TEF at *XbaI* and *ClaI* sites (Clone 2)	This study
p416TEFMET13_S361A HIS C1	ABE 5509	MET13 gene mutated at S361A with C terminal His tag cloned in 416TEF at *XbaI* and *ClaI* sites (Clone 1)	This study
p416TEFMET13_S361A HIS C2	ABE 5510	MET13 gene mutated at S361A with C terminal His tag cloned in 416TEF at *XbaI* and *ClaI* sites (Clone 2)	This study

p416TEFMET13_S340A HIS C2	ABE 5549	MET13 gene mutated at S340A with C terminal His tag cloned in 416TEF at *XbaI* and *ClaI* sites (Clone 1)	This study
p416TEFMET13_Y341A HIS C2	ABE 5551	MET13 gene mutated at S341A with C terminal His tag cloned in 416TEF at *XbaI* and *ClaI* sites (Clone 2)	This study
p416TEFMET13_R344A HIS C2	ABE 5553	MET13 gene mutated at R344A with C terminal His tag cloned in 416TEF at *XbaI* and *ClaI* sites (Clone 2)	This study
p416TEFMET13_T345A HIS C2	ABE 5555	MET13 gene mutated at T345A with C terminal His tag cloned in 416TEF at *XbaI* and *ClaI* sites (Clone 2)	This study
p416TEFMET13_W348A HIS C1	ABE 5556	MET13 gene mutated at S348A with C terminal His tag cloned in 416TEF at *XbaI* and *ClaI* sites (Clone 1)	This study
p416TEFMET13_W348A HIS C2	ABE 5557	MET13 gene mutated at S348A with C terminal His tag cloned in 416TEF at *XbaI* and *ClaI* sites (Clone 2)	This study
p416TEFMET13_F353A HIS C2	ABE 5559	MET13 gene mutated at F353A with C terminal His tag cloned in 416TEF at *XbaI* and *ClaI* sites (Clone 2)	This study
p416TEFMET13_P354A HIS C1	ABE 5560	MET13 gene mutated at P354A with C terminal His tag cloned in 416TEF at *XbaI* and *ClaI* sites (Clone 1)	This study
p416TEFMET13_P354A HIS C2	ABE 5561	MET13 gene mutated at P354A with C terminal His tag cloned in 416TEF at *XbaI* and *ClaI* sites (Clone 2)	This study
p416TEFMET13_G356A HIS C2	ABE 5563	MET13 gene mutated at G356A with C terminal His tag cloned in 416TEF at *XbaI* and *ClaI* sites (Clone 2)	This study
p416TEFMET13_G359A HIS C1	ABE 5564	MET13 gene mutated at G359A with C terminal His tag cloned in 416TEF at *XbaI* and *ClaI* sites (Clone 1)	This study
pNative-MET13 HIS C1	ABE 5615	MET13 gene promoter (500bp) cloned in 416TEFMET13 HIS (ABE 5347) at *SacI* and *XbaI* sites. (Clone 1)	This study
pNative-MET13 HIS C2	ABE 5616	MET13 gene promoter (500bp) cloned in 416TEFMET13 HIS (ABE 5347) at *SacI* and *XbaI* sites. (Clone 2)	This study
pNative-MET13_R357AHIS C1	ABE 5617	MET13 gene promoter (500bp) cloned in 416TEFMET13_R357A HIS vector (ABE 5507) using *SacI* and *XbaI* sites. (clone 1)	This study

pNative-MET13_R357AHIS C2	ABE 5618	MET13 gene promoter (500bp) cloned in 416TEFMET13_R357A HIS at (ABE 5507) using *SacI* and *XbaI* sites. (Clone 2)	This study
pNative-MET13_S361AHIS C1	ABE 5619	MET13 gene promoter (500bp) cloned in 416TEFMET13_S361A HIS at (ABE 5509) at *SacI* and *XbaI* sites. (Clone 1)	This study
pNative-MET13_S361AHIS C2	ABE 5620	MET13 gene promoter (500bp) cloned in 416TEFMET13_S361A HIS vector (ABE 5509) at *SacI* and *XbaI* sites. (Clone 2)	This study
pET21(d)MET13_F353AHIS	ABE 5638	MET13_F353A (ABE 5559) cloned with C terminal His tag subcloned in pET21(d)MET13 HIS (ABE 4246) at *BamHI* and *SalI* sites. (Clone 1)	This study
pET21(d)MET13_P354AHIS	ABE 5639	MET13_P354A (ABE 5560) cloned with C terminal His tag subcloned in pET21(d)MET13 HIS (ABE 4246) at *BamHI* and *SalI* sites. (Clone 2)	This study
pET21(d)MET13_G356AHIS	ABE 5640	MET13_G356A (ABE 5563) cloned with C terminal His tag subcloned in pET21(d)MET13 HIS (ABE 4246) at *BamHI* and *SalI* sites (Clone 1)	This study
pET21(d)MET13_R357AHIS	ABE 5641	MET13_R357A (ABE 5507) cloned with C terminal His tag subcloned in pET21(d)MET13 HIS (ABE 4246) at *BamHI* and *SalI* sites (Clone 1)	This study
pET21(d)MET13_G359AHIS	ABE 5642	MET13_G359A (ABE 5564) cloned with C terminal His tag subcloned in pET21(d)MET13 HIS (ABE 4246) at *BamHI* and *SalI* sites (Clone 2)	This study
p416TEFMTHFR-Chimera1 HIS C1	ABE 5659	Chimeric MTHFR [Yeast MET13 (N-terminal) and *Arabidopsis thaliana* MTHFR (C-terminal)] was amplified from ABE 5373 (pVT-301-U Chimera) and cloned in p416TEF at *EcoRI* and *SalI* sites. (Clone 1)	This study
p416TEFMTHFR-Chimera1 HIS C2	ABE 5660	Chimeric MTHFR [Yeast MET13 (N-terminal) and *Arabidopsis thaliana* MTHFR (C-terminal)] was amplified from ABE 5373 (pVT-301-U	This study

		Chimera) and cloned in p416TEF at *EcoRI* and *SalI* sites. (Clone 2)	
p416TEFMET13_E22A HIS C1	ABE 5676	MET13 gene mutated at E22A with C terminal His tag cloned in 416TEF at *XbaI* and *ClaI* sites (clone 1)	This study
p416TEFMET13_E22A HIS C2	ABE 5677	MET13 gene mutated at E22A with C terminal His tag cloned in 416TEF at *XbaI* and *ClaI* sites (Clone2)	This study
p416TEFMET13_R357A.E22A HIS C1	ABE 5678	MET13 gene mutated at E22A with C terminal His tag cloned in 416TEFMET13_R357A (ABE 5507) at *XbaI* and *ClaI* sites (Clone 1)	This study
p416TEFMET13_R357A.E22A HIS C2	ABE 5679	MET13 gene mutated at E22A with C terminal His tag cloned in 416TEFMET13_R357A (ABE 5507) at *XbaI* and *ClaI* sites (Clone 2)	This study
p416TEFAtMTHFR C1	ABE 5791	Complete AtMTHFR cDNA (Arabidopsis thaliana) with C-terminal His tag cloned in 416TEF at *SpeI* and *SalI* sites (Clone 1)	This study
p416TEFAtMTHFR C2	ABE 5792	Complete AtMTHFR cDNA (Arabidopsis thaliana) with C-terminal His tag cloned in 416TEF at *SpeI* and *SalI* sites (Clone 2)	This study
p416TEFMET13_N355H C1	ABE 5802	MET13 gene mutated at N355H with C terminal His tag cloned in 416TEF at *XbaI* and *ClaI* sites (Clone 1)	This study
p416TEFMET13_Y404A HIS C1	ABE 5871	MET13 gene mutated at Y404A with C terminal His tag cloned in 416TEF at *XbaI* and *ClaI* sites (Clone 1)	This study
p416TEFMET13_E422A HIS C1	ABE 5872	MET13 gene mutated at E422A with C terminal His tag cloned in 416TEF at *XbaI* and *ClaI* sites (Clone 1)	This study
p416TEFMET13_E422A HIS C2	ABE 5873	MET13 gene mutated at E422A with C terminal His tag cloned in 416TEF at *XbaI* and *ClaI* sites (Clone 2)	This study
pET21(d)MET13_Y404A HIS C1	ABE 5875	MET13_Y404A (ABE 5871) cloned with C terminal His tag subcloned in pET21(d)MET13 HIS (ABE 4246) at *BamHI* and *SalI* sites. (Clone 1)	This study
pET21(d)MET13_Y404A HIS C2	ABE 5876	MET13_Y404A (ABE 5871) cloned with C terminal His tag subcloned in	This study

		pET21(d)MET13 HIS (ABE 4246) at *BamHI* and *SalI* sites. (Clone 2)	
pET21(d)MET13_E422A HIS C1	ABE 5877	MET13_E422A (ABE 5872) cloned with C terminal His tag subcloned in pET21(d)MET13 HIS (ABE 4246) at *BamHI* and *SalI* sites (Clone 1)	This study
pET21(d)MET13_E422A HIS C2	ABE 5878	MET13_E422A (ABE 5872) cloned with C terminal His tag subcloned in pET21(d)MET13 HIS (ABE 4246) at *BamHI* and *SalI* sites (Clone 1)	This study

2.1.4. Primers

Primers used for plasmid construction, gene disruptions, and confirmation of gene disruption are listed in Table 2.3. Primers were designed using Snapgene software (version 2.4.3). De-salted primers were purchased from Integrated DNA Technologies (IDT) or Sigma Aldrich.

Table 2.3 List of oligonucleotides and their sequences used in the present study.

Primer Name	Sequence (5' to 3')
Primers used for cloning	
MET13_*XbaI* F	TGACGATCTAGAATGAAGATCACAGAAAAATTAGAGCAACATAG
MET13-His Cla I R	GATCCTATCGATTTAATGGTGGTGATGGTGATGTAGGCTTAGTAGGATGGAATGG
MET13_*SacI* F	TGACGAGAGCTCATGAAGATCACAGAAAAATTAGAGCAACATAG
MET13_Y404A F	TTGGTCATCAACGCCTTGAATGGAAAC
MET13_Y404A R	GTTTCCATTCAAGGCGTTGATGACCAAGAAGG
MET13_E422A F	CCCATCAATGATGCAATAAATCCAATC
MET13_E422A R	GATTGGATTTATTGCATCATTGATGGG
MET13_M1 F	TGGAAGAGAAGACCTTACGCCTATGTCGCAGCAGCCTCTCAATGGGCCGTGGACG
MET13_M1 R	GTCCACGGCCCATTGAGAGGCTGCTGCGACATAGGCGTAAGGTCTTCTCTTCCAG
MET13_M2 F	GGGCCGTGGACGAATTCCCCAACGGTGCATTCGGTGATGCGTCTTCTCCTGCGTTCGG
MET13_M2 R	CCGAACGCAGGAGAAGACGCATCACCGAATGCACCGTTGGGGAATTCGTC
MET13_M4 F	AACCAGCATTCTATCATCGCTATAGCCGCTGCAGCTCAAGTCAACGGCATTAGGTC

MET13_M4 R	CCTAATGCCGTTGACTTGAGCTGCAGCGGCTATAGCGATGATAGAATGCTGGTTCAGC
MET13_M5 F	TCCAAGTCCAACGCTGTGGCTGCGGGTATTTTCCCCGGCAGAG
MET13_M5 R	TCTGCCGGGGAAAATACCCGCAGCCACAGCGTTGGACTTGGAG
MET13_M6 F	GCTGTGACTTGGGGTATTGCCGCCGGCAGAGCAATTCTTCAACCTACCATTGTCG
MET13_M6 R	AATGGTAGGTTGAAGAATTGCTCTGCCGGCGGCAATACCCCAAGTCACAGCG
MET13_S340A F	TGGAAGAGAAGACCTTACGCCTATGTCGCAAGAACC
MET13_S340A R	GGTTCTTGCGACATAGGCGTAAGGTCTTCTCTTCC
MET13_Y341A F	GAGAAGACCTTACTCCGCTGTCGCAAGAACCTCTCAATGG
MET13_Y341A R	TGAGAGGTTCTTGCGACAGCGGAGTAAGGTCTTCTCTTCC
MET13_R344A F	TTACTCCTATGTCGCAGCAACCTCTCAATGGGCCG
MET13_R344A R	ACGGCCCATTGAGAGGTTGCTGCGACATAGGAGTAAGG
MET13_T345A F	ACTCCTATGTCGCAAGAGCCTCTCAATGGGCCGTGG
MET13_T345A R	CCACGGCCCATTGAGAGGCTCTTGCGACATAGGAGTAAGG
MET13_W348A F	CGCAAGAACCTCTCAAGCGGCCGTGGACGAATTCCC
MET13_W348A R	GGGAATTCGTCCACGGCCGCTTGAGAGGTTCTTGCG
MET13_F353A F	ATGGGCCGTGGACGAAGCCCCCAACGGTAGATTCGG
MET13_F353A R	CCGAATCTACCGTTGGGGGCTTCGTCCACGGCCCATTGAGAGG
MET13_P354A F	GGGCCGTGGACGAATTCGCCAACGGTAGATTCGGTG
MET13_P354A R	CACCGAATCTACCGTTGGCGAATTCGTCCACGGCCC
MET13_G356A F	GGACGAATTCCCCAACGCTAGATTCGGTGATTCG
MET13_G356A R	CGAATCACCGAATCTAGCGTTGGGGAATTCGTCC
MET13_R357A F	CGAATTCCCCAACGGTGCATTCGGTGATTCGTCTTCTCCTGCG
MET13_R357A R	GAGAAGACGAATCACCGAATGCACCGTTGGGGAATTCGTCC
MET13_G359A F	CCCCAACGGTAGATTCGCTGATTCGTCTTCTCCTGC
MET13_G359A R	GCAGGAGAAGACGAATCAGCGAATCTACCGTTGGGG
MET13_S361A F	CCAACGGTAGATTCGGTGATGCGTCTTCTCCTGCGTTCGG
MET13_S361A R	CCGAACGCAGGAGAAGACGCATCACCGAATCTACCGTTGG
MET13_E22A F	ACTTACTCATTCGCGTACTTCGTCCCG
MET13_E22A R	CGGGACGAAGTACGCGAATGAGTAAGT
Primers used for sequencing and verification	
TEF_F	TTGATATTTAAGTTAATAAACGG
TEF_R	TTCAGGTTGTCTAACTCCTTC
T7 Promoter	TAATACGACTCACTATAGGG
T7 Terminator	GCTAGTTATTGCTCAGCGG
Primers used for deletion and verification	
LEU2-MET13-DEL F	ATGAAGATCACAGAAAAATTAGAGCAACATAGACAGACCTAACTGTGGGAATACTCAGGT

LEU2 MET13 DEL R	TAGGCTTAGTAGGATGGAATGGATTTGATCATCTGGAGAATTAAGCAAGGATTTTCTTAA
MET13 prom F	TCATTCTATCCCTCGGATTATAGACTGTG
MET13_Seq (600bp) F	TGGTGTTCCCAAGTTAGAGCTGCG

2.1.5. Antibiotics

Ampicillin (100 mg/ml) stocks were prepared in autoclaved Millipore elix3 deionized water; filter-sterlized using 0.22μm syringe filters (MDI) and stored at -20°C and chloramphenicol (35 mg/ml) stocks were prepared in 100% Ethanol and stored at 4°C.

2.1.6. Media

All the media, buffers, and stock solutions were prepared using Millipore elix3 deionized water unless otherwise mentioned. They were sterilized, as recommended, either by autoclaving at 15 lb/inch^2 (psi) pressures at 121ºC for 15 minutes or by using membrane filters (Advanced Microdevices Pvt. Ltd., India) of pore size 0.2-0.45 μm (for heat-labile compounds). Agar was added, if required, at a final concentration of 2.2%. Ampicillin was added at a final concentration of 100 μg/ml. Chloramphenicol was added at a concentration of 35 μg/ml.

2.1.6.1. Rich Media for bacteria (LB-Lysogeny Broth)

5 g/litre yeast extract, 10 g/litre Bacto Tryptone, and 5 g/liter NaCl. The components were dissolved in 1 liter Millipore elix3 deionized water and autoclaved.

2.1.6.2. Rich Media for yeast (YPD)

10 g/litre yeast extract, 20 g/litre Bacto peptone, and 20 g/liter dextrose. The components were dissolved in 1 litre Millipore elix3 deionized water and autoclaved.

2.1.6.3. Synthetically Defined (SD) Minimal Media

1.7 g/litre yeast nitrogen base (YNB) without amino acids and ammonium sulphate, 5g/litre ammonium sulphate, and 20 g/litre dextrose. Additional amino acids were added as per the auxotrophy at a concentration of 80 mg/litre

2.1.7. Buffers and Stock Solutions

2.1.7.1. GSH Stock Solution (200 mM)

The required amount of glutathione (reduced form) was dissolved in 10 ml of deionized water and was filter-sterilized using a 0.2 μm filter membrane. It was stored at -20°C in aliquots.

2.1.7.2. Methionine Stock Solution (200 mM)

The required amount of methionine was dissolved in 10 ml of deionized water and was filter-sterilized using a 0.2 μm filter membrane. It was stored at 4°C.

2.1.7.3. SAM Stock Solution (25 mM)

The required amount of SAM was dissolved in 2 ml of deionized water containing 20 mM HCl. The stock was divided into aliquots of 0.2 ml and stored at -80°C in these aliquots.

2.1.7.4. Folic acid Stock Solution (100 mM)

The required amount of folic acid was dissolved in 1 ml of deionized water along with the addition of 0.05 ml of 10N NaOH. This solution was always prepared fresh.

2.1.7.5. 50% Glycerol (used for preparing –70°C stocks of *E. coli*)

50 ml glycerol is dissolved in 50 ml of deionized water and mixed properly. The solution was autoclaved and stored at room temperature.

2.1.7.6. Alkaline Lysis Buffer

The composition of alkaline lysis buffer solution used for Plasmid DNA preparation from *E. coli* was as follows:

Table 2.4 Composition of Alkaline Lysis Buffer.

Solution-I (Resuspension Solution)	50 mM Glucose 25 mM Tris-HCl (pH 8.0) 10 mM EDTA (pH 8.0) Autoclaved and stored at 4ºC.
Solution-II (Lysis Solution) (freshly prepared)	0.2 N NaOH (freshly diluted from a 10N stock) 1% SDS (freshly diluted from a 10% stock) Stored at room temperature.

Solution-III (Neutralization Solution) (100ml)	5 M Potassium acetate 60 ml Glacial acetic acid 11.5 ml Deionized water 28.5 ml The resulting solution is 3 M for potassium and 5 M for acetate. It was stored at 4ºC.
TE Buffer (Tris-EDTA) (pH 8.0)	10 mM Tris-HCl (pH 8.0). 1 mM EDTA (pH 8.0).
TE-RNAse (stock prepared at 10 mg/ml)	Working stock 20µg/ml in TE Buffer, pH 8.0.
PCI (Phenol-chloroform-isoamyl alcohol) Solution (100ml)	Phenol 50 ml [Equilibrated with Tris-HCl (pH 7.6)] Chloroform 48 ml Isoamyl alcohol 2 ml Stored at 4°C in a dark brown bottle.

2.1.7.7. Agarose Gel Electrophoresis Reagents

Table 2.5 Composition of Agarose Gel Electrophoresis Buffer

1× TAE (Tris-Acetate-EDTA) Buffer (per 1000 ml) (prepared from 50× TAE stock)	40 mM Tris-Acetate. 1mM EDTA (pH 8.0). Autoclaved and stored at room temperature.
Orange-G dye (Gel loading dye, 6X)	0.25% Orange-G 30% Glycerol
0.7-1% Agarose gel in 1× TAE	
Ethidium Bromide (10 mg/ml) Stock	Final working concentration was used at 0.5 µg/ml.

2.1.7.8. Solution for *E. coli* competent cell preparation

Table 2.6 Composition of buffer for *E.coli* competent cell preparation

SOB	Bactotryptone 20 g/litre Yeast extract 5 g/litre NaCl 0.5 g/litre
SOC	SOB + 20 mM Glucose 20 mM $MgCl_2.6H_2O$* 2.5 mM KCl* *added after filter sterilization.

0.1 M $CaCl_2$	Dissolve 1.47 g $CaCl_2$ in 15% glycerol solution and autoclave

2.1.7.9. Yeast Transformation Solutions

Table 2.7 Composition of yeast transformation buffer

0.1 M Lithium acetate (pH 7.5) (LiAc)	10.02 g in 1 litre water Autoclave this solution
TE Buffer (Tris-EDTA) (pH 8.0)	10 mM Tris-HCl (pH 8.0). 1 mM EDTA (pH 8.0).
50% PEG-3350 in 0.1 M Lithium acetate in TE (pH 7.5)	Prepare 10mM LiAcTE Buffer (For 100 ml) 5 ml LiAc (10 mM) 5 ml TE (10 mM) 40 ml deionized water Dissolve 50 g PEG to the above solution by intermittent heating in microwave, make up the volume to 100 ml and autoclave.

2.1.7.10. STES lysis mixture for plasmid / genomic DNA isolation from yeast

10 mM Tris-HCl (pH 8.0)

1 mM EDTA (pH 8.0)

100 mM NaCl

1% SDS

2% Triton X-100

2.1.7.11. SDS-PAGE Solutions and Reagents

Table 2.8 Composition of SDS PAGE Buffers

30% Acrylamide Mix	29.2% (w/v) Acrylamide 0.8% (w/v) N, N'- methylenebisacrylamide Filtered before use.
Resolving (Lower) Gel 1.5 M Tris-HCl (pH 8.8)	18.18 g Tris pH adjusted to 8.8 with 6N HCl and volume made up to 100 ml. (0.4% SDS can be added to the buffer itself).
Stacking (Upper) Gel 0.5 M Tris-HCl (pH 6.8)	6.06 g Tris pH adjusted to 6.8 with 6N HCl and volume made up to 100 ml. (0.4% SDS can be added to the buffer itself).
0.4% SDS	
TEMED	

10% Ammonium persulphate (APS)	
Tris-Glycine Gel Running Buffer (Laemmli Buffer) (pH 8.3)	25 mM Tris base 250 mM Glycine (electrophoresis grade) 0.1% SDS
5× Sample Buffer/Gel Loading Buffer (pH 6.8)	0.15 M Tris-HCl (pH 6.8) 5% SDS 25% Glycerol 12.5% β-mercaptoethanol 0.006% Bromophenol blue
Gel Staining Solution	40% Methanol 10% Glacial Acetic acid 0.1% Coomassie Brilliant Blue (R250)
Gel Destaining Solution	40% Methanol 10% Glacial Acetic acid

2.1.7.12. Resolving Gel Solutions

Table 2.9 Composition of Resolving gel buffer

Component	**Volume**
Distilled water	3.3 ml
Resolving (Lower) Gel Tris Buffer (Stock) (4×) 1.5 M Tris-HCl (pH 8.8) with 0.4% SDS	2.5 ml
30% Acrylamide Mix	4.0 ml
10% APS (Ammonium persulphate)	0.1 ml
TEMED (N, N, N', N'-Tetramethylethylenediamine)	0.004 ml

2.1.7.13. Stacking Gel Solutions

Table 2.10 Composition of Stacking gel buffer

Component	**Volume**
Distilled water	3.4 ml
Stacking (Upper) Gel Tris Buffer (Stock) 0.5 M Tris-HCl (pH 6.8) with 0.4% SDS	0.63 ml
30% Acrylamide Mix	0.83 ml
10% APS (Ammonium persulphate)	0.05 ml
TEMED (N, N, N', N'-Tetramethylethylenediamine)	0.005 ml

2.1.7.14. Yeast Lysis Buffer

Table 2.11 Composition of yeast lysis buffer

Component	Concentration
KH_2PO_4	100mM
Sorbitol	1.2 M
Zymolase	0.3 mg/ml

2.2. Methods

2.2.1. Strains and growth conditions

Yeast and bacterial strains used in the study are described in Table 2.1. The yeast strains were regularly maintained on a nonselective YPD medium, which is composed of yeast extract (1%), peptone (2%), and dextrose (2%) medium. For yeast transformation experiments, synthetically defined minimal medium containing yeast nitrogen base (0.17%), ammonium sulfate (0.5%), and dextrose (2%) supplemented with histidine, leucine, and lysine (when not used as an auxotrophic marker) at 80 mg/liter was used. Growth, handling of bacteria and yeast, and all the molecular techniques used in the study were according to the standard protocols (Guthrie & Fink, 1991; Sambrook et al., 1989). Yeast transformation was carried out by the lithium acetate method (Gietz et al., 1995). *Escherichia coli* strain DH5-α and Rosetta^{TM} were maintained in LB medium.

2.2.2. Transformation of yeast

The transformation of *S. cerevisiae* strains was carried out by the modified lithium acetate method (Gietz et al., 1995). *S. cerevisiae* cultures were grown in YPD at 30^{o}C with shaking for 16-24 hrs and then reinoculated in fresh YPD to an initial OD_{600} of 0.1, cells were allowed to grow at 30^{o}C for 4-5 hrs with shaking. Cells were harvested at 6000 rpm for 5 min, then were washed with sterile water followed by subsequent wash with 0.1 M lithium acetate solution (prepared in TE, pH 7.5) and were finally resuspended in the same solution. The cells were spun down, suspended in 0.1 M lithium acetate solution to a cell density of 1×10^{9} cells/ml and

divided into 100µl aliquots. Approximately 50 µg (5 µl of 10 mg/ml stock solution) of heat-denatured, salmon sperm carrier DNA (ssDNA), followed by 0.3 µg- 0.7µg of plasmid/DNA fragment were added to each aliquot along with 0.3 ml of 50% PEG 3350 (prepared in 0.1 M lithium acetate, pH 7.5) and was then subjected to heat shock at 42^{o}C for 20 min. The cells were pelleted down at 7000 rpm for 3 min. The cell pellet was resuspended in sterile water, and the appropriate volume of cell suspension was plated on selection plates.

2.2.3. Bioinformatics analysis and Multiple sequence alignment

Methylene tetrahydrofolate reductase (MTHFR) protein sequence from yeast (NP_011390.2) was used to identify MTHFR orthologs using BLASTp in a plant, roundworm, human, and zebrafish. The sequences obtained were further used to carry out the reverse BLASTp to confirm the orthology. The protein sequences of MTHFR protein from *Arabidopsis thaliana* (NP_191556.1), *Caenorhabditis elegans* (NP_005948.3), *Homo sapiens* (NP_741028.1), *and Danio rerio* (NP_001121727.1) were retrieved from the NCBI. The multiple sequence alignment of the protein sequences was generated using Clustal Omega (http://www.ebi.ac.uk/Tools/msa/clustalw2/) using default parameters.

2.2.4. Modeling of yeast MTHFR and docking with ligands

The crystal structure of human MTHFR was downloaded from Protein Data Bank (PDB id: 6FCX) and used as a template structure for modelling the yeast MTHFR. The missing coordinates for residues 161 to 171 in the human template structure were modelled using Modeller9v20. The refined human structure was used to generate a collection of 5000 homology models, and the best representative structure was selected based on the evaluation of discrete optimized protein energy (DOPE) potential. The model was further subjected to the loop refinement module of Modeller9v20 to refine the connecting loops, and an energetically favorable model was selected among the 1000 generated models based on the DOPE score.

The selected model was then used as a receptor structure for docking. For SAM, coordinates were obtained from the PubChem database in sdf format and docked using a computational docking program, AutodockVina. The human template structure consists of a SAH binding site, and comparative analysis of both human and modeled yeast structure showed the presence of a similar binding pocket for yeast MTHFR as well. Therefore, the SAM molecule was docked within the box volumes of 65Åx 65Åx 65Å, enclosing the SAH binding pocket. The residues within the binding pocket were defined as flexible residues to accommodate the SAM molecule. AutodockVina predicted favorable docking poses for SAM, and the most favorable docked conformation was used to identify critical residues for further experimental evaluation.

2.2.5. MET13 cloning and construction of site-directed mutants

MET13 was cloned with a hexahistidine tag at the C-terminus downstream of the TEF promoter at *XbaI* and *ClaI* sites of p416TEF vector, resulting in plasmid p416TEF-MET13-His. This construct was further used as a template for the creation of the different mutants of MET13 by splice overlap extension strategy. The PCR products were cloned back into the p416TEF-MET13-His vector. Clones were confirmed by sequencing for the presence of the desired changes.

2.2.6. Growth studies by dilution spotting

For growth assays, the different strains were grown overnight in minimal medium with amino acid supplements and glutathione as a sulfur source without uracil. They were re-inoculated in fresh medium containing methionine at an OD_{600} of 0.15 and grown until the cells attained an OD_{600} of 0.6 - 0.8. The exponential-phase cells were harvested, washed with water, and re-suspended in water to an OD_{600} of 0.2. These were serially diluted to 1:10, 1:100, and 1:1000. Of these cell resuspensions, 10 µl were spotted on the desired minimal medium plates. The plates were incubated at 30˚C for 2-3 days, and then the images were taken using Bio-Rad Gel Doc™ XR+ Imaging System.

2.2.7. Cloning, expression, and purification of yeast WT and mutant MET13

The WT and mutant MET13 genes were first cloned with a His-tag at the C-terminus in the pET21d vector. His tag was incorporated in the WT MET13 gene with the help of PCR based approach using MET13_*NheI*-F and MET13_HIS *SacI*-R primers. The amplified 1.8 kb gene was digested with *NheI* and *SacI* restriction enzymes and cloned into the *NheI* and *SacI* sites in the pET21d vector. The in-frame fusions were confirmed by sequencing. The MET13 mutant genes were sub-cloned from their respective yeast expression clones, generated in 416TEF vector, into the bacterial expression plasmid pET21d using *BamHI* and *SalI* restriction sites.

All the proteins were expressed as C-terminal 6XHis-tagged fusion proteins in *E. coli* Rosetta^{TM} strains. Rosetta^{TM} strains harboring either WT or the mutant MET13 clones were inoculated in LB (Luria–Bertani) broth, with 25 μg/ml chloramphenicol and 100 μg/ml ampicillin, to an OD_{600} of 0.05, and grown aerobically at 37˚C to an OD_{600} of ∼0.6. These cultures were then induced with 1mM isopropyl β-D-thiogalactopyranoside (IPTG) and allowed to grow for 16 h at 18˚C. Cells were harvested after induction by centrifugation at 5000 g for 20mins at room temperature (RT). At this stage, the pellet was stored at -80˚C until further.

The pellet was re-suspended in 20mM KP_i buffer (pH 7.2) containing 10% glycerol, 500mM sodium chloride (NaCl), 0.3mM EDTA, 20mM imidazole, 1mM phenylmethylsulfonyl fluoride (PMSF) and protease inhibitor cocktail. The cells were lysed by sonication at 20 amplitude, 10s sonication cycles were alternated with 20s recovery periods. The lysate was centrifuged at 10,000g for 45 mins at 4°C, and the supernatant was collected. The cleared lysate was loaded onto a Ni-NTA column equilibrated with 20mM KP_i containing 10% glycerol, 500mM NaCl, and 0.3mM EDTA and subsequently washed with 20mM KP_i, 10% glycerol, 0.3mM EDTA, and 50mM imidazole. Elution was performed in the presence of an elution buffer carrying 300mM imidazole. MET13 being a flavoprotein, can be visually

identified by its intense yellow color. The purified proteins were analysed by SDS PAGE (12% gel). Protein concentration estimations were done by the Bradford method (Bradford, 1976) with Bovine Serum Albumin (BSA) as standard after the removal of imidazole by means of dialysis. The dialysis was done for 3 hours against 20mM KP_i buffer (pH 7.2) containing 10% glycerol and 0.3mM EDTA at 4˚C. The dialysis buffer was changed four times, twice after completion of 1 hour and twice after an interval of 30 minutes.

2.2.8. MTHFR activity and inhibition studies: NADPH-menadione oxidoreductase assay

MTHFR activity and inhibition studies were performed with several modifications in the NADPH-menadione oxidoreductase assay (Matthews & Haywood, 1979). In a total volume of 800µl, the reaction mixture consisted of 400µl of 100mM potassium phosphate buffer (pH7.2) with 0.6 mM EDTA, 80µl menadione from a stock concentration of 2mM (menadione stock was prepared freshly in methanol), and 25-100nM of the enzyme. This mixture was incubated for 5 mins at 25°C. To initiate the enzyme activity, NADPH at a final concentration of 200µM was added to the reaction mix. For inhibition studies, in the same reaction mix, 200µM of SAM was added just before adding the NADPH. In both cases, the rate of reaction was monitored as a decrease in the absorbance of NADPH at 343nm. Activities are presented as the initial rate of NADPH oxidation observed, using an extinction coefficient of 6220 M^{-1} cm^{-1}. Activity units represent nanomoles of NADPH oxidized per min per milligram protein.

2.2.9. Protein estimation

Protein estimation of the samples was done by Bradford Assay (Bradford, 1976) using Bradford reagent as per the manufacturer's instructions. The protein samples were dilute, and 5µl of the diluted sample was used for protein estimation, using BSA (Albumin, Fraction V, Sigma) as standard. Protein estimations were done in Triplicates taking absorbance reading at 595nm.

2.2.10. Limited Proteolysis

Limited proteolysis was performed for both the WT and mutant proteins as described below. 1.5 mg/ml of the MET13_WT, MET13_P354A, and MET13_R357A were treated with 0.01mg/ml of trypsin prepared in 1mM HCl with and without the addition of 200 μM SAM (ligand). The reactions were incubated at room temperature, and aliquots were removed at different time intervals (0, 10, 20, 40, 60, 120, and 180 minutes). These samples were boiled with SDS-sample loading buffer to stop any further digestion and were run on 15% SDS-PAGE to observe the digestion pattern.

2.2.11. Circular Dichroism

Thermal denaturation studies were performed by monitoring the signal change at 208 nm using a Chirascan spectrophotometer (Applied Photophysics). Purified protein at a concentration of 5μM, in 50 mM Potassium Phosphate buffer, pH 7.4, and 20 mM NaCl was used for these investigations, with a temperature ranging from 25˚C to 90˚C. The spectra were collected at 25°C using 5μM MET13_WT-6XHis in a quartz cuvette with a 1 mm path length. The average values of each spectrum were corrected for the contribution of the buffer. Data obtained were plotted as a function of mean residue ellipticity against temperature. Spectra were also collected for the wild-type and mutant proteins with a wavelength range of 205–280 nm in the presence of buffer (50 mM Potassium Phosphate buffer, pH 7.4, and 20 mM NaCl).

2.2.12. Targeted metabolite analysis: extractions and estimations

For metabolite analysis (Amino acids, sulfur intermediates, and nucleotides), the *S. cerevisiae* (ABC2613) transformants with MET13_WT or MET13_R357A were grown overnight in minimal media with amino acid supplements and glutathione. These were then re-inoculated at 0.15 OD_{600} in fresh SD media without any sulfur source. Methionine was added to the transformants after 3 h of secondary inoculation, and samples were collected in duplicate at 0.5 and 1.0 OD. Samples were rapidly quenched in a quenching solution, following which

metabolite extraction was done. Metabolite quenching and extraction were performed as described previously (Walvekar et al., 2018). Metabolite extracts were dried down in a speed-vacuum (3-4 h), and stored at -80°C until analyzed by a mass spectrometer.

These metabolites were estimated by LC/MS/MS, using an HPLC coupled to a triple-quadrupole mass spectrometer (ABSciex 6500). Details of the analysis are described in (Walvekar et al., 2018). In brief, metabolites were extracted, resolved, and estimated as described. For each metabolite, parameters for quantitation of the two most abundant daughter ions (that is, two MRMs per metabolite) were included. To quantify metabolites, the area under each peak was quantitated by using the Analyst software (ABSciex), inspected for accuracy, and normalized against total ion count, after which relative amounts were quantified.

Polyamines and folate intermediates were measured in QTRAP 6500^{+}. Metabolites were extracted from the cells using the chilled methanol method. Briefly, 20 OD cells were quenched with chilled methanol (Kept at -80˚C) and followed by bead beating using acid-washed glass beads. The cell suspension was transferred to a fresh tube and centrifuged at 15000g for 15 mins at 4˚C temperature. The supernatant was vacuum dried and reconstituted in 100µl of 50% methanol. 5µl was injected for LC-MS/MS analysis. The data was acquired using a Sciex Exion LC^{TM} analytical UHPLC system coupled with a triple quadrupole hybrid ion trap mass spectrometer (QTRAP 6500^{+}) in a positive ion mode. To quantify these metabolites, the area under each peak was measured using the Multiquant software (ABSciex), inspected for accuracy, and normalized against total ion count, after which relative amounts were quantified.

For PE, PC, and PS estimation, the modified Bligh and Dyer method (Bligh & Dyer, 1959) was used for extraction. 1.8 OD cells were taken, and 2.0 mL methanol was added with 1 mL dichloromethane, vortexed, and made sure to have a mono-phase. The mixture was allowed to be incubated for 30 mins at room temperature. After incubation, 500 µL water, and

1 ml dichloromethane was added to the solution and vortexed for 5 seconds. The mixture was centrifuged at 1200 rpm for 10 mins. The lower layer was collected into a fresh glass tube. 2 mL dichloromethane was added to the remaining mixture in the extraction tube, centrifuged, and the above step was repeated once again. The solvent was evaporated in a vacuum dryer, and the lipids were suspended in 100µl of 100% ethanol; vortexed for 5 mins followed by sonication for 10 mins and again vortexed for 5 mins. Their suspension was transferred to LC-vials and subjected to LC-MS run.

2.2.13. Cell growth for ^{13}C labelling experiments

WT yeast (MET13_WT) and deregulated MTHFR (MET13_R357A) mutant strain were grown in SD media 0.17% Yeast Nitrogen Base (YNB), 0.5% Ammonium sulphate; 80 mg/l leucine, 80 mg/l histidine, methionine, or glutathione (GSH) as per experimental requirement (200µm), 2% Glucose. For ^{13}C feeding experiments, the strains were grown in parallel in SD minimal media with either 99% [1-^{13}C] glucose or unlabeled glucose. Cells were harvested during the mid-exponential phase of the growth (at ~13 h for MET13_WT and 26 h for MET13_R357A mutant) that represent pseudo-steady state conditions. Cell pellets were quenched in liquid nitrogen, lyophilised, and stored at -80˚C till further analysis.

2.2.14. Acid hydrolysis of cell pellets and derivatization of amino acids

Lyophilized yeast cell pellets (approx. 2 mg each) were resuspended in 600µl of 6N HCl. The samples were incubated at 100°C for 18 h to hydrolyze the protein and get the amino acid released (Hayakawa et al., 2018). The hydrolysates were centrifuged, and 50µl supernatant was transferred to a fresh vial and subjected to vacuum drying in a speed-vacuum (Thermo scientific) to ensure the complete removal of moisture. The dried pellets were derivatized using TBDMS for the detection of amino acids using GC-MS (Jyoti et al., 2020). This is achieved by first dissolving the dried extracts in 30µl of pyridine (Sigma Aldrich) and incubated at 37°C, 900 rpm for 30 mins. The resuspended extracts were topped up with 50µl of MtBSTFA + 1%

t-BDMCS (N-methyl-N-(t-butyldimethylsilyl) trifluoroacetamide + 1% t-butyl-dimethylchlorosilane) and incubated at 60 °C on a thermoshaker set at 900 rpm for 30 mins. The derivatized samples were centrifuged for 10 mins at 13000 rpm, and the supernatant was transferred to new GC-MS vials followed by sealing with a septum screw cap.

2.2.15. GC-MS based analysis of amino acids

Samples were analysed by GC-MS (Agilent 7890B GC, electron impact ionization (70 eV). Agilent HP 5-ms ultra-inert chromatography column (Agilent 19091S-433UI, 30m x 250μm x 0.25μm) with 1μL injection volume, splitless mode, 1.3ml/min helium carrier gas flow was used to separate the TBDMS derivatized amino acids (Masakapalli et al., 2014). The initial oven temperature was constant at 120°C for 5 mins, followed by a ramp of 4°C per min to 270°C, hold for 3 mins, then a ramp of 20°C per min to 320°C and hold for 1 min. After 30 mins, the run temperature was reduced to 70°C with a ramp of 100°C per min. The solvent delay was set for ~10 mins. MassHunter (Agilent Technologies, USA) was used to control the data acquisition parameters (both GC separation and mass spectrometry) during all the sample runs. The raw GC-MS spectra of each sample obtained were baseline corrected using MetAlign with default parameters for accurate assessment of MIDs of the metabolites. National Institute of Standards and Technology (NIST), Maryland database, and authentic standards, were used for amino acid peak and fragment identification. The intensity of amino acid fragment mass ions ranging from 40-600 was obtained using Agilent chemstation software. Once the MIDs of all amino acid fragments were obtained from the averaged scans, the values were corrected for the presence of naturally occurring heavy isotopes attached to the carbon backbone of derivatives using IsoCor (Millard et al., 2012). The average ^{13}C abundance of each fragment was calculated for all mass corrected MIDs (Shree & S, 2018). The MIDs of each amino acid fragment can retro-biosynthetically be correlated to the label incorporation from the central precursors. The analysis further gives us a quantitative and qualitative understanding of the

incorporation of glucose into amino acid via various metabolic pathways in the WT and deregulated mutant strain.

The WT and mutant bearing cells were grown in minimal media supplemented with leucine, lysine, histidine, and methionine were fed either [^{12}C]-, or [1-^{13}C] glucose. The derived mass isotopomer fragments were successfully validated by comparing the corrected MID with expected theoretical proportions in unlabelled fragments. Among these fragments, the reliable mass ions (m/z) of fragments [M-85] or [M-57] were considered for comparison of label incorporation and distribution. In the case of the fragments derived from unlabelled amino acids (obtained from ^{12}C tracer feeding), the fractions of ^{13}C in these fragments were observed to be less than the natural abundance (i.e., <1.13%). In parallel, the cells fed with [1-^{13}C] glucose confirmed the label redistribution of 15 amino acids under pseudo-steady state conditions via different pathways of the central metabolism in MET13_WT and in MET13_R357A.

2.2.16. Generation of MET13 disruptions in different deletion strains

The MET13 gene was disrupted in the *mup1Δ* and *met6Δ* strain backgrounds using the one-step PCR-mediated gene disruption (Baudin et al., 1993). The *met13Δ*::LEU2 disruption cassette was generated using the primer pair MET13Δ-LEU2F and MET13Δ-LEU2R and the plasmid pRS315TEF (ABE 3488, lab stock) as a template. The 1.6-kb PCR product obtained was transformed into the strains mentioned above, and the transformants were selected on minimal medium without leucine but containing methionine as the successful disruptants would be methionine auxotrophs. For *met13Δ*::LEU2 disruption in *mup1Δ* strain background, transformants were confirmed by lack of growth on SD plates without methionine. The transformants in *met6Δ* strain were confirmed for the disruption by diagnostic PCR using the primer pair MET13promF and MET13Δ-LEU2-R.

2.2.17. Isolation of genomic DNA from yeast

Genomic DNA from *S. cerevisiae* strains was isolated as described by (Kaiser, 1994) using the glass bead lysis method and the STES lysis buffer, described in the section below.

2.2.18. Preparation of Yeast whole-cell extract

Total crude cell extracts were prepared as described previously with certain modifications (Aggarwal & Mondal, 2006). Briefly, overnight cultures of transformants grown in minimal media containing methionine and other supplements without uracil were reinoculated at OD_{600} of 0.1 in 50 ml of fresh medium and grown to exponential phase (OD_{600} of ~0.6 to 0.8). Cells were harvested by centrifugation and resuspended in yeast breaking buffer for whole-cell extract preparation containing protease inhibitors (Section 2.5.14a). Acid-washed glass beads (425 to 600 µm) were added to the cell suspension, and cells were lysed by vigorous vortexing. The resulting homogenate was centrifuged for 10 min at 13,000 rpm, and the supernatant fraction was collected.

2.2.19. Estimation of Methylglyoxal sensitivity by disc diffusion assay

Disc diffusion assay has been performed after several modifications in the method (adapted from) (Kato et al., 2019). Transformants were grown overnight in SD minimal media along with reduced glutathione (200µM) as sulfur source and other amino acid supplements. These were then re-inoculated in fresh SD media to 0.15 OD_{600} after washing them twice with sterile distilled water. Methionine (200µM) was added to the culture 3 h post the secondary inoculation. At the exponential phase (1.0-1.5 OD), 5 OD of cells were plated onto SD plates supplemented with methionine and glutathione. Grade 1 filter paper with 1 cm in diameter (Whatman) was placed onto the SD plate, and 25µl of MG (6.49 M) was soaked into the filter paper. Cells were grown at 30°C for 48 h.

2.2.20. Total NADPH/NADP measurement by luminescence-based kit

For measurement of total NADPH/NADP pools of yeast cells, transformant expressing either WT or mutated MTHFR protein were grown overnight in SD minimal media along with reduced glutathione (200μM) as sulfur source and other amino acid supplements at 30 ºC for 12 h and re-inoculated in fresh SD medium lacking a sulfur source at an initial OD_{600} of 0.15. After 3 h of incubation, methionine was added to these transformants and allowed to grow at 30˚C till the early exponential phase of growth at 0.6–0.8 OD_{600} with shaking at 220 rpm. Details of the treatment given to cells were as described in (Yadav et al., 2020). An equal number of cells ($OD_{600\sim}$1.0) were harvested at 5000 rpm and washed with sterile MilliQ water, followed by resuspension of the cells in lysis buffer (100mM KH_2PO_4, 1.2M Sorbitol). Spheroplasts were prepared by adding the zymolase at the final concentration of 0.3mg/ml and a subsequent incubation at 30˚C with shaking at 100 rpm for 1 h. A 100µl aliquot of these spheroplasts were mixed with an equal volume of the NADP/NADPH Glo^{TM} detection reagent from NADP/NADPH-Glo^{TM} assay kit (Promega). The reaction mixture was incubated in dark at room temperature for 45 mins, and readings were taken using luminescence spectrometer. Data were analyzed using GraphPad Prism 5.0.

2.2.21. Statistical Tool

For menadione oxidoreductase enzyme activity and inhibition assays, standard deviation calculations were performed. All error bars represent the mean ± SD-based of the three technical replicates. In the targeted metabolite experiments, C^{13} labelling experiments, and luminescence-based NADPH estimation assay, statistical analyses were performed using a paired Student's t-test. p values were generated by analysis of variance (*, $p < 0.05$; **, $p < 0.01$; ***, $p < 0.001$; $n \geq 3$). All error bars represent mean ± SD based on three biological replicates.

Chapter 3

Isolation and characterization of deregulated mutants of yeast MTHFR, MET13

3. Chapter 3

3.1. Introduction

One-carbon (1C) metabolism is a universal metabolic process, where single-carbon methyl groups are transferred to enable the synthesis of several essential metabolites. These include DNA synthesis (thymidine and purines), amino acid homeostasis (serine, glycine, and methionine), redox balance, and epigenetic maintenance (Figure 1.1). This carbon partitioning across various cellular outputs involves three different pathways, namely, the folate cycle, the methionine cycle, and the trans-sulphuration pathways (Figure 1.2) (Locasale, 2013). It is one of the critical metabolic processes amongst all living beings regardless of minor differences in each of its constituent metabolic pathways across diverse organisms (reviewed in chapter 1).

The folate arm of this complex metabolic network in the cytoplasm takes up a 1C moiety from serine and transfers it to THF, the universal 1C acceptor. This, in turn, accepts 1C units derived from amino acids glycine or serine resulting in interchangeable forms of methylated-THF with variable chemical structures (Newman & Maddocks, 2017). These include 10-CHO-THF, 5-CH_3THF, and 5,10-CH_2THF, which respectively donate their 1C units to purine synthesis, methionine recycling pathway (via homocysteine methylation), and thymidylate synthesis (Newman & Maddocks, 2017; Tibbetts & Appling, 2010) (Figure 1.2). The methionine cycle generates methionine by transmethylation of cellular homocysteine pools, which is subsequently utilized in the production of SAM, a universal methyl donor in the cell. As a carrier of the 1C unit, SAM aids the methylation of different acceptor molecules, DNA, RNA, lipids, and proteins producing SAH as a side product. Homocysteine, a breakdown product of SAH, connects the trans-sulfuration pathway to the methionine cycle. Through the trans-sulfuration pathway, serine can be directly metabolized to synthesize GSH, one of the major reducing power in the cell.

MTHFR is found at a critical branch point in one-carbon metabolism and is one of the key regulatory nodes under allosteric feedback inhibition by SAM (Kutzbach & Stokstad, 1967, 1971) (Fig 3.1). Typical eukaryotic MTHFR enzymes have two domains: a catalytic domain of approximately 300 amino acids and an equally large regulatory domain for feedback regulation by SAM (Figure 3.1). This enzyme has been extensively studied; however, these studies have focused primarily on the catalytic domain (Burda et al., 2015; Trimmer, 2013). Several mutations leading to decreased catalytic activity have been implicated in several disorders like neural tube defects and pregnancy-related complications, motor and gait disturbances, seizures, psychiatric disturbances, and other neurological abnormalities and cardio-vascular diseases (Frosst et al., 1995; Goyette et al., 1994; Rosenblatt, 1995). The role of the regulatory domain, however, has not been as extensively studied. Considering that MTHFR essentially straddles the critical cycles of one-carbon metabolism, the folate cycle, and the methionine cycle, its regulation is likely to be critical. However, the consequences of its regulation by SAM is not at all understood. One approach for investigating this aspect is to examine mutants of MTHFR deregulated for SAM inhibition. Analysis of such mutants would not only lead to a deeper understanding of one-carbon metabolism but also aids in understanding the physiological implications of MTHFR regulation by SAM. However, such mutants are not known, and in fact, the SAM binding regions on the MTHFR regulatory domain are still not unequivocally recognized. While photo-affinity labelling identified a shorter region in the N-terminal region of the regulatory domain (Goyette et al., 1994), the recent structure of the human MTHFR has suggested a slightly different part of the regulatory region (Froese et al., 2018).

In this chapter, I describe the successful isolation and characterization of feedback insensitive, deregulated yeast MTHFR mutants. Since such mutants have not been isolated prior to this study, and the precise region within the regulatory domain that might be important

for the regulation was not known, we have used insights from both structure and sequence to identify such mutants. Importantly, we have discovered a growth phenotype of such mutants in methionine medium that enabled the characterization of such mutants and helped to define a region within the regulatory domain that is critical for regulation by SAM, which we wish to establish *in vitro*. Purification of some of the mutants and the wild-type protein as recombinant proteins from *Escherichia coli* further confirmed the absence of SAM regulation in these mutants relative to the wild-type. Attempts to identify possible differences among the wild-type and mutant proteins in terms of differences in oligomerization or conformation revealed that the protein did not display any significant changes in these properties.

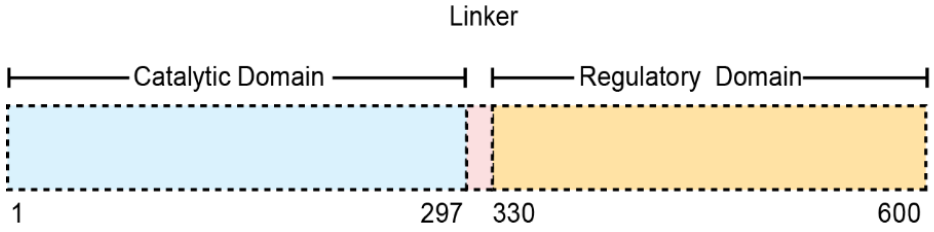

Figure 3.1 Schematic representation of eukaryotic MTHFR

Domain organization of the yeast MTHFR, Met13p, with approximately 300 amino acid long catalytic domain at the N-terminus and an equally large, regulatory domain at the C-terminus.

3.2. Results

3.2.1. The regulatory region of the yeast MTHFR protein, MET13p: predicting potential residues critical for SAM binding and enzyme inhibition

To create a deregulated eukaryotic MTHFR protein and examine the metabolic consequences, we sought to work with the yeast homologue of MTHFR, Met13p, since the yeast system is far more amenable to rapid phenotypic analysis. Towards the goal of creating a deregulated eukaryotic MTHFR protein in yeast that would be insensitive to allosteric inhibition by SAM, we initially carried out an analysis of the regulatory region of MTHFR. This region has not been subjected to any systematic investigations so far.

Figure 3.2 Sequence alignment analysis of MTHFR orthologs indicates three stretches of conserved regions within the regulatory domain.
Sequence alignment of the regulatory domain of yeast (NP_011390.2), plant (NP_191556.1), roundworm (NP_741028.1), human (NP_005948.3), and zebrafish (NP_001121727.1) MTHFR proteins performed using Clustal omega. *, identical residues; . and :, varying degree of conserved substitution; and –, gaps in the alignment. Putative SAM binding residues as predicted by modelling and docking studies are highlighted in yellow.

Comparative sequence analysis of yeast MTHFR and other eukaryotic MTHFRs (*Arabidopsis thaliana*, *Caenorhabditis elegans*, *Danio rerio*, and *Homo sapiens*) reveals that the catalytic domains of these proteins show high similarity amongst each other (42% identity with the human and yeast protein in the catalytic region). Surprisingly, these eukaryotic MTHFRs also show a high sequence similarity in the regulatory region with a 43% identity with the human and yeast proteins, across the entire regulatory region of the yeast MTHFR, residues 337-600 (Figure 1.11). Further, within the large regulatory domain, one observes short blocks of high identity across all these organisms. We have defined these regions as Conserved Region 1 (CR1) beginning from amino acids 340-361, Conserved Region 2 (CR2) corresponding to amino acids 440-445, and Conserved Region 3 (CR3) from amino acids 517-527 (Figure 3.2 and 3.3). Efforts to find any signature SAM binding domains in the regulatory

region or the short stretches were, however, unsuccessful. Indeed, it is known that there is a large and diverse family of SAM binding proteins with no sequence or structural similarities around the SAM binding pocket (Kozbial & Mushegian, 2005).

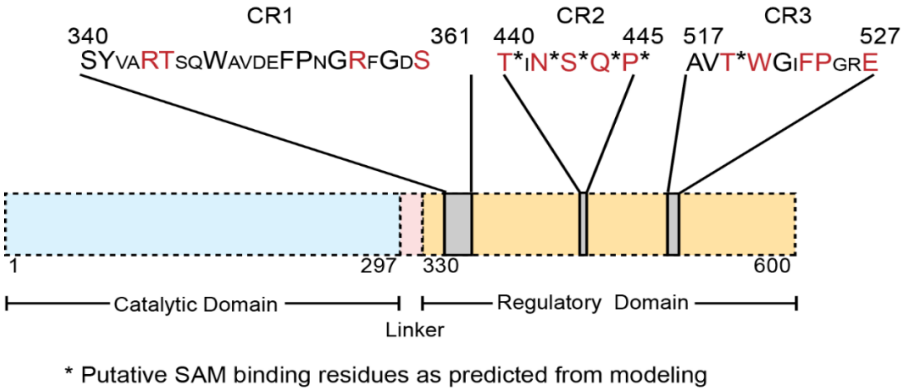

Figure 3.3 Schematic representation of Met13p indicating the conserved regions (CR1, CR2, and CR3) within the regulatory domain

Clustal omega analysis of the regulatory domain of the MTHFR protein across different eukaryotic organisms (*S. cerevisiae*, *A. thaliana*, *C. elegans*, *D. rerio*, and *H. sapiens*) shows three conserved regions which were defined as Conserved Region 1 (CR1) beginning from amino acids 340-361, Conserved region 2 (CR2) corresponding to amino acids 440-445, and Conserved Region 3 (CR3) from amino acids 517-527. Conserved residues are indicated in a bigger font, residues subjected to mutational analysis are marked in red, and * indicates the residues which were predicted to bind to SAM through modeling studies.

3.2.2. Molecular docking and structural analysis of the modeled MET13p predicts several residues within the regulatory domain as the probable SAM binding residues

Further, to obtain insights into the SAM binding domains of the MTHFR protein, we built a homology model of the yeast MTHFR, Met13p, based on the crystal structure of human MTHFR, which has been recently solved (Froese et al., 2018). This structure has provided the first insights into the eukaryotic MTHFR with its large regulatory region and was obtained using a truncated protein that has deletions, both, at the N and C-terminal ends. Moreover, the crystal structure could be attained only with SAH and not with SAM, the known inhibitor of the MTHFR enzyme. Although SAH is not an inhibitor of MTHFR, the similarity in structure to SAM was used to extract insights regarding residues involved in SAM binding. Using the

human MTHFR as a template that shows a 42% sequence identity with the full-length yeast homolog, we carried out the homology modeling studies with the help of Modeller 9v20. Modeled yeast MTHFR structure aligns well with human MTHFR protein, which exists as a homodimer with each monomer consisting of a catalytic domain and a regulatory domain. The two monomers are held together by interactions of the regulatory domain, as has been reported for the human MTHFR (Figure 3.4) (Froese et al., 2018).

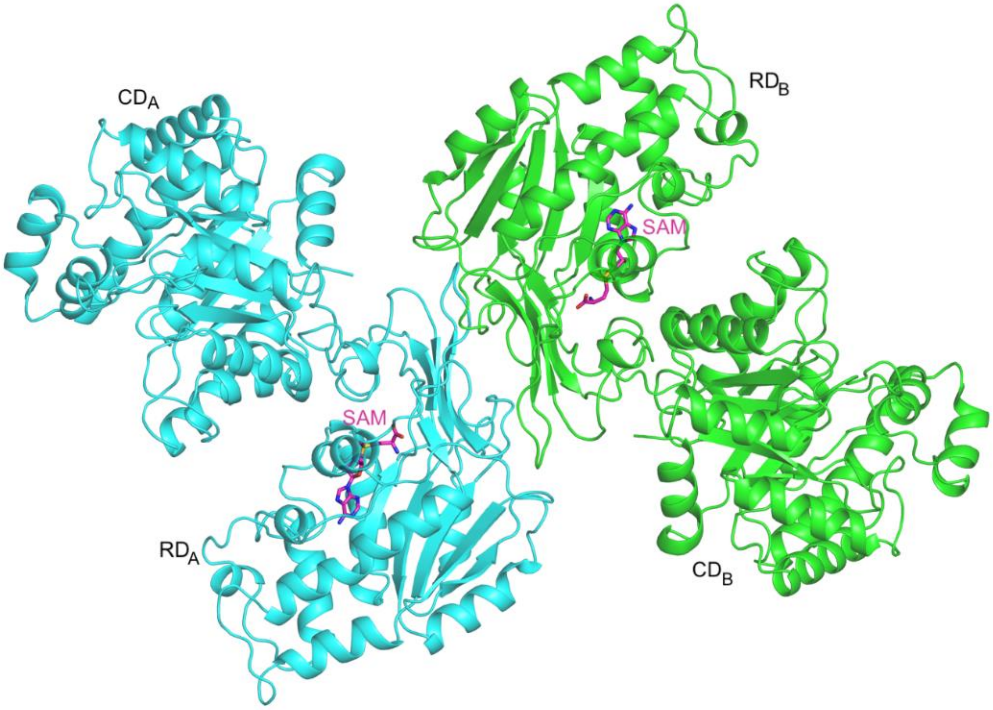

Figure 3.4 Cartoon representation of modeled yeast MTHFR structure.
Homology modeling studies using Modeler 9v20 indicates yeast MTHFR, Met13p, exists as a dimer where each monomer is composed of a catalytic domain and a regulatory domain. The two monomers interact with each other via the regulatory domain. Chain A is shown in cyan, and chain B in green. CD_A and CD_B- Catalytic domain of the two monomers (A and B); RD_A and RD_B- Regulatory domain of the two monomers (A and B); bound SAM is represented by sticks in pink.

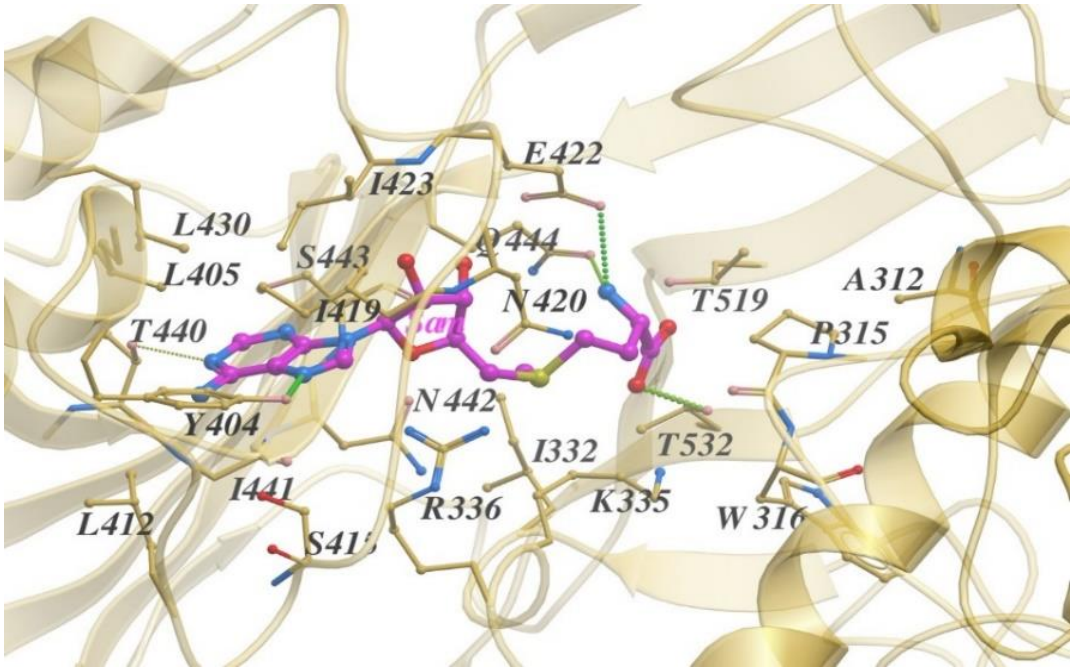

Figure 3.5 Yeast MTHFR docked with a molecule of SAM.
A SAM molecule (represented in pink sticks) was docked with modeled Met13p using AutodockVina. Amino acid residues that might be involved in SAM binding are marked with yellow sticks.

In order to predict the SAM binding residues of MET13, we docked the SAM molecule using a computational docking program, AutodockVina. In total, we identified twenty residues (Figure 3.5 and Figure 3.2) as the probable SAM binding candidates based on the distance cut-off around the SAM binding pocket, which was predicted using the docking studies. Of these, three amino acids (A312, P315, and W316) are present in the linker region, and the other seventeen (K335, R336, Y404, L405, L412, S415, I419, N420, E422, I423, T440, I441, N442, S443, Q444, T519, and T532) within the regulatory domain. In addition to the distance cut-off, we included two more parameters to select the residues for further mutational analysis. The first parameter was to restrict the residues to the regulatory domain; hence, this allowed the elimination of A312, P315, and W316 due to the location of these amino acids in the linker region. The second criterion was conservation. We selected the residues- Y404, E422, T440, N442, S443, Q444, T519, and T532, conserved across other organisms whose MTHFR protein is also regulated allosterically by SAM (Kutzbach & Stokstad, 1967, 1971; Roje et al., 2002).

From these selected eight residues, we focused on two amino acids, i.e., Y404 and E422, due to the likelihood of interactions with the side chains as observed by our modeling analysis and excluded the other six which are close enough but may interact with SAM through the amino or carboxyl group of the main chain. Among these, two residues- E422 and Y404, appeared critical. E422 is the equivalent of the mammalian E463 that has also been suggested to be involved in binding to SAM (Froese et al., 2018), and mutation of this residue showed protein characteristics that indicated lack of binding with SAM molecule; Y404 also appeared to be critical since its benzyl ring seemed to be interacting with the adenosyl group of SAM around the hydrophobic region within the the SAM binding pocket, although enzymatic studies were not carried out to confirm these suggestions (Froese et al., 2018).

These structural predictions, as well as the predictions made with the human enzyme (Froese et al., 2018), were not consistent with earlier experimental studies where photo-affinity labeling of SAM was carried out to find out the SAM binding regions of porcine and human MTHFR (Goyette et al., 1994). These studies had indicated a completely different region of the MTHFR regulatory domain, i.e., within a stretch of about 30 amino acids starting 30 residues after the junction between the two domains (Goyette et al., 1994; Raymond et al., 1999; Roje et al., 2002; Sumner, Jencks, Khani, Matthews, et al., 1986). In particular, a 6kDa region of the protein located at the N-terminal end of the regulatory domain was suggested in these studies to be important for SAM binding (Goyette et al., 1994) that approximates residues 340 to 390 in the yeast MTHFR. However, this region was quite distinct from the structural predictions.

3.2.3. MET13_E422A, but not MET13_Y404A mutant, predicted from the modeling studies, shows a partial loss of regulation by SAM

To identify which regions of the regulatory region might be important for SAM-mediated repression of MTHFR, we initially targeted and conducted a mutational analysis of the

probable SAM-binding residues selected based on structural predictions. We generated independent single-point alanine mutants of both Y404 and E422 using site-directed mutagenesis. Further, we expressed the mutants into an *E.coli* expression vector, purified the recombinant proteins (Figure 3.6), and evaluated them for enzymatic activity and SAM inhibition. We performed NADPH-menadione oxidoreductase assays for *in-vitro* MTHFR activity and inhibition measurements. All three purified proteins (MET13_WT, MET13_Y404A, and MET13_E422A) retained MTHFR activity (Figure 3.7). The MET13_Y404A mutant exhibited inhibition (~95%) in the presence of 200μM SAM and behaved like the wild-type protein (Figure 3.7). However, the mutant, MET13_E422A, showed mild repression (~30%) in the presence of SAM, indicating a partial loss of allosteric inhibition (Figure 3.4B).

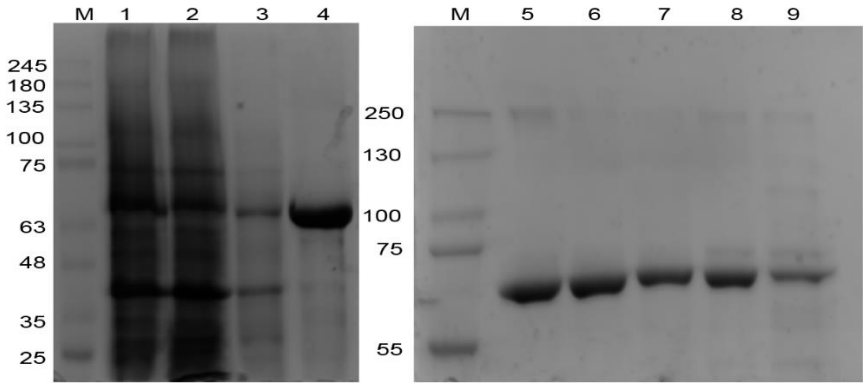

Figure 3.6 Protein purification of yeast MTHFR

Yeast MTHFR WT and mutant proteins were recombinantly expressed and purified from the bacterial expression system using NiNTA affinity chromatography. The purified protein was run on a 12% SDS PAGE, and a band corresponding to a molecular weight of WT MET13p (69 kDa) was observed. Lane 1 Crude extract, Lane 2 Flow-through, Lane 3 Wash, Lane 4 MET13_M2, Lane 5 MET13_WT, Lane 6 MET13_P354A, Lane 7 MET13_R357A, Lane 8 MET13_Y404A, and Lane 9 MET13_E422A.

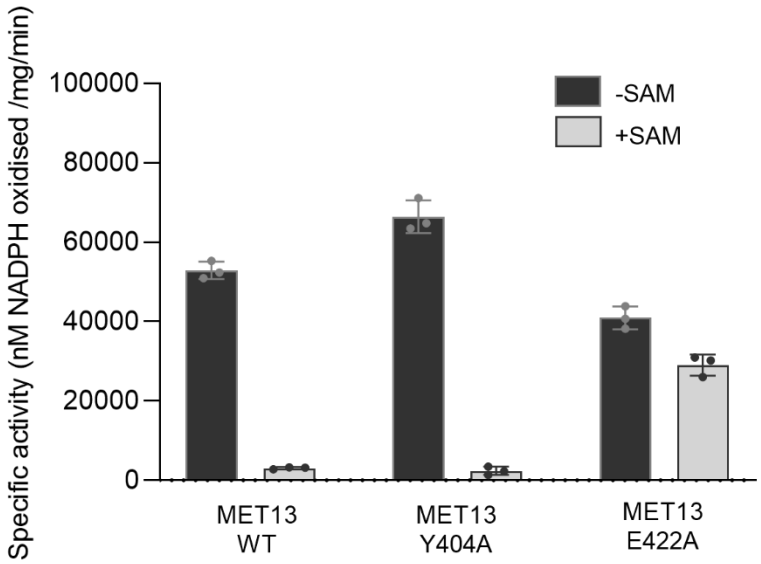

Figure 3.7 MET13_E422A, but not MET13_Y404A mutant, predicted from the modelling studies, shows a partial loss of regulation by SAM.

Measurement of catalytic activity of MET13_WT and its structural mutants, MET13_Y404A and MET13_E422A, without and with 200µM SAM, was performed using NADPH-menadione oxidoreductase assay as described in materials and methods section. The activity was calculated as the rate of disappearance of NADPH by monitoring absorbance at A_{343} nm and using the extinction coefficient of NADPH as 6220 M^{-1} cm^{-1}. The concentration of the protein samples measured using the Bradford assay was used for calculating the specific activities of all the purified protein samples. The experiment was done thrice, along with three technical replicates for each sample protein. The graph here corresponds to the representative data set plotted using the average of the three technical replicates along with ±S.D values.

3.2.4. MET13_E422A mutant with partial loss in SAM-mediated regulation shows a mild growth defect in methionine medium: A possible screen for deregulated mutants

The two mutants, MET13_Y404A and MET13_E422A, were also assayed for functionality, i.e., the ability to complement the *S. cerevisiae met13Δ* strain and for growth behavior in different media conditions. We transformed these mutants in a *met13Δ* strain, which is a methionine auxotroph, and monitored their growth on minimal media supplemented with different sulfur sources (GSH, cysteine, homocysteine, SAH, SAM, and methionine). Both the mutants were functional, as indicated in Figure 3.8. Interestingly, MET13_E422A but not the wild-type and MET13_Y404A mutant showed a minor defect in growth on methionine media (Figure 3.8). Considering the observation that MET13_E422A mutant was also defective in

SAM-mediated regulation, these results suggested that defective growth on methionine media as a possible screen for deregulated MTHFR mutants.

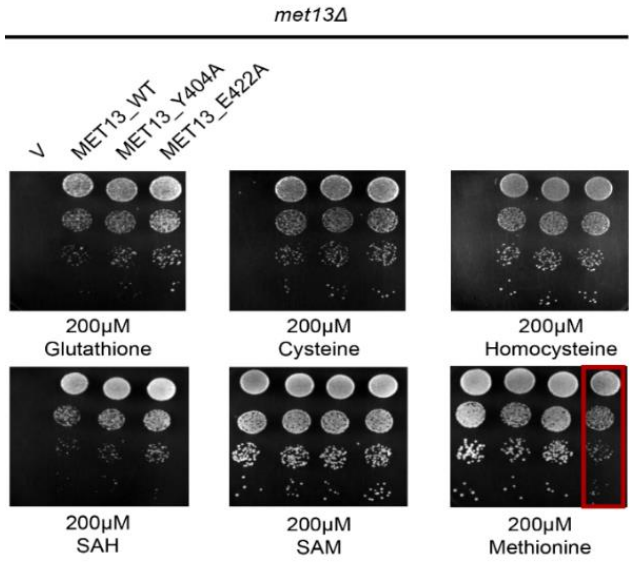

Figure 3.8 MET13_E422A mutant with partial loss in SAM-mediated regulation shows a mild growth defect in methionine medium: A possible screen for deregulated mutants.
The *S. cerevisiae met13*Δ strains transformed with vector control, MET13_WT, MET13_Y404A, and MET13_E422A, were grown to exponential phase in minimal medium containing 200μM glutathione, harvested, washed, re-suspended in water, and serially diluted to give 0.1, 0.01, 0.001, and 0.0001 OD_{600} of cells. Ten microliters of these dilutions were spotted on a minimal medium containing 200μM of different sulfur sources (GSH, cysteine, homocysteine, SAH, SAM, and methionine). The photographs were taken after 48 hours of incubation at 30°C. The experiment was repeated three times, and a representative data set is shown in the above figure.

To further examine the defective growth on methionine as a possible screen for evaluating MTHFR mutant proteins for deregulated phenotype, we examined a chimeric protein that has been previously cloned and characterized, in yeast, for being insensitive to inhibition by SAM (Roje et al., 2002). This clone had been generated by fusing the catalytic domain of *S. cerevisiae* MTHFR protein with the regulatory domain of *A. thaliana*. We expressed this chimeric protein downstream of the TEF promoter and compared the growth of the *met13Δ* strain transformed with the chimeric clone on GSH as well as methionine media. The clone was functional, as seen by its ability to complement the growth defect on GSH

(Figure 3.9). Interestingly, this clone, which has been reported to be devoid of SAM regulation, exhibited defective growth on methionine medium (Figure 3.9). These results further demonstrated that the defective methionine growth could be a valid aid for evaluating MTHFR mutants for deregulation in yeast.

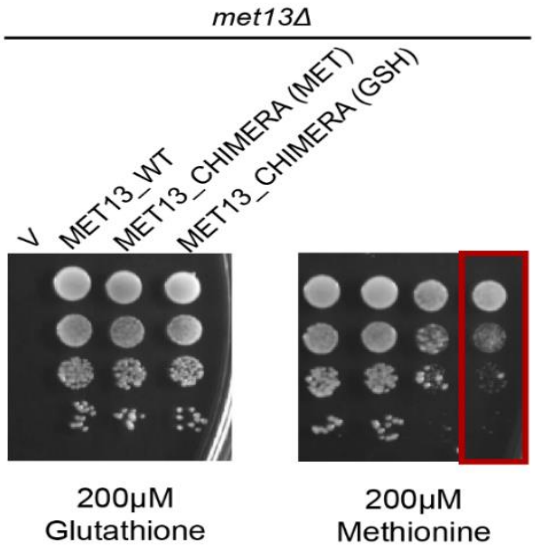

Figure 3.9 MET13_Chimera displays growth defect on methionine media
*S. cerevisiae met13*Δ strains transformed with vector control, MET13_WT, and MET13_Chimera were grown to exponential phase in minimal medium containing 200µM glutathione, harvested, washed, re-suspended in water, and serially diluted to give 0.1, 0.01, 0.001, and 0.0001 OD_{600} of cells. Ten microliters of these dilutions were spotted on a minimal medium containing either 200µM GSH or 200µM methionine as the sulfur source. The photographs were taken after 48 hours of incubation at 30°C. The experiment was repeated three times, and a representative data set is shown in the above figure.

3.2.5. Mutational analysis of different regions of the regulatory domain of MTHFR reveals a region in CR1 is critical for SAM regulation, with major defects in growth seen in these deregulated mutants

In addition to the residues predicted by structural modeling and docking, we also carried out, in parallel, a systematic mutational analysis of the regulatory domain. The three conserved regions within the regulatory domain- CR1, CR2, and CR3, were targeted for mutagenesis. In these regions, we created the mutants M1, M2, M4, M5, and M6. M1 (R344A, T345A) and

M2 (R357A, S361A) were mutants in the CR1 region, M4 (T440A, N442A, S443A, Q444A, P445A) was in the CR2 region, while M5 (T519A, W520A) and M6 (F523A, P524A, E527A) were mutations made in the CR3 region (Figure 3.3) (Table 3.1). We conducted a similar plate-based assay, as mentioned in section 3.2.3, to check these clones for functionality as well as for the deregulated phenotype. Mutants in all three conserved regions were functional (Figure 3.10). However, the MET13_M2 mutant showed a severe growth defect in the methionine medium (Figure 3.10). The mutation MET13_M1, also within the CR1 region, did not, however, show a growth defect. None of the other mutants of CR2 or CR3 (M4, M5, and M6) exhibited any growth defect in any of the tested sulfur sources. Therefore, among these three conserved regions (CR1, CR2, and CR3), we found that a specific region within CR1 might be critical for regulation by SAM, as suggested by the growth of methionine medium.

Table 3.1 Regulatory domain mutants of CR1, CR2, and CR3 of the Met13p

Mutant Name	Residues Mutated	Region of Regulatory Domain
M1	R344A.T345A	CR1
M2	R357A.S361A	CR1
M4	T440A.N442A.S443A.Q444A.P445A	CR2
M5	T519A.W520A	CR3
M6	F523A.P524A.E527A	CR3

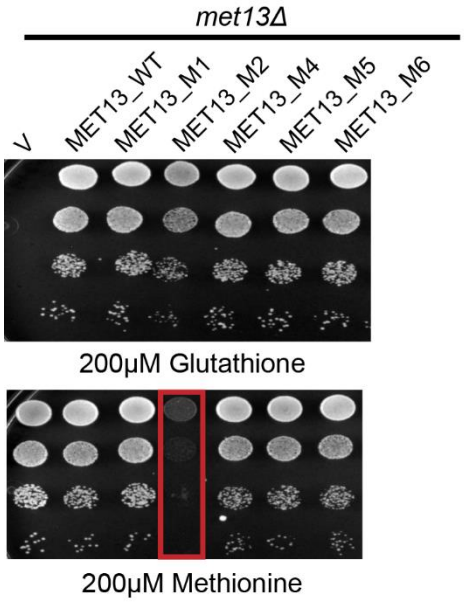

Figure 3.10 Combinatorial mutational assessment of CR1, CR2, and CR3 reveals that CR1 is critical for regulation by SAM

*S. cerevisiae met13*Δ strains transformed with vector control, MET13_WT, and conserved region mutants (MET13_M1, MET13_M2, MET13_M4, MET13_M5, MET13_M6) selected on 200μM glutathione were grown to exponential phase in minimal medium containing 200μM glutathione, harvested, washed, re-suspended in water, and serially diluted to give 0.1, 0.01, 0.001, and 0.0001 OD_{600} of cells. Ten microliters of these dilutions were spotted on minimal medium containing either 200μM GSH or 200μM methionine as the sulfur source. The photographs were taken after 48 hours of incubation at 30°C. The experiment was repeated three times, and a representative data set is shown in the above figure.

3.2.6. MET13_M2 mutant within the CR1 region completely lacks allosteric regulation by SAM

As the MET13_M2 (R357A, S361A) mutant presented a severe growth defect on methionine media, it suggested that the mutant enzyme might be displaying a deregulated phenotype. To evaluate this mutant for deregulation, we purified recombinant MET13_M2 from *E. coli* and performed the MTHFR assays. We measured the activity of the mutant in the absence and presence of SAM. In agreement with plate assays for functionality, the MET13_M2 mutant was functional and exhibited no inhibition of activity even in the presence of 200μM SAM (Figure 3.11). Thus, the MET13_M2 (R357A, S361A) mutant is completely devoid of allosteric inhibition by SAM.

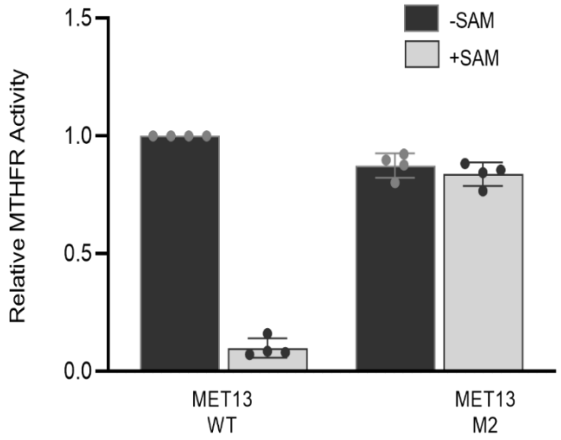

Figure 3.11 MET13_M2 mutant within the CR1 region completely lacks allosteric regulation by SAM

Measurement of catalytic activity of MET13_WT and MET13_M2 mutant, without and with 200µM SAM, was performed using NADPH-menadione oxidoreductase assay. The activity was calculated as the rate of disappearance of NADPH by monitoring absorbance at A_{343} nm and using the extinction coefficient of NADPH as 6220 M^{-1} cm^{-1}. The experiment was done twice, and relative activity was plotted by using the activity of the wild-type protein in the absence of SAM as the normalizing factor. The graph here corresponds to the representative data set for one of the experiments.

3.2.7. Alanine mutant of R357 residue of MET13_M2 mutant is responsible for the deregulated phenotype

The MET13_M2 carries two mutations, R357A and S361A. To determine whether both R357A and S361A together contributed to this phenotype or whether a mutation in any one of them alone was sufficient to cause deregulation, we generated independent single point alanine mutants, MET13_R357A and MET13_S361A. This was followed by an examination of their growth on media supplemented with 200µM GSH or 200µM methionine, respectively. Like the MET13_M2 mutant, both MET13_R357A and MET13_S361A were functional (Figure 3.12). However, the deregulated phenotype was presented only by MET13_R357A and not by the MET13_S361A mutant (Figure 3.12). Thus, the deregulation of MET13_M2 could be attributed to the R357A mutation of Met13p. This was subsequently confirmed by *in-vitro* purification and enzyme inhibition studies (Figure 3.13).

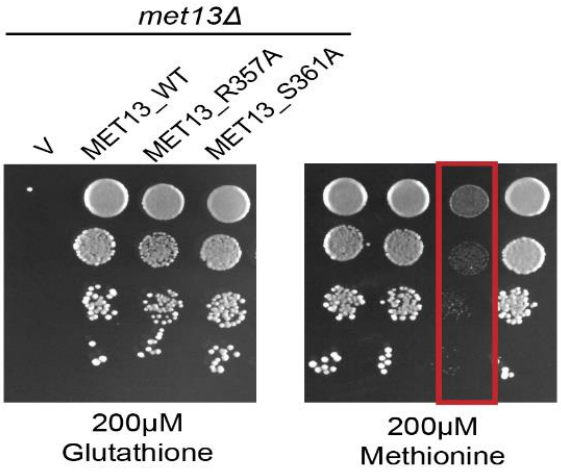

Figure 3.12 Alanine mutant of R357 residue of MET13_M2 mutant is responsible for the deregulated phenotype

*S. cerevisiae met13*Δ strains transformed with vector control, MET13_WT, MET13_R357A, and MET13_S361A selected on 200µM glutathione were grown to exponential phase in minimal medium containing 200µM glutathione, harvested, washed, re-suspended in water, and serially diluted to give 0.1, 0.01, 0.001, and 0.0001 OD_{600} of cells. Ten microliters of these dilutions were spotted on a minimal medium containing either 200µM GSH or 200µM methionine as the sulfur source. The photographs were taken after 48 hours of incubation at 30°C. The experiment was repeated thrice, and a representative data set is shown in the above figure.

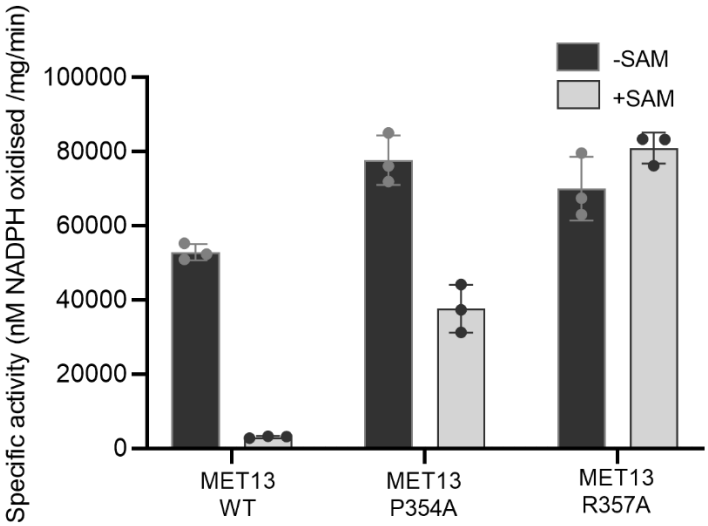

Figure 3.13 *In-vitro* MTHFR activity and inhibition assays reveal a complete loss of regulation of MET13_R357A mutant by SAM.

Measurement of catalytic activity of MET13_WT, MET13_P354A, and MET13_R357A, without and with 200µM SAM, was performed using NADPH-menadione oxidoreductase assay as described in the materials and methods section. The activity was calculated as the rate

of disappearance of NADPH by monitoring absorbance at A_{343} nm and using the extinction coefficient of NADPH as 6220 M^{-1} cm^{-1}. The concentration of the protein samples measured using the Bradford assay was used for calculating the specific activities of all the purified protein samples. The experiment was done thrice, along with three technical replicates for each sample protein. The graph here corresponds to the representative data set plotted using the average of the three technical replicates along with ±S.D values.

3.2.8. A short stretch (residues F353 to G359) within CR1 is critical for MTHFR regulation

To determine whether R357 alone was responsible for deregulation or whether other amino acids within the CR1 region might be important, we carried out a more detailed analysis of the CR1 region. We made individual alanine mutants for eleven of the conserved residues within CR1 (S340, Y341, R344, T345, W348, F353, P354, G356, R357, G359, and S361) and checked their growth on methionine medium. The mutants were functional, as seen by functional complementation of *met13Δ* strain on GSH supplemented media. The methionine specific growth defect was demonstrated by F353A, P354A, G356A, R357A, G359A mutants of Met13p (Figure 3.14A). This analysis of the CR1 region spanning 340-361 residues indicated that the stretch 353-359 seems critical for MTHFR regulation by SAM (Figure 3.14B) since residues outside this region did not exhibit any growth defect on methionine medium.

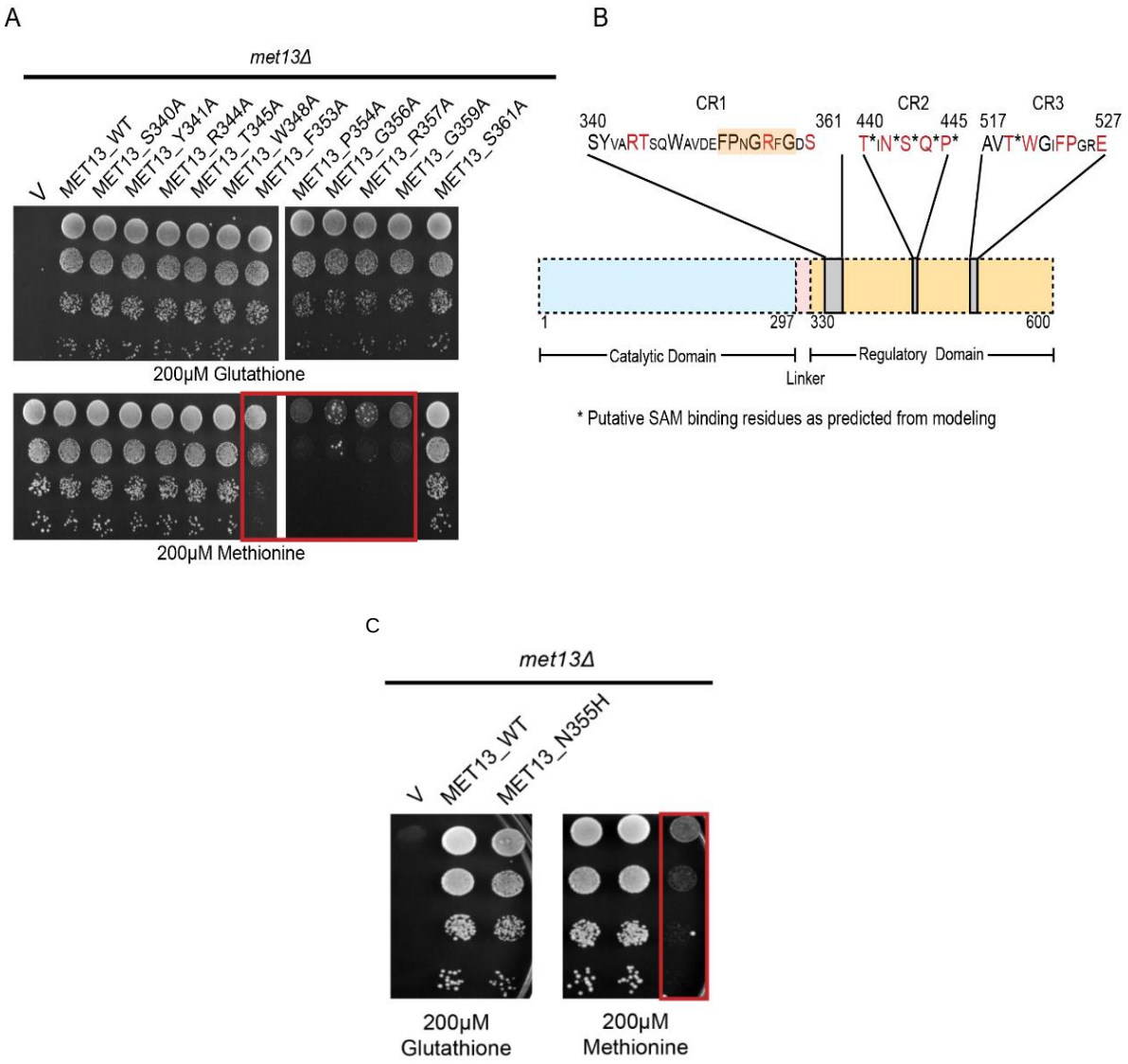

Figure 3.14 A short stretch (residues from F353 to G359) within CR1 is critical for MTHFR regulation.

(A) *S. cerevisiae met13*Δ strains transformed with vector control, MET13_WT, and single point alanine mutants of conserved residues (S340A, Y341, R344, T345, W348, F353, P354, G356, R357, G359, and S361) within CR1 were selected on 200μM glutathione. These transformants were grown to exponential phase in minimal medium containing 200μM glutathione, harvested, washed, re-suspended in water, and serially diluted to give 0.1, 0.01, 0.001, and 0.0001 OD_{600} of cells. Ten microliters of these dilutions were spotted on a minimal medium containing either 200μM GSH or 200μM methionine as the sulfur source. The photographs were taken after 48 hours of incubation at 30°C. The experiment was repeated three times, and a representative data set is shown in the above figure. (B) Schematic with residues highlighted in orange within CR1 that are crucial for MTHFR regulation by SAM, as indicated by plate-based growth assays. (C) Dilution spotting of *S. cerevisiae met13*Δ strains transformed with MET13_N355H clone was performed by growing the transformants to exponential phase in minimal medium containing 200μM glutathione, which was later harvested, washed, re-suspended in water, and serially diluted to give 0.1, 0.01, 0.001, and 0.0001 OD_{600} of cells. Ten

microliters of these dilutions were spotted on minimal medium containing either 200μM GSH or 200μM methionine as the sulfur source. The photographs were taken after 48 hours of incubation at 30°C. The experiment was repeated three times, and a representative data set is shown in the above figure.

In the above results, we inferred that the residues 355 and 358, sandwiched between amino acids 353-359, might be crucial for the regulation of Met13p; however, these residues were not examined since they were not conserved among other organisms. At position 355, asparagine, a neutral amino acid residue, was replaced by histidine, a positively charged amino acid, exclusively in plants, and at 358, there was a synonymous substitution in the case of yeast by phenylalanine as opposed to tryptophan in all the others. *A. thaliana* MTHFR has been previously shown to be SAM insensitive (Roje et al., 1999) and only differ at this particular amino acid in this short stretch within CR1. Hence, rather than making an alanine mutant, we substituted asparagine to histidine and studied its impact using the plate-based assay. MET13_N355H mutant was functional as seen by growth on GSH plates, and like the other deregulated mutants of CR1, presented a growth defect on methionine media (Figure 3.14C). Together these results confirmed that a short stretch of amino acids (F353, P354, N355, G356, R357, and G359) within CR1 is critical for the regulation of MTHFR protein by SAM.

3.2.9. *In-vitro* MTHFR activity and inhibition assays reveal a complete loss of regulation of MET13_R357A mutant by SAM

MET13_P354A and MET13_R357A, two of the representative CR1 mutants, which display the most severe growth defect in the methionine supplemented media, were examined by NADPH-menadione oxidoreductase assay for SAM insensitivity. The catalytic activity in the absence of SAM for both MET13_P354A and MET13_R357A was slightly higher than the wild-type protein (Figure 3.13). Additionally, both these mutants retained MTHFR activity even in the presence of SAM (Figure 3.13). MET13_P354A was partially inhibited (repression, 50%), whereas MET13_R357A completely lacked inhibition. This fully deregulated yeast

MTHFR protein that we have isolated for the first time (MET13_R357A), which exhibits a methionine specific growth defect in SD minimal media and is insensitive to SAM as evaluated by *in-vitro* inhibition assay, should be a useful aid in understanding the physiological implications MTHFR regulation by SAM.

3.2.9.1. The methionine growth defect of feedback insensitive, deregulated MET13 mutant (MET13_R357A) requires a functionally active enzyme

The feedback insensitive, deregulated mutants showed a severe growth defect on methionine plates. The possibility existed that the growth defect of these mutants was unrelated to their activity and was a consequence of the interference of these mutants with some other protein or an unrelated pathway. It was, therefore, necessary to establish that the growth defect of these mutants was due to their unregulated activity. One way of establishing this link was to create a catalytically inactive mutation of the deregulated MTHFR. Therefore, we created a mutation of the active site residue of MTHFR, E22 (Trimmer et al., 2001). An E22A led to an inactive MTHFR, as seen by its inability to complement the *met13Δ* defect (Figure 3.15). We then introduced this E22A mutation in the R357A deregulated mutant background. Here, we observed that the R357A deregulated mutant carrying the E22A mutation no more displayed the growth defect on methionine (Figure 3.15). This result established that the deregulated mutants displayed the methionine growth defect due to the deregulated property of MTHFR.

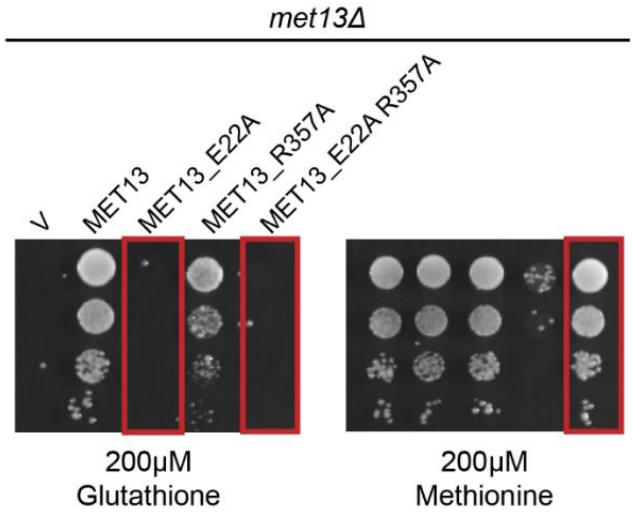

Figure 3.15 The methionine growth defect of feedback insensitive, deregulated MET13 mutant (MET13_R357A) requires a functionally active enzyme.
*S.cerevisiae met13*Δ strains transformed with vector control, MET13_WT, MET13_E422A (catalytically inactive mutant), MET13_R357A, and MET13_E22A.R357A were selected on 200µM glutathione. These transformants were grown to exponential phase in minimal medium containing 200µM glutathione, harvested, washed, re-suspended in water, and serially diluted to give 0.1, 0.01, 0.001, and 0.0001 OD_{600} of cells. Ten microliters of these dilutions were spotted on a minimal medium containing either 200µM GSH or 200µM methionine as the sulfur source. The photographs were taken after 48 hours of incubation at 30°C. The experiment was repeated three times, and a representative data set is shown in the above figure.

3.2.9.2. MET13_R357A mutant exhibits a deregulated phenotype even under the native promoter

The plate-based assays described so far have all been done with the Met13p expressed downstream of the TEF promoter, which is a strong and constitutive promoter. Thus, it was possible that these phenotypes were a consequence of substantial overexpression. To establish if even the natively expressed Met13p bearing the deregulated mutation showed a growth phenotype, we cloned the MET13_R357A gene under its native promoter and tested it for deregulation using different concentrations of methionine (0.005mM, 0.05mM, 0.2mM, 0.5mM, 1.0mM, and 2.0mM). The clone was functional, as seen by the complementation of *met13Δ* in GSH media (Figure 3.16). The growth defect exhibited by MET13_R357A expressed under the TEF promoter was observed at 0.005mM methionine and became more

severe at 0.2mM methionine. In contrast, MET13_R357A, when expressed under its native promoter, showed deregulation only at 10 fold higher methionine concentrations starting from 0.05mM and was more severe at 2mM (Figure 3.16). Thus even when expressed under the native promoter, the growth defects were observed, although owing to the slightly weaker promoter (compared to TEF), the effects were more visible only at higher methionine concentration.

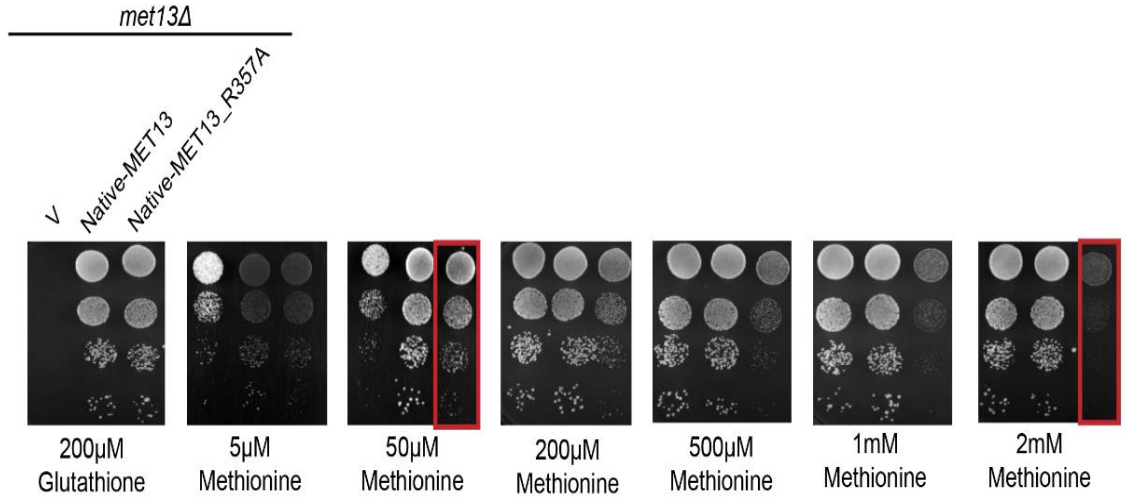

Figure 3.16 MET13_R357A mutant exhibits a deregulated phenotype even under the native promoter.
*S. cerevisiae met13*Δ strains transformed with vector control, MET13_WT, and MET13_R357A expressed under native promoter were selected on 200µM glutathione. These transformants were grown to exponential phase in minimal medium containing 200µM glutathione, harvested, washed, re-suspended in water, and serially diluted to give 0.1, 0.01, 0.001, and 0.0001 OD_{600} of cells. Ten microliters of these dilutions were spotted on a minimal medium containing 200µM GSH and a range of methionine concentrations (0.005- 2.0mM) as the sulfur source. The photographs were taken after 48 hours of incubation at 30°C. The experiment was repeated three times, and a representative data set is shown in the above figure.

3.2.9.3. Defective growth of MET13_R357A on methionine media in the presence of endogenous WT copy of gene suggests the dominant nature of this mutation

The functional complementation of the mutants and the growth defects on methionine were all examined in a *met13Δ* background. Therefore, we were interested in determining whether the defective growth on methionine shown by the deregulated mutant was observed even in the

presence of a wild-type Met13p. We, therefore, transformed a wild-type strain, with a functional Met13p, with the mutant. We also used a strain that was wild-type for MET15 so that it was not a methionine auxotroph. A similar methionine specific growth defect of the MET13_R357A clone was observed at identical methionine concentration (200µM) in the parental background, BY4742 (Figure 3.17). This suggests a dominant nature of the deregulated MTHFR mutant.

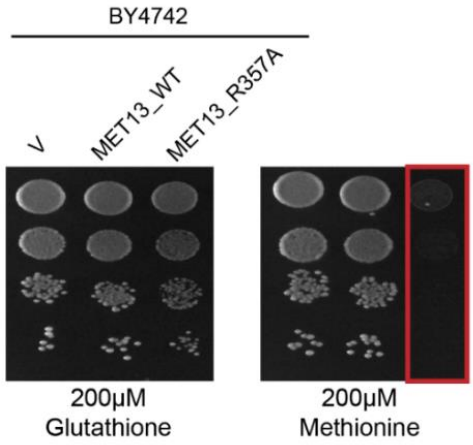

Figure 3.17 Defective growth of MET13_R357A on methionine media in the presence of endogenous wild-type copy of gene suggests the dominant nature of this mutation.
WT *S. cerevisiae* strains transformed with vector control, MET13_WT and MET13_R357A selected on 200µM glutathione were grown to exponential phase in minimal medium containing 200µM glutathione, harvested, washed, re-suspended in water, and serially diluted to give 0.1, 0.01, 0.001, and 0.0001 OD_{600} of cells. Ten microliters of these dilutions were spotted on a minimal medium containing either 200µM GSH or 200µM methionine as the sulfur source. The photographs were taken after 48 hours of incubation at 30°C. The experiment was repeated thrice, and a representative data set is shown in the above figure.

3.2.10. Analysis of SAM insensitive mutants for conformational changes

To understand the basis of the deregulated phenotype of the mutations based on the structure, we mapped these residues on the modeled crystal structure of yeast MTHFR. Interestingly, the residues, F353 to G359, mapped on the interfacial region of the two monomers of the protein, which interacted through its regulatory domain (Figure 3.18). It was possible, therefore, that these SAM insensitive mutants led to an altered oligomerization state and was responsible for the lack of inhibition by SAM. Hence, we examined the oligomeric status of these mutants with

the help of gel filtration chromatography. Both MET13_WT, as well as the deregulated mutants, MET13_P354A and MET13_R357A, presented similar profiles with two peaks, a smaller one corresponding to higher oligomer (tetramer) and a major peak of the dimeric form of the protein (Figure 3.19). Thus, the deregulated behavior of these conserved region mutants could not be explained by the altered oligomeric condition of the protein.

Next, we examined these SAM insensitive mutants for the lack of SAM binding using modified limited proteolysis experiments, as has been described previously for mammalian MTHFR protein (Sumner, Jencks, Khani, Matthews, et al., 1986). The tryptic digestion pattern for wild-type as well as mutant protein (MET13_R357A) with and without SAM (200μM) seemed more identical, each having a half-life of approximately 20 minutes for the full-length protein of about 70 kDa (Figure 3.20). In one of the experiments, the mutant degraded in less than 20 minutes (data not shown), but these results were not reproducible. To further probe the presence of any conformational differences among the wild-type and mutant proteins, we probed the melting temperatures of these proteins using Circular Dichroism (CD) studies. The CD studies gave identical Tm values of 57.19˚C for MET13_WT protein and 57.78˚C for MET13_R357A mutant protein (Figure 3.21). Therefore, these experiments fail to show any significant differences in the conformation of the mutant protein.

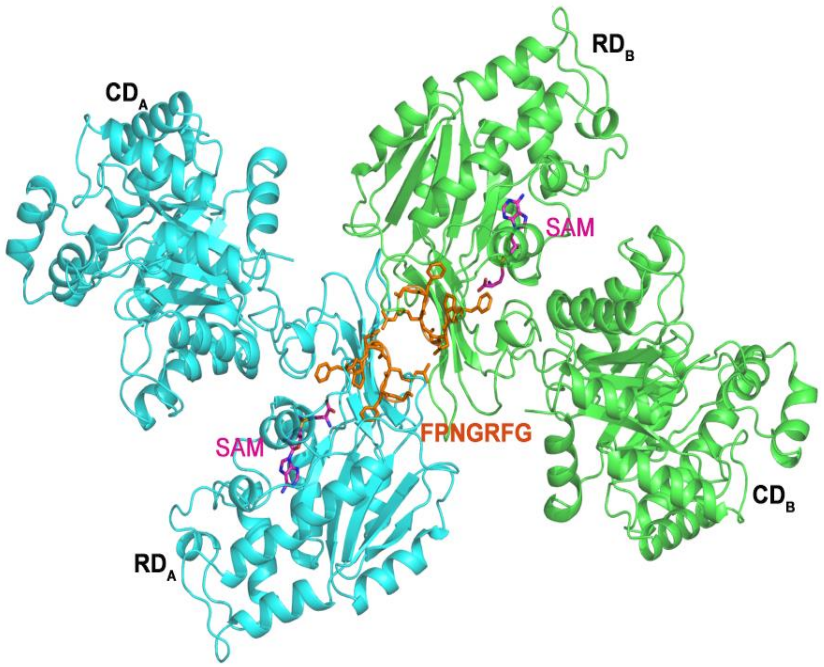

Figure 3.18 Deregulated MET13 mutants mapped to the interfacial region of the two monomers.

The panel on the right is a zoomed out version of the figure on the left specifying the position of the deregulated Met13p mutants (indicated in orange sticks) on modeled yeast MTHFR. The cartoon representations in light cyan and green were used for distinguishing between the two monomers.

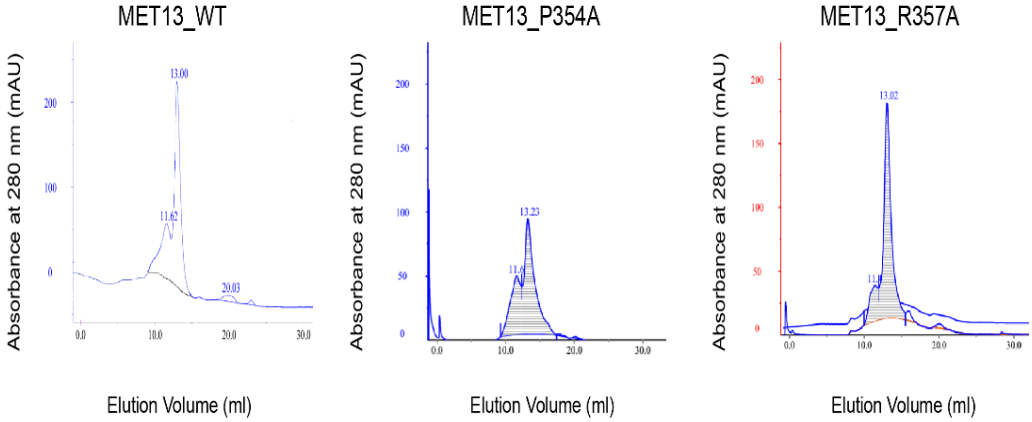

Figure 3.19 Size-exclusion chromatograms of wild-type and deregulated Met13p

Purified proteins of MET13_WT and two representatives of the deregulated proteins, MET13_P354A and MET13_R357A (1.5mg/ml), were examined for changes in oligomeric status using analytical size-exclusion chromatography on Superdex-200 column. Peak area calculations, which have been depicted in Table 3.2, were done using the Unicorn Analysis software of GE healthcare.

Table 3.2 Size-exclusion chromatography profiles of wild-type and deregulated mutant

Protein Sample	Elution Volume Peak 1 (ml)	Area Peak 1 (mAU*ml)	Elution Volume Peak 2 (ml)	Area Peak 2 (mAU*ml)
MET13_WT	11.62	39.8 (17.1%)	13.00	192.9 (82.9%)
MET13_P354A	11.62	80.7 (33.7)	13.23	158.8 (66.3%)
MET13_R357A	11.42	35.8 (15.3%)	13.02	198.3 (84.7)

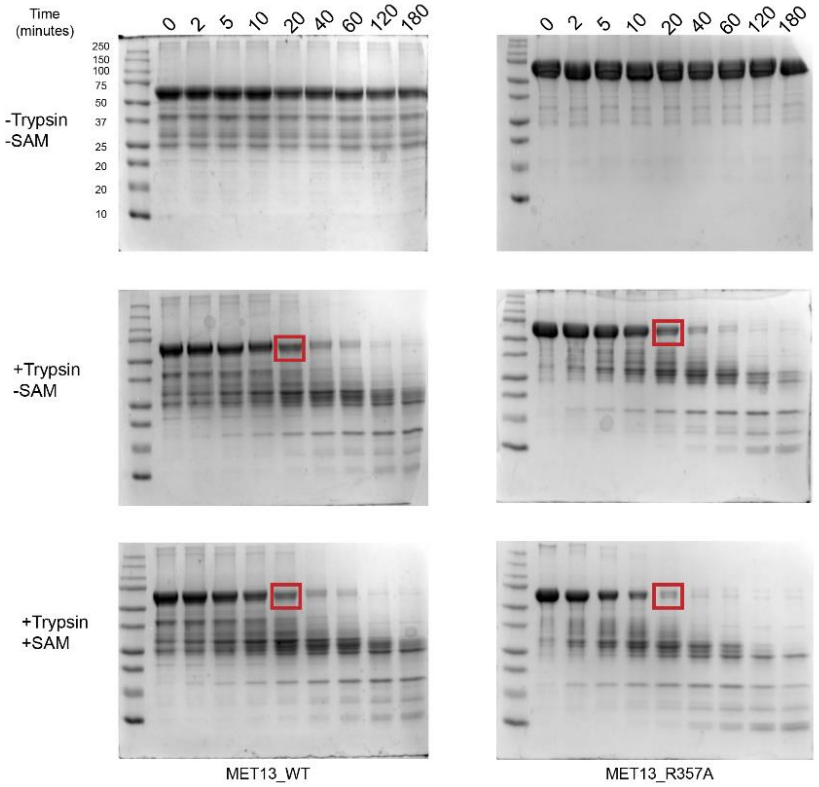

Figure 3.20 Limited proteolysis analysis of wild-type and deregulated Met13p.
Purified MTHFR wild-type and deregulated enzyme (5µM) was treated with trypsin (0.01% w/w) with and without 200µM SAM, the mixture was incubated at 25˚C, and the aliquots were removed at the indicated time points. The digestion reaction was quenched by boiling the samples in SDS PAGE sample loading buffers. Aliquots were then subjected to SDS PAGE and stained using coomassie brilliant blue R-250 (0.25% w/v). As indicated, different gels represent different reaction conditions; top panel: no trypsin, middle panel: enzyme+trypsin, lower panel: enzyme+SAM+trypsin. The experiment was repeated at least three times, and a representative data set that was most consistent is shown in the above figure.

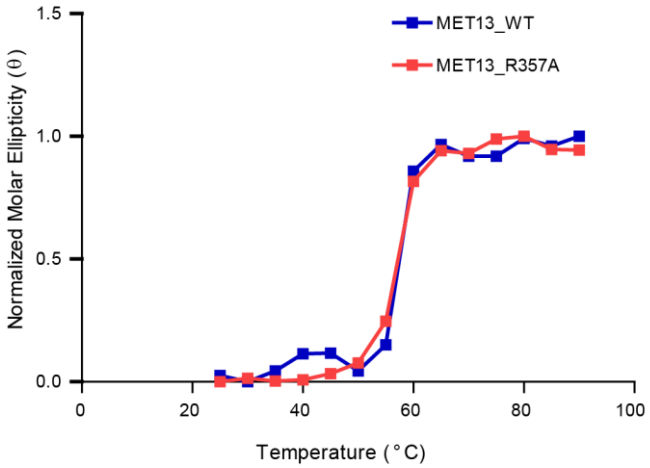

Figure 3.21 Melting temperature studies of MET13_WT and MET13_R357A mutant using CD spectroscopy.

Tm analysis for MET13_WT and MET13_R357A (3µM) proteins was performed using Circular dichroism. CD Spectra (200-280 nm) for both the proteins diluted in potassium phosphate buffer (50mM, pH 7.2) containing 0.3mM EDTA was collected beginning at 25˚C. An increment of 5˚C was done until the temperature was increased to 90˚C. Protein was held at a given temperature for 5 minutes. This experiment was done only once.

3.3. Discussion

I have described in this chapter the isolation of mutants in the regulatory region of MTHFR that shows a lack of inhibition by SAM. SAM mediated inhibition of MTHFR has been considered to be a key regulatory feature in one-carbon metabolism ever since the discovery of allosteric inhibition of mammalian MTHFR by SAM (Kutzbach & Stokstad, 1967, 1971). However, there was neither direct evidence for the presence of this regulation *in vivo* nor clear demonstrations of the regions in the regulatory region that was important for this control. The current studies, therefore, provide this evidence for regulation *in vivo* and helps in delineating the residues in MTHFR critical for this feedback inhibition. We have been able to demonstrate this by isolating, for the first time, mutants in the regulatory region of MTHFR that show a lack of inhibition by SAM.

Although peptide mapping and photo affinity labelling of the mammalian enzymes that were carried out more than 2 decades ago had suggested that the SAM binding domain lay within a 6kDa region of the regulatory region close to the junction of the Catalytic and

Regulatory domains of MTHFR, the exact residues were never delineated (Goyette et al., 1994). Recent crystal structural studies, however, had suggested residues that conflicted with the earlier mapping data (Froese et al., 2018). Therefore, we combined both structural and targeted mutagenic approaches to precisely identify SAM binding residues.

One of these mutants, E422A, was predicted to be involved in SAM binding based on the modeled structure. However, this showed only partial loss of regulation as the mutant still demonstrated partial inhibition by SAM. However, a mutation (MET13_M2) in the conserved region of the regulatory domain, CR1, showed an almost complete loss of regulation and represented the first MTHFR mutant known so far that completely lacks SAM regulation. Since this mutant also exhibits a severe growth defect in methionine medium, we used this phenotype to further define potential deregulated mutants by a systematic mutational analysis of the regulatory region. This rigorous investigation led us to pinpoint a 7 amino acid stretch, 353-F-P-N-G-R-F-G-359, within the CR1 region of the regulatory domain, as being critical for the regulation by SAM. This region falls within the 6kDa region that was earlier suggested from the photo-affinity labelling studies (Goyette et al., 1994; Matthews et al., 1998). The residue, E422, which was predicted by the modelled yeast MTHFR structure to bind to SAM (both from our work with the yeast model and the earlier human MTHFR structural studies), was, surprisingly, completely outside the CR1 region. The structural model does not indicate any proximity of E422 with the CR1 region, so the participation and involvement of E422 is unclear at present. One possibility is that at some early point of the conformational transitions, when the SAM first binds to the region in CR1, it may also be in proximity to the E422. However, this awaits more dynamic insights into the process. Importantly, the CR1 region mapped to the interfacial region between the two monomers on the structure, and thus it would have been difficult to predict the involvement of these regions based on the modelled structure. Therefore,

combining both structural approaches and targeted mutagenic approaches yielded valuable insights into the regions of the protein that are likely to determine regulation by SAM.

One important outcome of this study is also the development of a simple assay or screen for isolating or evaluating deregulated mutants of MTHFR. This was the methionine-dependent growth defect, which was consistently observed with the deregulated mutants. The reason for this growth defect is the subject of the investigation of the next chapter.

Chapter-4

Deregulation of MTHFR disrupts the redox and metabolic homeostasis in *S. cerevisiae*

4. Chapter 4

4.1. 4.1 Introduction

MTHFR is an enzyme that links the folate cycle to the methionine cycle in one-carbon metabolism. As explained earlier, previous studies with the purified eukaryotic MTHFR have revealed that the enzyme is under allosteric inhibition by S-Adenosyl methionine (SAM) (Appling, 1991; Bagley & Selhub, 1998; Kutzbach & Stokstad, 1967, 1971). Although this allosteric regulation has been known for decades, the importance of this regulatory control to one-carbon metabolism has never been adequately understood, as mutants defective in this regulation have never been obtained.

In the earlier chapter, I have described the isolation and characterization of deregulated mutants of MTHFR that lack feedback inhibition by SAM. Importantly, we had discovered a growth phenotype of such mutants in methionine medium. In this chapter, we have tried to explore in detail the consequences of MTHFR deregulation and the reason behind the greater growth defect seen in the methionine medium. To understand the metabolic consequences, we have carried out biochemical and metabolite analysis. We have investigated the folate and methionine cycles. In addition, we have also investigated the transsulfuration pathway metabolites. Since NADPH and FAD are the cofactors of the MTHFR enzyme, we investigated how the levels of these cofactors were affected as a consequence of deregulation. The impact on redox homeostasis was also examined. We have observed that both the folate and methionine cycles were affected in these mutants, as was the transsulfuration pathway leading to decreased formation of glutathione and its precursors critical for redox homeostasis. The major consequences appeared to be in the depletion of nucleotides. Folates are precursors to nucleotides, but folate supplementation led to only partial recovery. ^{13}C isotope labelling and metabolic studies revealed that the deregulated MTHFR cells undergo continuous transmethylation of homocysteine by CH_3THF to form methionine, which drives SAM

formation accentuating the ATP depletion. SAM was also cycled back, leading to futile cycles of SAM synthesis and recycling. This also explains the need for MTHFR to be regulated by SAM, and the study has yielded valuable insights into one-carbon metabolism.

4.2. 4.2 Results

4.2.1. MTHFR deregulation disrupts the cellular folate and nucleotide pools

MTHFR is an enzyme that straddles two cycles, the folate cycle and the methionine cycle. It is also a key regulatory step in 1-C metabolism. Therefore, it was possible that the deregulated enzyme might impact the metabolic homeostasis of both cycles, although which of the cycles might be primarily affected was difficult to predict. As MTHFR deregulated enzymes have not been isolated earlier, it was, therefore, important for us to investigate the metabolic consequences. We, in particular, exploit the acute phenotype seen in the methionine medium for our analysis.

We first examined the folate pools and whether cells might be facing folate deficiency owing to the deregulated MTHFR. Although plasma membrane folate transporters have not yet been reported in yeast, we nevertheless supplemented cells with an increasing concentration of folic acid in the medium. At higher concentrations of folic acid, we observed a significant rescue of growth (Figure 4.1A). To further define which pools were deficient, we decided to examine the steady-state levels of the different folate pools. Although folate pools are continuously cycling and are also difficult to measure reliably owing to their lability, we nevertheless attempted to estimate these pools. Using LC-MS/MS analysis, we observed a decrease in the levels of the substrate of MTHFR, CH_2THF (p-value = 0.1) in the deregulated mutant, MET13_R357A, whereas pools of the product of MTHFR, CH_3THF, appeared to be higher in the mutant (p-value = 0.25) (Figure 4.1 B). The levels of these two folate intermediate (CH_2THF, and CH_3THF) indicated increased activity of MTHFR while suggesting that the

cells could be facing some limitations in the pools of CH_2THF. Interestingly, an increase in the THF pools (p-value = 0.07) (Figure 4.1B) for the deregulated mutant suggested that the activity of the downstream enzyme, methionine synthase (MET6) involving the donation of the CH_3 group to homocysteine could be increased.

As CH_2THF, the substrate of MTHFR is also essential for the synthesis of nucleotides (purines and thymidine); depleted CH_2THF pools would be reflected in depleted nucleotide pools. Therefore, we determined the nucleotide levels in the MTHFR deregulated strains as a read-out of an impaired folate cycle. We observed a striking, 10-fold depletion of the cellular AMP, GMP, and CMP pools in the mutant bearing cells (Figure 4.1B). To examine whether external supplementation might rescue the growth, we performed a growth assay by supplementing mutant cells with either adenine or guanine (0.05-1mM). We observed that adenine supplementation as little as 0.05mM rescued the growth defect of the deregulated MTHFR mutant (Figure 4.1C). However, guanine at even 1mM did not restore the growth of the deregulated mutant (Figure 4.1C). A likely explanation for the inability of guanine to complement the growth defect is the inability of guanine to interconvert to adenine, while adenine is able to interconvert to guanine intracellularly (Rebora et al., 2001). Hence, the restoration of both would be required to restore cell growth. While these observations are consistent with the depletion of CH_2THF, which is the precursor in nucleotide biosynthesis, the much steeper decreases in the nucleotide levels suggested that folate depletion might be only one of the causative factors.

Figure 4

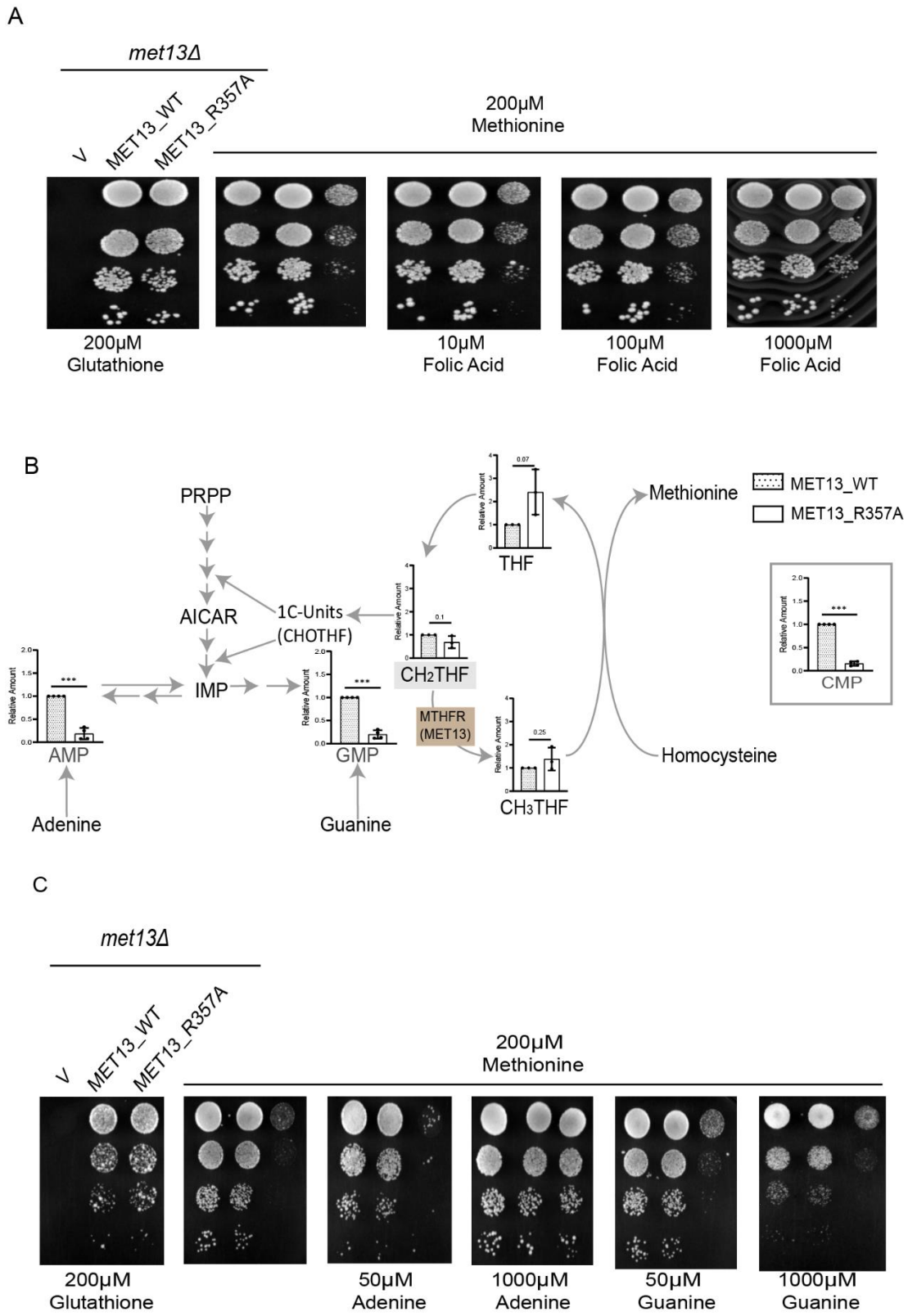

Figure 4.1 MTHFR deregulation disrupts cellular folate and nucleotide pools

(A) Yeast *met13*Δ strains transformed with vector control, MET13_WT, and MET13_R357A were grown to exponential phase in minimal medium containing 200μM glutathione, harvested, washed, re-suspended in water, and serially diluted to give 0.1, 0.01, 0.001, and

0.0001 OD_{600} of cells. Ten microliters of these dilutions were spotted on a minimal medium containing either 200μM GSH, methionine, and methionine, along with the increasing concentration of folic acid (10-1000 μM). The photographs were taken after 72 hours of incubation at 30°C. The experiment was repeated three times, and a representative data set is shown in the above figure. (B) The relative abundance of folate and nucleotide pools in transformants bearing the wild-type MET13 or deregulated mutant of yeast MTHFR, MET13_R357A. Transformants were grown overnight in SD minimal media along with GSH (200μM) as a sulfur source and re-inoculated in a medium containing methionine (200μM) and different types of folate intermediates and nucleotide intermediates were determined by LC-MS/MS. Error bars indicate SD. n = 3. *p < 0.05, **p < 0.01, ***p < 0.001. The graphs show a representative data set of three biological replicates. (C) Growth conditions same as (A) Ten microliters of these dilutions were spotted on minimal medium containing 200μM GSH, 200μM methionine, and different concentrations of either adenine or guanine (50-1000μM) in methionine supplemented plates. The photographs were taken after 48 hours of incubation at 30°C. The experiment was repeated three times, and a representative data set is shown in the above figure.

4.2.2. Cells bearing deregulated MTHFR display depleted cofactor pools

The MTHFR enzyme uses NADPH as the reducing equivalent for the catalytic activity. Additionally, it has a FAD moiety non-covalently bound to it, which is also essential for the oxidoreductase activity. Both NADPH/NADP and FAD/FADH2 derive from adenine pools. Thus with adenine pools significantly lower in the cells, these pools would also be expectedly lower. Furthermore, with unregulated MTHFR activity, the reduced NADPH pools that are required for numerous anabolic reactions would be further depleted, while the specific oxidized FAD pools that are cofactors in many essential enzymes would also be similarly depleted. We measured total NADPH/NADP pools in the cellular extracts of transformants bearing either MET13_WT or MET13_R357A plasmid. We observed an approximate 2-3 fold reduction in total NADPH/NADP pools in cells expressing the deregulated MET13 mutant when compared with the wild type cells upon growth in minimal media containing 200μM methionine media (Figure 4.2A). Deficiency in the nucleotide pools could be responsible for this significant decrease. Further, since NADPH represents approximately 95% (ratio of NADPH/NADP varies from 15-60) of the content of NADPH and NADP pools, it indicates a depletion in the

reduced NADPH pools (Zhang et al., 2016) primarily. If this is the case, then merely replenishing the reduced pools might in itself provide some benefit to the cells. We attempted to examine this by replenishing the NADPH pools by overexpression of the ZWF1 gene, which encodes glucose-6- phosphate dehydrogenase (G6PDH) enzyme. G6PDH, the first step in the pentose phosphate pathway (PPP), is the major enzyme converting NADP to NADPH, and this is the main NADPH generating enzyme in living cells (Thomas et al., 1991). We observed that the co-expression of ZWF1 with the deregulated mutant, MET13_R357A, led to a significant growth rescue (Figure 4.2B). These findings confirm that the unregulated MTHFR activity leads to the depletion of the cellular reserves of NADPH, which can be partly restored by the reductive biosynthetic activity of G6PDH.

The cofactor FAD that is bound to MTHFR plays a critical role in many other oxidoreductase reactions as well, where it aids in transferring electrons in several redox reactions. MTHFR is a flavin-dependent oxidoreductase that requires oxidized FAD for transferring the electrons and reducing equivalents to its substrate, CH_2THF (Figure 1.10). Since FAD is also derived from adenine, the deregulated cells would have lower total pools of $FAD/FADH_2$ and a higher demand for oxidized FAD. We investigated this possibility by restoring the cellular reserves of oxidized FAD. Fumarate reductase is a flavoprotein and catalyses the reduction of fumarate to succinate along with the synthesis of oxidized FAD (Figure 4.2C) (Camarasa et al., 2007). Yeast has two fumarate reductases: FRD1, a cytosolic fumarate reductase, and OSM1, a mitochondrial fumarate reductase (Enomoto et al., 2002). We co-expressed the cytosolic fumarate reductase FRD1 gene along with a deregulated Met13p and examined the growth on methionine plates. FRD1 over-expression significantly rescues the defective growth of our deregulated mutant on methionine media (Figure 4.2D). These results confirm that NADPH and oxidized FAD, both of which are required for the catalytic activity of MTHFR, becomes limiting in a deregulated mutant of MTHFR.

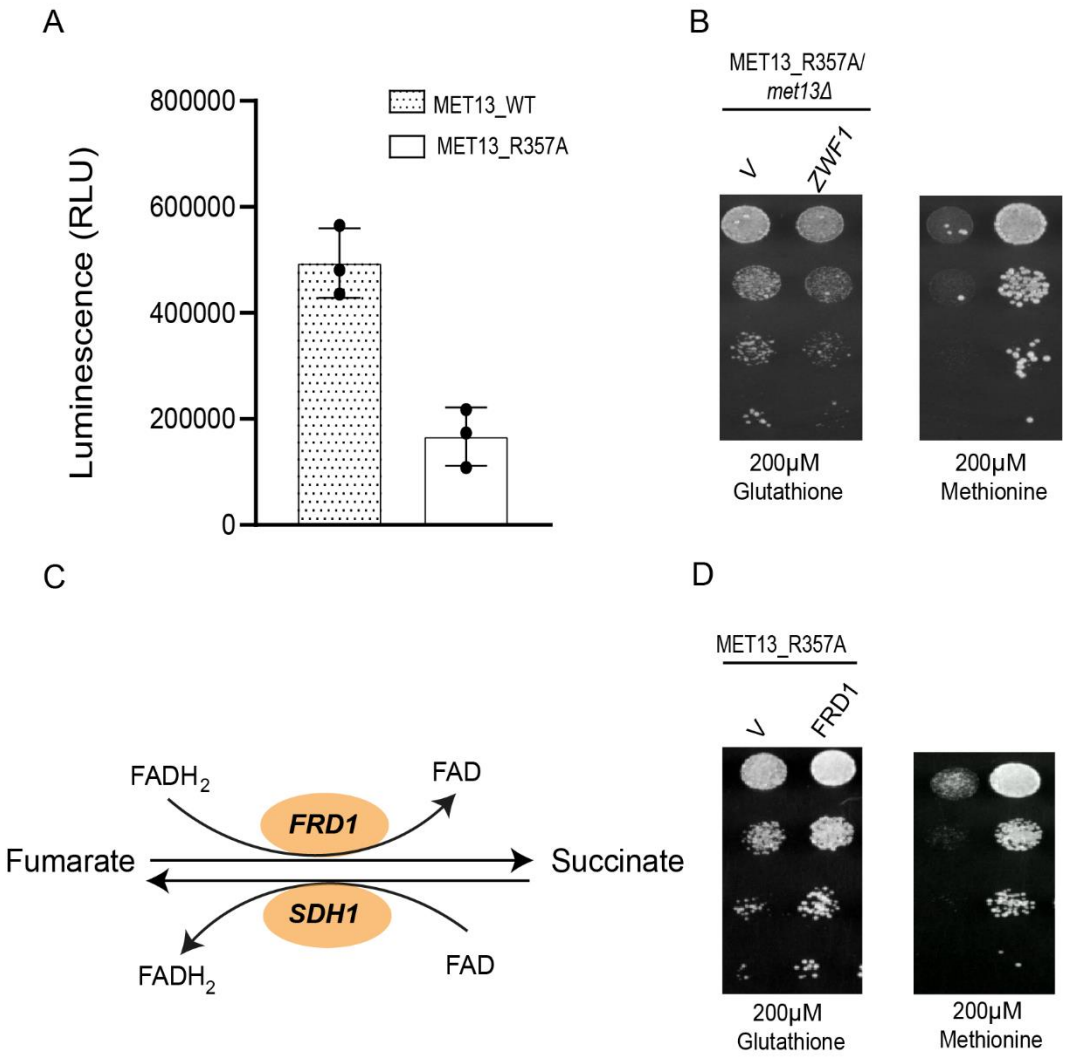

Figure 4.2 Cells bearing deregulated MTHFR display depleted cofactor pools.
(A) Intracellular levels of NADPH in transformants bearing the wild-type MET13 or deregulated mutant of yeast MTHFR, MET13_R357A. Transformants were grown overnight in SD minimal media along with GSH (200µM) as a sulfur source and re-inoculated to medium containing methionine (200µM) and NADPH estimated using NADP/NADPH-Glo™ assay kit. The graph shows a representative data set of three biological replicates. Error bars indicate SD. n = 3. *p < 0.05, and **p < 0.01 (B) The *S. cerevisiae met13*Δ strains were co-transformed with MET13_R357A and vector control of ZWF1, the transformants were grown to exponential phase in minimal medium containing 200µM glutathione, harvested, washed, re-suspended in water, and serially diluted to give 0.1, 0.01, 0.001, and 0.0001 OD_{600} of cells. Ten microliters of these dilutions were spotted on a minimal medium containing either 200µM GSH or methionine. The photographs were taken after 72 hours of incubation at 30°C. The experiment was repeated three times, and a representative data set is shown in the above figure. (C) Reaction of fumarate reduction and oxidation (D) *S. cerevisiae* wild-type strains (BY4742) were co-transformed with MET13_R357A and either vector control or FRD1. The transformants were grown, as mentioned in (B).

4.2.3. Impact of the deregulated MTHFR on amino acid pools, SAM, and glutathione

MTHFR links the folate cycle to the methionine cycle that leads to the synthesis of methionine, SAM, cysteine, and glutathione (Figure 1.2). In addition to the sulfur amino acids, cysteine, and methionine, that are required for protein biosynthesis, SAM is required for methylation in a host of reactions with lipids, proteins, and DNA. At the same time, glutathione is critical for redox homeostasis. We were, therefore, interested in understanding the consequences of MTHFR deregulation on the levels of these different sulfur metabolites, their intermediates that fall in the reverse transsulfuration pathway, and amino acid pools in general.

We carried out the analysis of the sulfur metabolites in a *met15Δmet13Δ* background. MET15 deletions are deficient in inorganic sulfur assimilation; thus, all the sulfur in such cells is derived from the organic sulfur supplemented in the medium (methionine or glutathione). The cells carried a deletion in the MET13 gene and thus lacked the endogenous MTHFR (*met13Δ*). The strains thus only carried on the plasmids, either the wild-type or mutant MTHFR. The transformants exposed to methionine were harvested at two different cell densities, i.e., OD_{600} 0.5 and 1.0, corresponding to the early and mid-exponential phase of growth, respectively, and these samples were used immediately to extract metabolites for targeted LC-MS/MS-based metabolite estimations.

Even though the cells were deregulated for MTHFR and were also grown in media containing exogenous methionine, the methionine levels surprisingly remained almost unchanged; instead, they showed a minor reduction (1.2 fold) in the mutants (Figure 4.3A-B). SAM levels were, however, increased, whereas SAH showed decreased levels in the deregulated mutant (Figure 4.3A-B). The metabolites of the reverse trans-sulfuration pathway, homocysteine, cystathionine, and cysteine, showed decreased levels, the most striking being in the levels of cystathionine (Figure 4.3A-B). We also observed lower levels of both oxidized and reduced forms of glutathione (GSH and GSSG) (Figure 4.3A-B). To confirm if the cells

were indeed facing a glutathione depletion, we examined sensitivity to methylglyoxal (MG) since GSH is required for detoxification of MG (Figure 4.4A) (Jain et al., 2018). Indeed, cells transformed with MET13_R357A showed enhanced sensitivity to MG in comparison with wild-type Met13p, suggesting that glutathione was getting depleted in these strains (Figure 4.4 B-C).

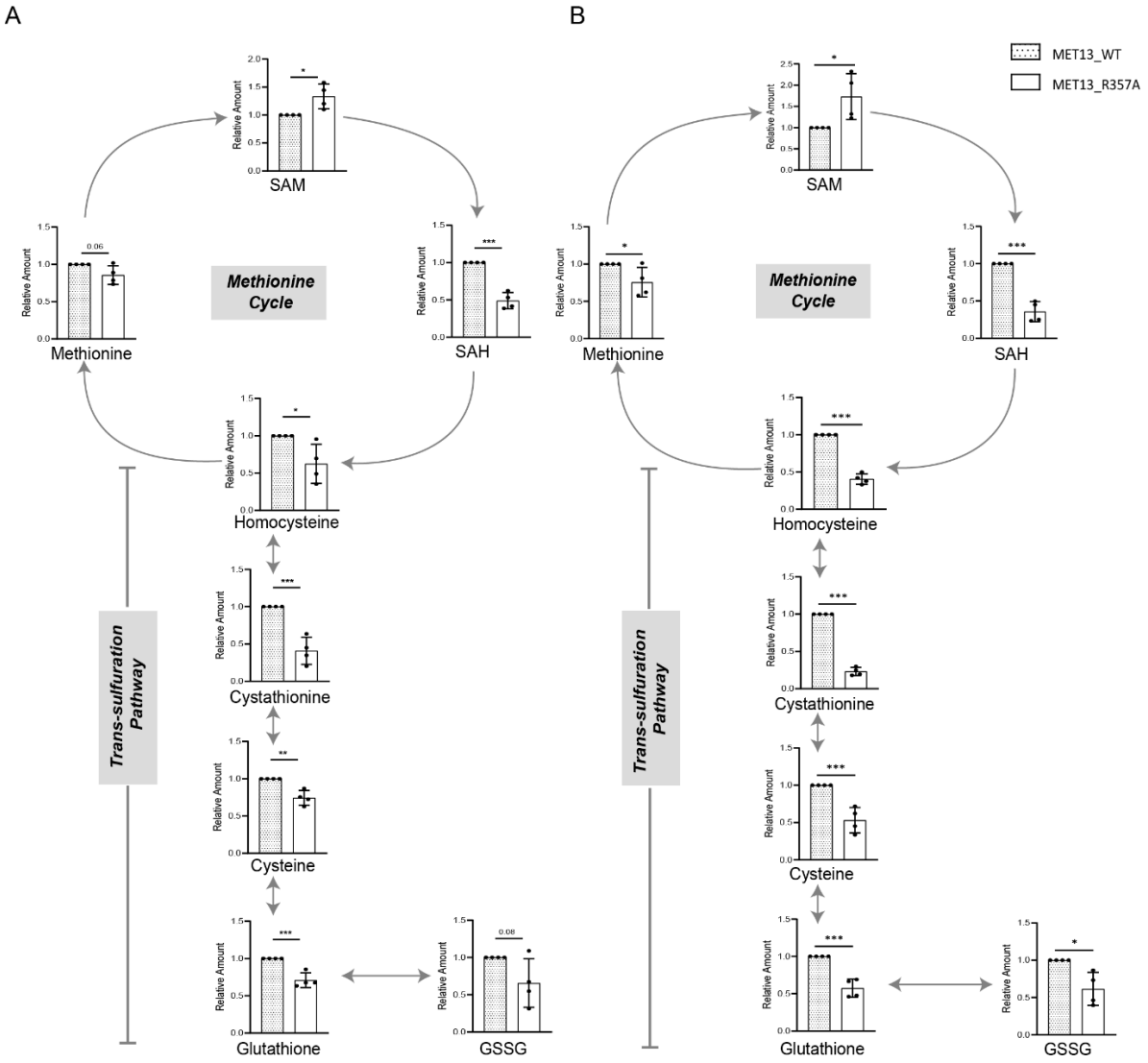

Figure 4.3 Impact of the deregulated MTHFR on amino acid pools, SAM, and glutathione.

Relative intracellular levels of different intermediates in the methyl cycle and transsulfuration pathway positioned in the context of the sulfur amino acid pathway, from the *S. cerevisiae* (ABC2613) transformants with MET13_WT or MET13_R357A that were grown overnight in the minimal media with amino acid supplements, and GSH. These were then re-inoculated at 0.15 OD600 in fresh SD media without any sulfur source. Methionine was added to the transformants after 3 hours of secondary inoculation, and samples were collected for metabolite

extraction at 0.5 (A) and 1.0 (B) OD. The graph here corresponds to the representative data set plotted using the average of four biological replicates along with ±S.D values. Error bars indicate SD. n = 4. *p < 0.05, **p < 0.01, and p***< 0.001.

Estimations of the pools of the other non-sulfur amino acids were also carried out, and while the pools of the majority of amino acids were low, a few of the amino acids revealed sharper differences (Figure 4.5A-B). These included aspartic acid, threonine, and arginine. The trends for all the metabolites were similar at 0.5 (Figure 4.5 A-B) and 1.0 OD cells. However, the differences were more striking for sulphur metabolites and arginine at the mid-exponential phase of growth corresponding to 1.0 OD cells.

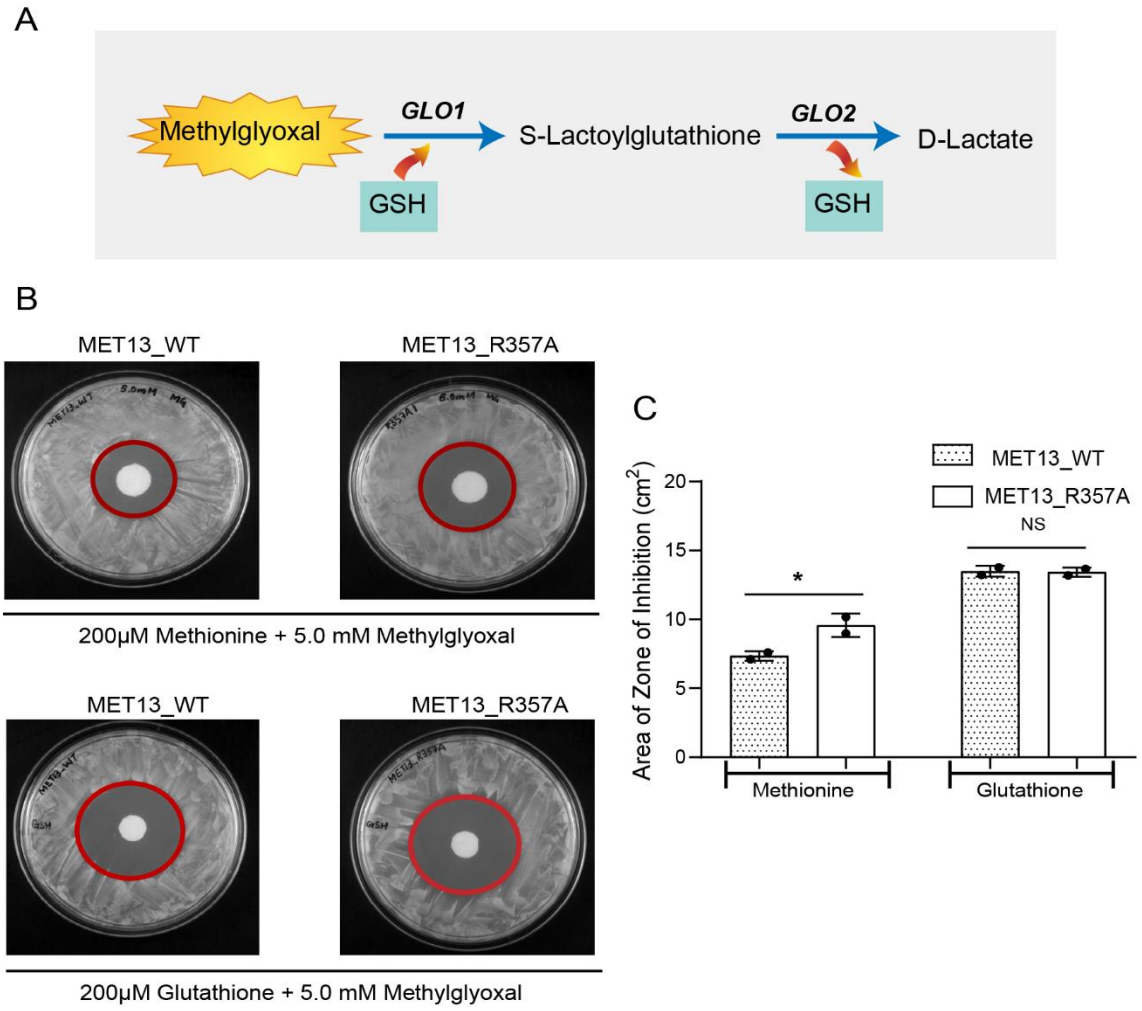

Figure 4.4 Increased sensitivity of deregulated MET13_R357A mutant towards methylglyoxal (MG), GSH specific oxidizing agent.
(A) Methylglyoxal detoxification pathway in yeast by utilization of GSH. (B) Transformant bearing the deregulated mutant, MET13_R357A, exhibits sensitivity to MG when grown

overnight in SD minimal media along with GSH (200μM) as sulfur source and re-inoculated to medium containing methionine (200μM). At the exponential phase (1.0-1.5 OD), 5 OD of cells were plated onto SD plates supplemented with either methionine or glutathione. Filter disc containing 5.0 mM MG was placed onto the lawn of cells, which were allowed to grow at 30°C for 48 h. The experiment was repeated twice, and a representative data set of two biological replicates is shown in the above figure. (C) The graph corresponds to the zone of inhibitions calculated using the average of two independent biological replicates. Error bars indicate SD. n = 2. *p < 0.05, NS is not significant.

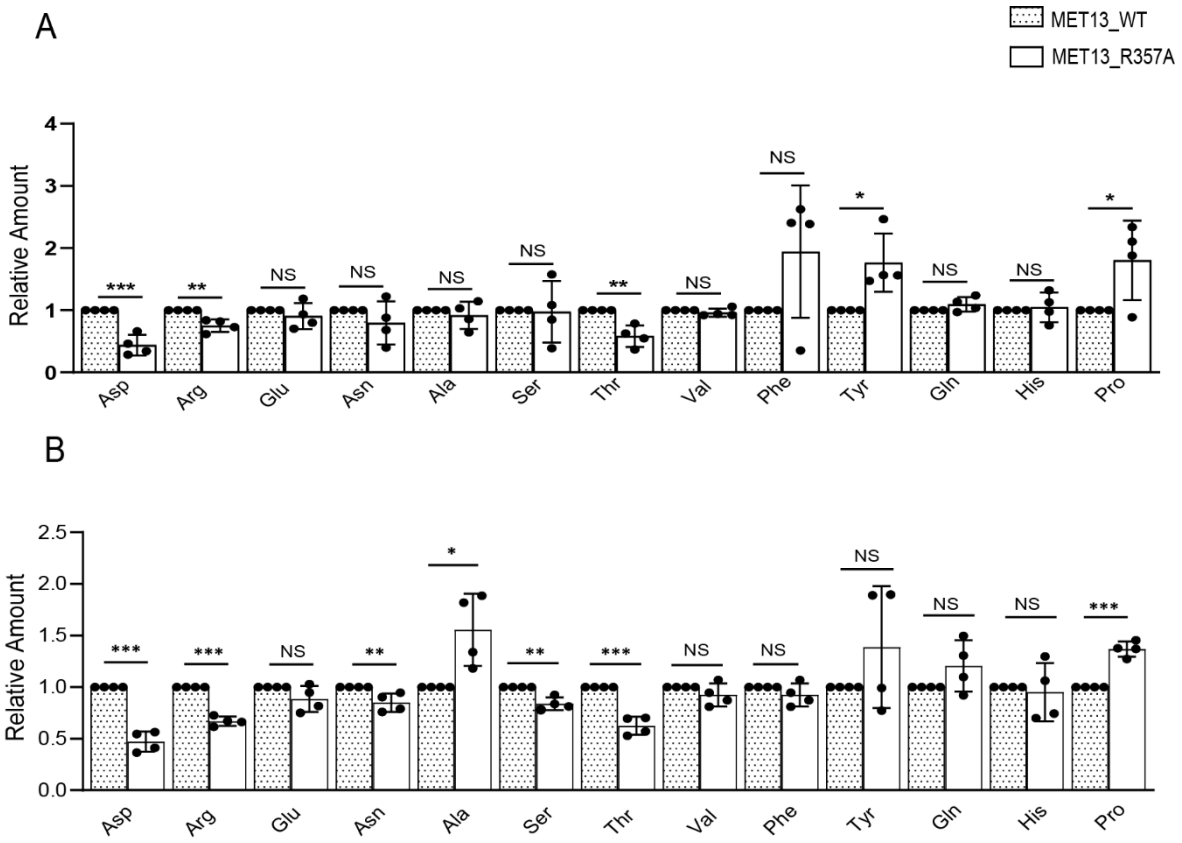

Figure 4 5 Impact of the deregulated MTHFR on amino acid pools.
Relative intracellular levels of different amino acid pools from the *S. cerevisiae* (ABC2613) transformants with MET13_WT or MET13_R357A that were grown overnight in minimal media with amino acid supplements and GSH. These were then re-inoculated at 0.15 OD600 in fresh SD media without any sulfur source. Methionine was added to the transformants after 3 hours of secondary inoculation, and samples were collected for metabolite extraction at 0.5 (A) and 1.0 (B) OD. The graph here corresponds to the representative data set plotted using the average of four biological replicates along with ±S.D values. Error bars indicate SD. n = 4. *p < 0.05, **p < 0.01, and p***< 0.001.

4.2.4. Methionine biosynthesis continues in the deregulated MTHFR even in the presence of exogenous methionine

The surprisingly unchanged levels of methionine suggested that in the presence of exogenous methionine, the homeostasis of cellular methionine might be maintained by repression of synthesis. To determine the relative importance of endogenous biosynthesis of methionine and direct uptake of exogenous methionine in the observed phenotype, we initially adopted a genetic strategy to investigate the phenomenon. MET6 encodes the methionine synthase enzyme that accepts the methyl group from CH_3THF to convert homocysteine to methionine. When we deleted this gene, we observed that the strain, *met6Δ* lacked methionine biosynthetic capacity. This was evident from its inability to grow on glutathione as the sulfur source since the strain had now become strictly auxotrophic for methionine. Importantly, the strain also showed a reduced growth defect when transformed with the deregulated MTHFR (Figure 4.6A). We then evaluated the contributions of methionine uptake, where we deleted MUP1, a high-affinity transporter of methionine. Interestingly, the *mup1Δ* strains also did not show the growth defect on methionine in the presence of the deregulated MTHFR (Figure 4.6B). These experiments seemed to indicate that both endogenous biosynthesis and the transport of exogenous methionine were essential factors in the growth defect on methionine.

Despite the suggestions from the genetic experiments, we needed more rigorous confirmation as to whether methionine biosynthesis by CH_3THF was indeed taking place. Although methionine biosynthesis appeared to be required (based on the *met6Δ* observations), this normally does not occur in a strain which is supplemented by methionine, since in the presence of exogenous methionine, methionine biosynthesis is repressed. To evaluate this aspect, we resorted to ^{13}C metabolic studies.

The wild-type and mutant bearing cells were grown in minimal media supplemented with leucine, lysine, histidine, and methionine were fed either [^{12}C]-, or [1-^{13}C] glucose. The

TBDMS derivatized protein hydrolysate from these cells was subjected to GC-MS for accurate analysis of mass isotopomer distribution in amino acids. The total ion chromatogram of 15 amino acids derived from protein hydrolysates was obtained (Figure 4.7A and Table 4.1). The derived mass isotopomer fragments were successfully validated by comparing the corrected mass isotopomer distributions (MID) with expected theoretical proportions in unlabelled fragments. Among these fragments, the reliable mass ions (m/z) of fragments [M-85] or [M-57] were considered for comparison of label incorporation and distribution (Antoniewicz et al., 2007). In the case of the fragments derived from unlabelled amino acids (obtained from ^{12}C tracer feeding), the fractions of ^{13}C in these fragments were observed to be less than the natural abundance (i.e., <1.13%). In parallel, the cells fed with [1-^{13}C] glucose confirmed the label redistribution of 15 amino acids under pseudo-steady state conditions via different pathways of the central metabolism in MET13_WT as well as in MET13_R357A (Figure 4.7B).

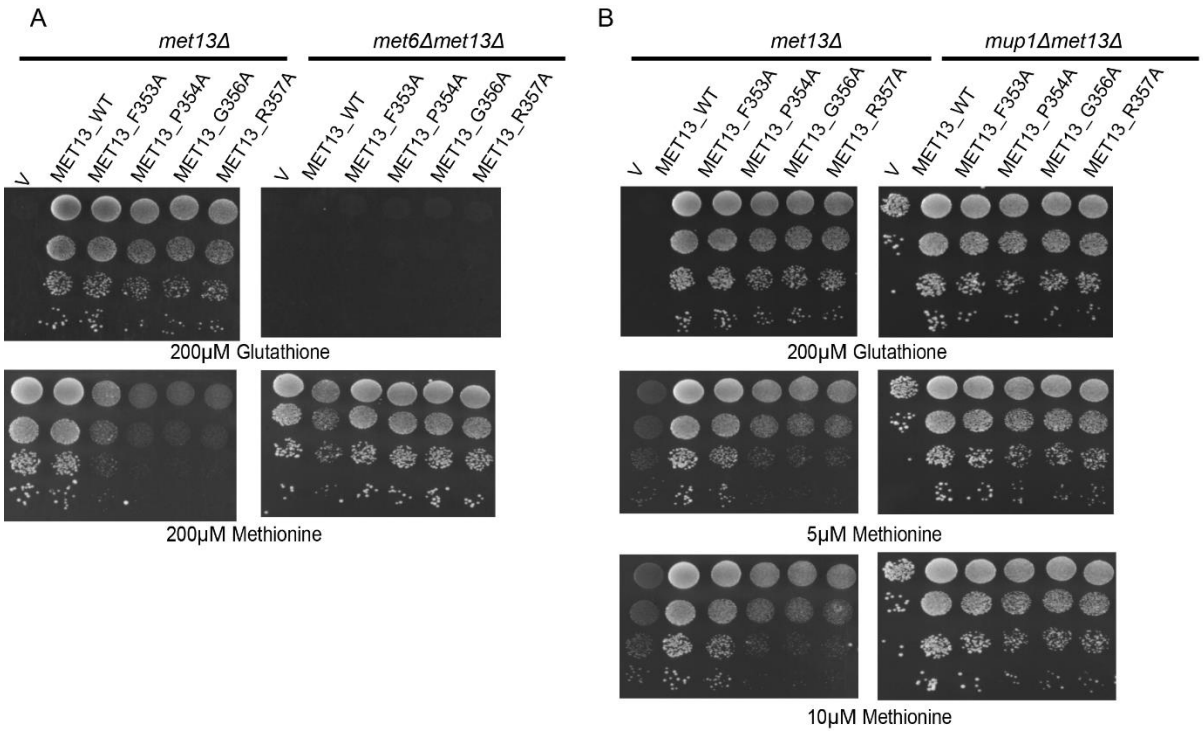

Figure 4.6 Methionine synthesis as well as uptake critical for the deregulated phenotype of MTHFR.

Yeast *met13*Δ*, (A) met6*Δ*met13*Δ *and (B) mup1*Δ*met13*Δ strains were transformed with vector control, MET13_WT, MET13_F353A, MET13_P354A, MET13_G356A, and

MET13_R357A were grown to exponential phase in minimal medium containing 200µM glutathione, harvested, washed, re-suspended in water, and serially diluted to give 0.1, 0.01, 0.001, and 0.0001 OD_{600} of cells. Ten microliters of these dilutions were spotted on a minimal medium containing 200µM GSH or different methionine concentrations. The photographs were taken after 48 hours of incubation at 30°C. The experiment was repeated three times, and a representative data set is shown in the above figure.

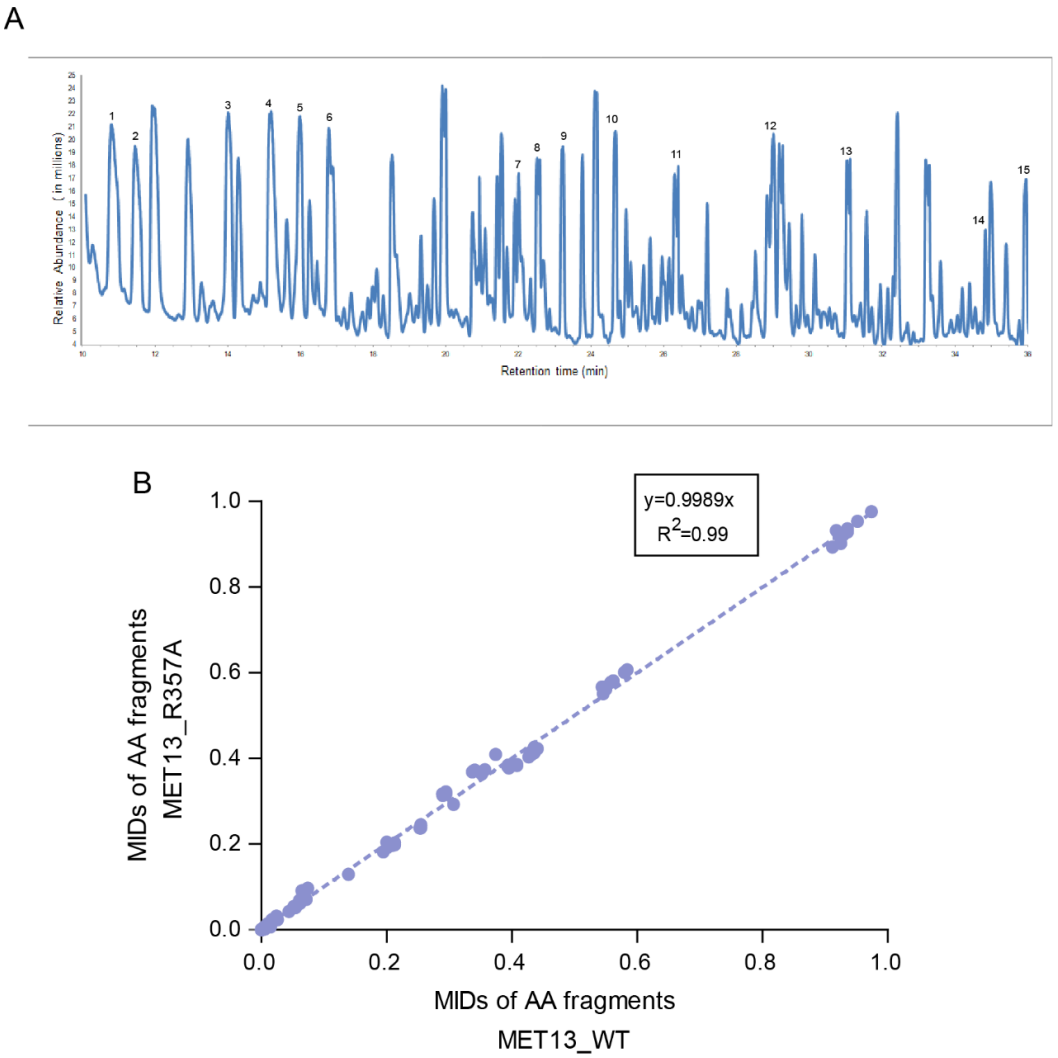

Figure 4.7 MIDs of ^{13}C Metabolite analysis

(A) GC-MS spectra of amino acids derived from the yeast cells. 15 TBDMS derivatized amino acids were detected from the cell hydrolysates of MET13_WT and MET13_R357A. The m/z fragments of each amino acid resulted in Mass isotopomer distributions. (B) Mass isotopomer distributions of amino acid pools observed between the MET13_WT and MET13_R357A obtained from [1-^{13}C] glucose feeding. The TBDMS derivatized protein hydrolysate from these cells was subjected to GC-MS for accurate analysis of mass isotopomer distribution in amino acids. Due to ionization in mass spectroscopy, the TBDMS derivatized amino acids formed different fragments such as $[M-0]^+$, $[M-15]^+$, $[M-57]^+$, $[M-85]^+$, $[M-159]^+$, and $[M-R]^+$ (where, R denotes the side chain of an amino acid often resulting in fragment $[f302]^+$), where $[M-57]^+$, $[M-85]^+$ fragments of each amino acid were plotted using linear regression.

Table 4.1 List of TBDMS derivatized amino acids detected using GC-MS from the yeast cell hydrolysates

S. No.	Retention Time (RT)	Amino acids identified	Derivatives
1	10.787	Alanine	2TBDMS
2	11.438	Glycine	2TBDMS
3	14.009	Valine	2TBDMS
4	15.151	Leucine	2TBDMS
5	15.967	Isoleucine	2TBDMS
6	16.762	Proline	2TBDMS
7	21.894	Methionine	2TBDMS
8	22.504	Serine	3TBDMS
9	23.200	Threonine	3TBDMS
10	24.657	Phenylalanine	2TBDMS
11	26.381	Aspartic acid	3TBDMS
12	28.928	Glutamic acid	3TBDMS
13	31.033	Lysine	3TBDMS
14	34.986	Histidine	TBDMS
15	35.942	Tyrosine	3TBDMS

We first examined the ^{13}C incorporation in the four externally fed amino acids: leucine, lysine, histidine, and methionine that were added to fulfil the nutritional requirement. When external amino acids are supplemented, the corresponding biosynthetic pathway is strongly repressed. Thus, as expected, in the case of leucine, lysine, and histidine, *de novo* biosynthesis was not observed, and thus these amino acids are principally used from the external medium (Figure 4.8). We see only an exception with methionine (Figure 4.8). The [1-^{13}C] fed cells indicated significantly higher m+1 isotopomer for all these fragments of methionine in the case of deregulated MTHFR bearing cells compared to the wild-type (Figure 4.8). The first four carbon backbone of methionine are derived from aspartate, and the last carbon, which is ^{13}C-labelled, is derived from one-carbon metabolism (Figure 4.11). The presence of higher m+1 isotopomer in fragment ions of methionine, Met-292[C2-5] lacking C1 and Met-320[C1-5] (Figure 4.8 and 4.11) confirms CH_3THF (a 1C intermediate of folate cycle) as the precursor for the increased label of methionine in the mutant. These results reveal a continuous biosynthesis of methionine

in yeast (with significantly higher rates in the mutants) through the substrates of ^{13}C-labelled CH_3 and homocysteine. The mass isotopomer distributions of methionine also show that the homocysteine, one of the substrates of methionine synthesis, is primarily derived from SAM via methionine cycle rather than from aspartate, which would have otherwise led to m+2 mass isotopomers in methionine (Figure 4.11). This finding confirms the significance of externally fed methionine for the defective growth phenotype of the deregulated mutant.

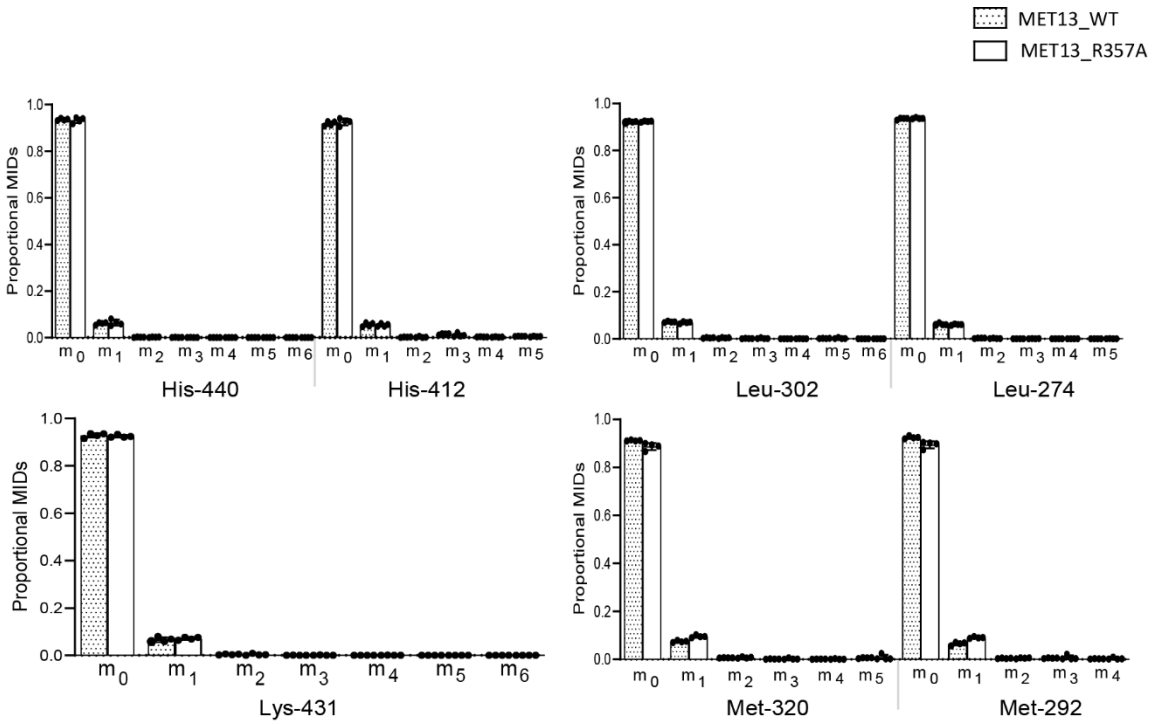

Figure 4.8 Methionine biosynthesis continues in the deregulated MTHFR even in the presence of exogenous methionine.

^{13}C label redistribution, the fate of externally fed, histidine, lysine, leucine, and methionine is depicted. The proportional mass isotopomer distribution (MIDs) of protein derived amino acid fragments retro-biosynthetically report on the labelling of precursors. These amino acid fragments were obtained by TBDMS derivatisation and GC-MS ionisation and are presented by their m/z and carbon backbone.

4.2.5. Cells with deregulated MTHFR show minor readjustments in relative metabolic fluxes

The continuous synthesis of methionine, even in the presence of exogenous methionine and its specific effect on growth retardation, required a better understanding of the impact of methionine over the metabolic fluxes and the cellular metabolism of the deregulated mutant.

Interestingly, one observes a dramatic difference in growth seen on plates; however, when the growth was analysed in the liquid medium, the generation time of the mutant bearing cells was only about 2.3 times the wild-type (Generation time of 10.5 hours for the mutant as compared to 4.5 hours for the wild-type) (Figure 4.9).

To examine alterations in pathway preferences, we further analysed the ^{13}C isotope labelling data to analyse the fluxes of these pathways under pseudo-steady state conditions, as mentioned in the previous section (Figure 4.10). The label incorporation in all the amino acids except leucine, lysine, histidine (discussed in the previous section), and glycine were observed as indicated by the relative mass isotopomer distributions.

The ^{13}C redistribution in the amino acids retro-biosynthetically reporting on the central precursors of different pathways of central metabolism shows that the relative fluxes in the wild-type and mutant are predominantly stable with only minor but appreciably significant readjustments as supported by the quantitative analysis of the extent of ^{13}C proportions in the mass isotopomers.

Glycolysis is active in both wild-type and mutant cells based on ^{13}C incorporation in serine and alanine that retro-biosynthetically report of the label incorporations in the glycolytic intermediates, 3-Phosphoglycerate (3-PG) and Pyruvate, respectively (Figure 4.11).^{13}C label incorporation detected in Phenylalanine MIDs indicates active pentose phosphate pathway (PPP) for both the MET13_WT and MET13_R357A transformed cells. Likewise, the label incorporation in aspartate, glutamate, and proline confirms an active TCA cycle (Figure 4.11).

However, minor differences in the relative abundances of mass isotopomers were observed between the wild-type and the mutant, suggesting minor readjustments of central metabolism.

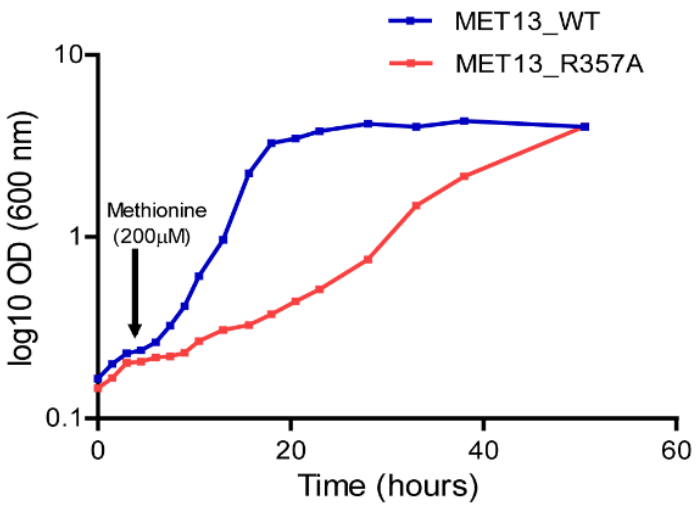

Figure 4.9 Cells bearing the deregulated MTHFR do not show major changes in relative metabolic fluxes.
(A) MET13_WT or MET13_R357A bearing transformants in *met13Δmet15Δ* (ABC2613) were harvested after ~ 13 hours and ~26 hours post methionine addition.

From the [1-^{13}C] glucose fed cells, two amino acids, serine, and alanine, displayed minor but significant differences in ^{13}C incorporation between wild-type and mutant, highlighting readjustment in glycolysis. The relative proportion of m+1 in Ser-362[C2-3] fragment (lacking C1) in comparison to the Ser-390[C1-3] confirms that C3 was labelled via glycolysis (Figure 4.11). The relative levels of m+1 in the mutant for both serine and alanine (that are derived from glycolysis) were marginally yet significantly lower than the wild-type implying a slightly lesser rate of glucose oxidation (significant based on t-test) (Figure 4.11).The data provides strong evidence that glucose metabolism via glycolysis was marginally lower in the mutant as compared to the wild-type, and this could be a consequence of the depleted ATP levels in the cell. With lower glycolysis, it can be speculated that the relative activities via PPP would be higher. The conversion of serine to glycine releases the labelled C3 into 1-carbon pools (CH_2THF), which was ^{13}C enriched (Figure 4.11).

However, regardless of these minor differences, our data suggest that the deregulated mutant, which has a slower growth rate, is undergoing minor metabolic readjustments to behave metabolically like the wild-type without any major changes in the fluxes.

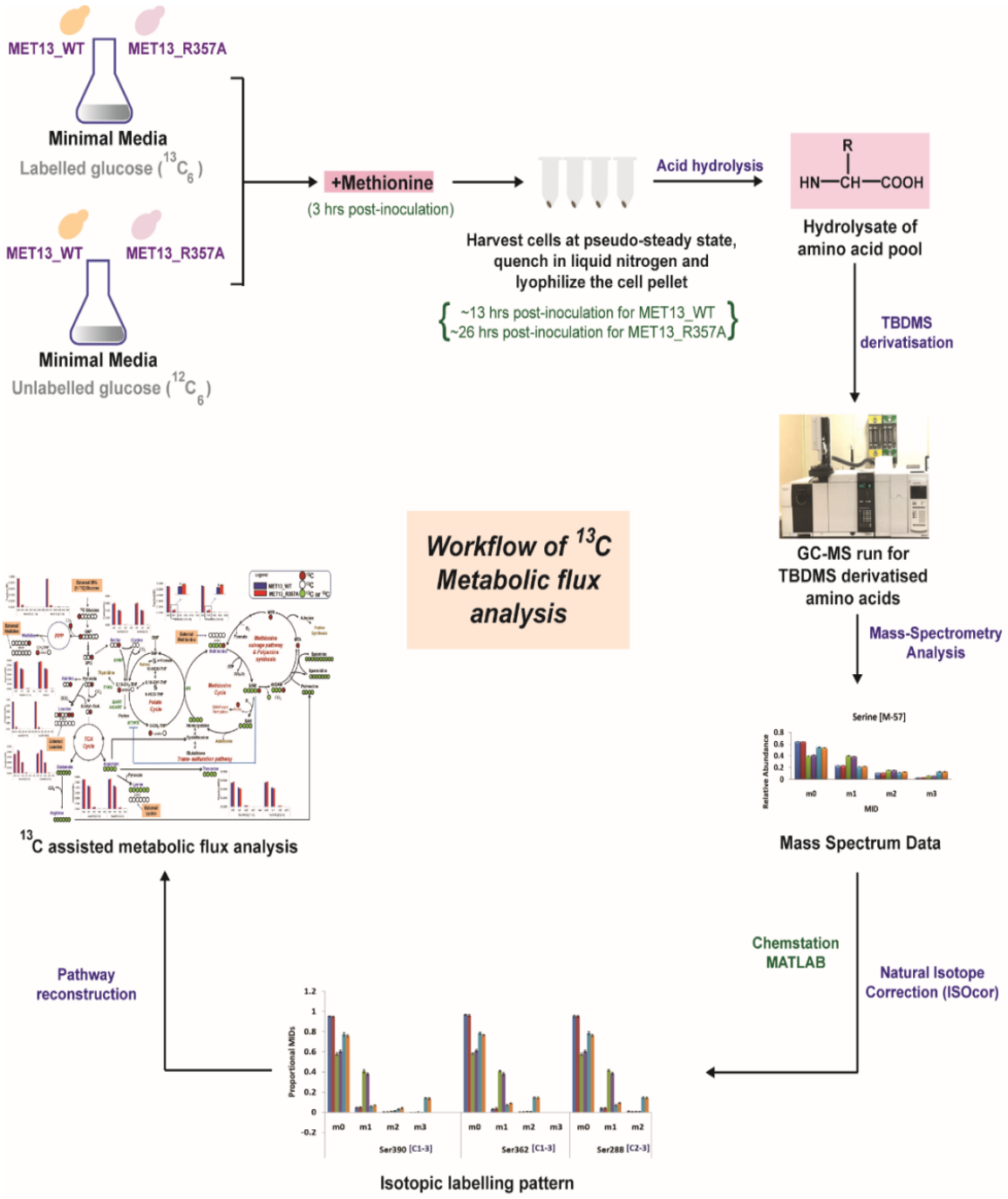

Figure 4.10 Work-flow for 13C metabolic flux analysis experiment.

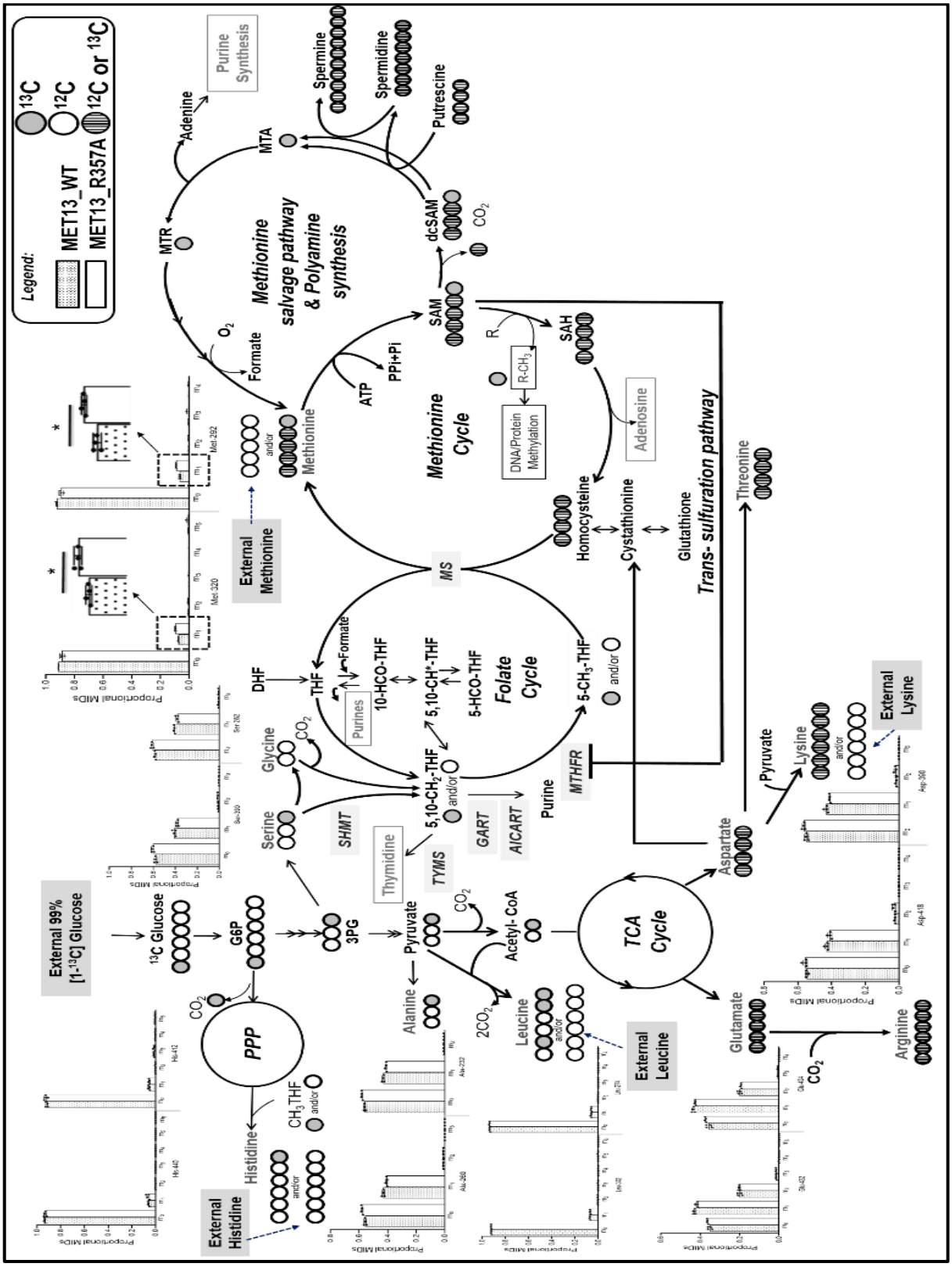

Figure 4.11 Cells bearing the deregulated MTHFR do not show major changes in relative metabolic fluxes.

The ^{13}C label redistribution via glycolysis, pentose phosphate pathway, TCA cycle, the folate cycle, methionine cycle, methionine salvage pathway, polyamine synthesis, transsulfuration pathway, and amino acid biosynthesis are highlighted. Also, the fate of externally fed histidine,

lysine, leucine, and methionine is depicted. The proportional mass isotopomer distribution (MIDs) of protein derived amino acid fragments retro-biosynthetically report on the labelling of precursors. These amino acid fragments were obtained by TBDMS derivatisation and GC-MS ionisation and are presented by their m/z and carbon backbone. The ^{13}C redistribution in the carbon atoms of central metabolites is derived from our analysis and highlighted via red circles. The open circles represent unlabelled carbon, while the circles in green represent either unlabelled ^{12}C or labelled ^{13}C incorporation. In the methionine cycle and methionine salvage pathway, additional carbons from ATP (Adenine and ribose unit) are depicted in circles with close vertical lines. * represents significance at 99% significance level analysed via t-test. The abbreviations used are as follows:

MID: Mass Isotopomer distributions; $^{13}C_{red}$: Labeled carbon; $^{12}C_{white}$: Unlabeled carbon; $^{12}C_{green}$ or $^{13}C_{red}$: Unlabeled carbon or labeled carbon. PPP: Pentose phosphate pathway; TCA: Tricarboxylic acid cycle; G6P: Glucose-6-Phosphate; 3PG: 3-Phosphoglycerate; DHF:Dihydrofolate; THF: Tetrahydrofolate; 5,10-CH_2THF: 5,10-methylene tetrahydrofolate; 5-CH_3THF: 5-methyl tetrahydrofolate; 5-HCO-THF: 5- formyltetrahydrofolate; 10-HCOTHF: 10-formyltetrahydrofolate; 5,10-CH^*THF: 5,10-methenyl tetrahydrofolate; SAM: S-Adenosyl methionine; SAH: S-Adenosyl homocysteine; dcSAM: Decarboxylated S-Adenosylmethionine; MTA: Methylthioadenosine; MTR: Methylthioribose; SHMT:Serine hydroxymethyl transferase; TYMS: Thymidylate synthase; GART:Glycinamide ribonucleotide transformylase; AICART: Aminoimidazolecarboxamide ribonucleotide formyltransferase; MTHFR: Methylenetetrahydrofolate reductase; MS: Methionine synthase.

4.2.6. In the deregulated MTHFR mutant cells, SAM cycles in futile salvage pathways wherein both methionine and adenine are continuously utilized and recycled

The absence of any major metabolic readjustments in the deregulated mutant as compared to the wild-type suggested that pathways downstream of methionine were responsible for the methionine-dependant growth defect in the MTHFR deregulated mutants. Methionine formation drives the ATP dependant enzymatic synthesis of S-adenosyl methionine (SAM). The metabolite analysis had indicated an increase in SAM, which can meet two distinct fates (Figure 1.7). In the first case, SAM is involved in the methylation of a variety of cellular substrates such as nucleic acids, proteins, and lipids. Recent studies in yeast have reported phosphatidylethanolamine (PE) methylation as the major SAM consumer (Ye et al., 2017). Therefore, we quantified the relative abundance of phospholipids [phosphotidyl ethanolamine (PE) and phosphatidylcholine (PC)] in the deregulated MTHFR mutant. Mutant harboring cells

show a noticeable increase (≈1.6 fold) in the total PC levels along with a marginal decline in cellular abundance of PE (Figure 4.12). An increase in SAH, a side product of PE methylation and other methylation reactions, is generally observed with increased methylation. However, SAH, in turn, is hydrolysed to homocysteine and adenosine, both of which are in increased requirements in the mutant (Figure 4.3A). Adenosine is required because of the depleted adenine pools, while homocysteine is required owing to the continuous unregulated formation of CH_3THF. The methyl group of CH_3THF is accepted by homocysteine to form methionine again, and subsequently, the methionine formed drives the ATP-dependant formation of SAM. The second route of SAM metabolism is through the methionine salvage pathway. In this pathway, the methionine, which converts to SAM, is converted back to methionine with the release of adenine and polyamine following the decarboxylation of SAM. In the polyamine pathway, the decarboxylated-SAM can be used in the synthesis of spermidine from putrescine or in the formation of spermine, which eventually releases into methyl-thioadenosine (MTA), subsequently yielding methionine and adenine (Chan & Appling, 2003). We measured the relative abundance of polyamines (spermidine and spermine) in the wild-type and mutant bearing cells. While there was no significant change observed in the relative abundance of spermidine in the wild-type and mutant transformed cells, we observed a significant increase of 2.5 fold in the amount of spermine for the deregulated mutant (MET13_R357A) (Figure 4.12). This clearly suggested a significant conversion of SAM back to methionine and adenine, with the concomitant formation of spermine. The methionine so formed would again drive the ATP-dependant formation of SAM.

Thus, based on the metabolite data, it is clear that the methionine and ATP driven formation of SAM is recycled back through both pathways of SAM metabolism. The first is via SAH and homocysteine, while the other is through decarboxylated SAM and the polyamines. As a consequence of this, with continuous methionine formation that is leading

again to the formation of SAM, one observes futile cycles of ATP-dependant SAM formation and its recycling to methionine and adenine/adenosine. The activities of both the pathways in yeast with higher rates in the mutant, in particular, is supported by the higher proportion of mass isotopomer m+1 in methionine mainly contributed by the incorporation of ^{13}C of CH_3THF due to enhanced activities of either methionine cycle and/or methionine salvage pathway via SAM.

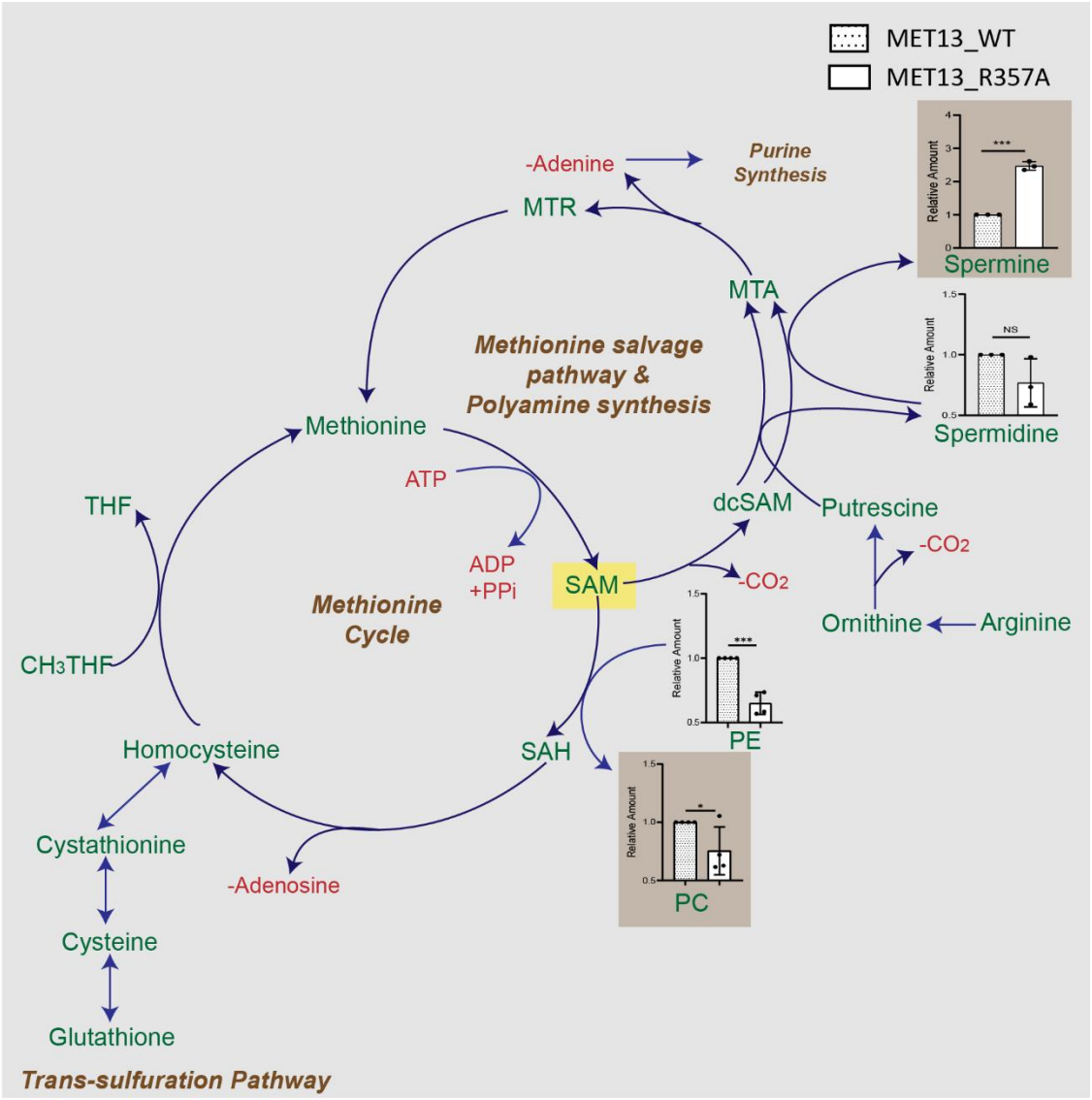

Figure 4.12 Increased SAM pools of the deregulated MTHFR mutant is metabolized via both pathways metabolism.

(A) A schematic for the metabolism of SAM in budding yeast. Major catabolism of SAM to SAH occurs by methylation of phosphatidylethanolamine (PE), or SAM may also be consumed for the production of spermidine, spermine, and MTA via polyamine synthesis, the latter then enters a futile methionine salvage pathway producing adenine as a side-product (B-C) Relative

intracellular levels of (B) the two phospholipids intermediates involved in PE methylation (C) polyamines (spermidine and spermine) estimated from yeast transformants of MET13_WT or MET13_R357A in *met13Δmet15Δ* (ABC2613) that were grown overnight in minimal media with amino acid supplements and GSH. These were then re-inoculated at 0.15 OD_{600} in fresh SD media without any sulfur source. Methionine was added to the transformants after 3 hours of secondary inoculation, and samples were collected in triplicates at 1.0 OD. The graph here corresponds to the representative data set plotted using the average of three biological replicates and three technical replicates of each of these biological replicates along with ±S.D values. Error bars indicate SD. n = 3. *p < 0.05, **p < 0.01, p***< 0.001 and NS is not significant.

4.3. Discussion

In this chapter, we have been able to show the critical role of SAM-mediated allosteric control of MTHFR in the maintenance of overall metabolic homeostasis in the cell. The growth defect seen in the feedback-insensitive deregulated MTHFR mutant on methionine medium provided an opportunity to understand the metabolic reasons behind the regulation of MTHFR by SAM. In the deregulated MTHFR mutant, we observed a drastic reduction in the nucleotide pools (which are derived from folate pools). However, growth could only be partly recovered by supplementation with external folate. Thus, while depleted folate pools appeared to be part of the explanation for the growth defects, additional mechanisms seemed to be important. Our investigations further revealed the presence of ongoing methionine synthesis driven by CH_3THF formation that occurred even in the presence of biosynthetically repressive levels of methionine in the medium. Using stable isotope labelling studies, we could demonstrate that the ^{13}C label seen in methionine arises from CH_3THF and quantitative estimations indicated a 31% increased consumption of CH_2THF by the deregulated MTHFR mutant. Methionine, when it is in excess of its requirement in protein biosynthesis, is activated by ATP to the universal methyl donor, SAM. As the continuous generation of SAM would exacerbate nucleotide depletion, it suggests, therefore, that severe nucleotide depletion is a consequence of sustained SAM synthesis in a deregulated, feedback-insensitive MTHFR mutant. Besides its impact on folate and nucleotide metabolism, MTHFR deregulation also results in the depletion

of essential cofactors, i.e., NADPH and FAD (oxidized form). These results provide evidence that the regulation of yeast MTHFR is crucial for maintaining cellular NADPH and FAD pools.

In addition to the folate cycle, we also observed consequences on both the methionine cycle and the transsulfuration pathway. Methionine biosynthesis occurs in the methionine cycle through the transmethylation of homocysteine (Finkelstein, 1990). However, homocysteine also stands at the junction of another competing pathway, the transsulfuration pathway, towards the formation of cystathionine and cysteine (Selhub & Miller, 1992; Thomas & Surdin-Kerjan, 1997). As a consequence of the deregulated MTHFR, its product, CH_3THF, is formed continuously, and these higher CH_3THF pools push the transmethylation of homocysteine towards methionine biosynthesis despite the presence of adequate external methionine. This depletes the homocysteine pools and limits their availability for the transsulfuration pathway. That this phenomenon is indeed occurring is reflected not only by the lower levels of homocysteine but also by the significantly lower levels of cystathionine and cysteine observed in these mutants. With lower cysteine, there is consequently decreased glutathione, and thus redox homeostasis is also partially disrupted as seen by the sensitivity to methylglyoxal. In contrast to the transsulfuration pathway, the methionine cycle is overactive, with the consequence that the accumulating methionine (through both *de novo* biosynthesis and external uptake) drives the formation of SAM despite the depleted ATP levels. This also explains the methionine dependence of the phenotype.

SAM is a critical methyl donor for various substrate-specific methyltransferases that enables the methylation of DNA, RNA, and proteins, and these can have profound metabolic consequences in the cell. In yeasts, excess SAM can also be trapped in the methylation of phosphatidylethanolamine to form phosphatidylcholine, and this has been reported in yeast to function as a ‘methyl sink’ (Ye et al., 2017). Irrespective of the substrates, though, the methyltransferases generate S-adenosyl homocysteine (SAH). SAH, in turn, is hydrolyzed to

adenosine and homocysteine through the action of the enzyme, S-adenosyl homocysteine hydrolase. The homocysteine so generated is normally diverted to the synthesis of cysteine and glutathione through the transsulfuration pathway. However, this is prevented, as we have seen earlier, owing to the continuous transmethylation of homocysteine by CH_3THF and its diversion towards the formation of methionine in the deregulated MTHFR. The binding constants of SAM and SAH for mammalian MTHFR protein are approximately 2.7µM and 2µM, respectively (Froese et al., 2018; Kutzbach & Stokstad, 1971). The human intracellular concentration of SAM is well within this range, i.e., 1-3 µM. On the other hand, in the yeast grown on a minimal medium, steady-state concentrations of SAM is almost tenfold higher. It varies between 10-30µM for SAM and between 100-400µM for SAH (Laxman et al., 2013). The kinetic parameters for yeast MTHFR homolog have not been determined yet. However, if we consider the dissociation constant of SAM for MET13p similar to human MTHFR, our study would be completely relevant in the physiological setting where the SAM concentration varies between 10-30µM.

SAM is also metabolized through the methionine salvage pathway, wherein SAM is first decarboxylated and then recycled with the release of methionine, adenosine, and polyamines (Murin et al., 2017). In the deregulated MTHFR mutant, we observed a 2.5 fold increase in the amount of spermine, suggesting that the pathway is indeed active in the mutant. This possibly also explains why arginine, a precursor for spermine, is also observed at significantly lower levels in the deregulated mutant. Thus, in effect, the methionine and ATP-driven formation of SAM enters both the pathways of SAM metabolism. It is difficult to conclude at this point which of the two pathways might be the predominant one in the regeneration of adenosine. However, irrespective of whether one or the other is a major contributor to the recycling process, one observes futile cycles of SAM formation, and it's recycling to methionine and adenosine. This unregulated, 'wasteful' synthesis of SAM and

recycling further accentuates the nucleotide depletions seen in the cell and consequently also affects the cell growth. Spermine levels are also dependant on their catabolism. In yeast, spermine is catabolized by a FAD utilizing enzyme, FMS1 (White et al., 2001). As the SAM-insensitive mutants face the depletion of FAD pools, it is possible that the activity of this FAD utilizing enzyme might also be compromised. Therefore, inefficient catabolism of spermine might also be contributing to the increased spermine levels in the deregulated mutant.

Even though both yeast and human MTHFR enzymes require NADPH for their activity and are feedback regulated by SAM, it is interesting to note that the plant enzyme is naturally feedback-insensitive while also requiring NADH for the activity in place of NADPH. In an effort to investigate the importance of SAM-insensitivity in yeast, a previous study made use of *Arabidopsis* enzymes and yeast-arabidopsis chimeric enzymes (Roje et al., 2002). However, the enzyme had quite different cofactor requirements compared to the native enzyme, and thus these studies, while yielding interesting results, could not be generalized to the actual situations in vivo, and, not surprisingly, led to significantly different metabolic consequences than what was observed in the current study.

Although the findings described in this report are restricted to yeasts, they have implications for human MTHFR. Human MTHFR shares 43% identity with the yeast protein. This similarity extends to both the catalytic and regulatory domains of the protein. The 7 amino acid region in CR1 important for regulation by SAM that we have shown here is also conserved in the human protein. Therefore, it is likely that mutations or polymorphisms in these regions of the human MTHFR might also exhibit a deregulated phenotype and exhibit similar metabolic consequences in humans. In fact, few of the polymorphisms in human MTHFR protein are indeed present in the CR1 region (Table 4.2); however, they have not been characterized sufficiently yet. Innumerable studies on SNPs of human MTHFR have been carried out over the years owing to their relevance to many diseases, but these have focused on SNPs exhibiting

a loss of function (Burda et al., 2015; Lopez-Lopez et al., 2013; Rummel et al., 2007; Wang et al., 2018). Mutations or SNPs that might result in a gain of function have not been identified or even recognized so far. This study with the feedback-insensitive, deregulated MTHFR reveals that a single polymorphism in the critical region could significantly disrupt cellular folate and nucleotide homeostasis while also impacting homocysteine levels and affecting redox homeostasis. Investigations of patient MTHFR polymorphisms that affect MTHFR regulation are therefore likely to be important, but are likely to manifest quite different phenotypes than what has been reported so far for the loss of function/decreased function SNPs. One of the possible phenotypes that might be predicted would be increased sensitivity of cancer patients to drugs targeting the folate pathway, as has been recently observed with polymorphisms in the histidine catabolic pathway (Kanarek et al., 2018). In conclusion, these studies with the isolation and investigation of deregulated mutants of MTHFR have yielded valuable new insights into SAM cycle and one-carbon metabolism, and future investigations with these mutants, both in yeasts and humans, will throw more light on the interaction of these two pathways.

Table 4.2 List of polymorphism in human MTHFR corresponding to CR1 region of yeast

S. No.	Nucleotide Change		Amino acids change		Residual Activity (% Control)
	Catalytic Domain	Regulatory Domain	Human	Yeast	
1		C1141T 1359+1G>A	Arg377Cys splice site	Arg344	7.4
2		G1142A G1142A	Arg377His Arg377His	Arg344, Arg344	34.8
3	G358A	C1134G	Ala116Thr Tyr374*	Ala73 Tyr341	29.1
4	C553G	C1141T	His181Asp Arg377Cys	Tyr140 Arg344	15.0
5	G590A	C1141T	Cys193Tyr Arg377Cys	Gly152 Arg344	nd

6	T980C	C1141T	Leu323Pro Arg377Cys	Met284 Arg344	2
7	G1016A	1179-2delA	Arg335His Trp389fs*1	Arg296 Phe358	5.3

Text in red indicates SNPs in the CR1 region (Burda et al., 2015)

* STOP codon mutation

nd: no data

Bibliography

Aggarwal, M., & Mondal, A. K. (2006). Role of N-terminal hydrophobic region in modulating the subcellular localization and enzyme activity of the bisphosphate nucleotidase from *Debaryomyces hansenii*. *Eukaryot Cell, 5*(2), 262-271.

Antoniewicz, M. R., Kraynie, D. F., Laffend, L. A., Gonzalez-Lergier, J., Kelleher, J. K., & Stephanopoulos, G. (2007). Metabolic flux analysis in a nonstationary system: fed-batch fermentation of a high yielding strain of *E. coli* producing 1,3-propanediol. *Metab Eng, 9*(3), 277-292. doi:10.1016/j.ymben.2007.01.003

Applebaum, J., Shimon, H., Sela, B. A., Belmaker, R. H., & Levine, J. (2004). Homocysteine levels in newly admitted schizophrenic patients. *J Psychiatr Res, 38*(4), 413-416. doi:10.1016/j.jpsychires.2004.01.003

Appling, D. R. (1991). Compartmentation of folate-mediated one-carbon metabolism in eukaryotes. *FASEB J, 5*(12), 2645-2651. doi:10.1096/fasebj.5.12.1916088

Bagley, P. J., & Selhub, J. (1998). A common mutation in the methylenetetrahydrofolate reductase gene is associated with an accumulation of formylated tetrahydrofolates in red blood cells. *Proc Natl Acad Sci U S A, 95*(22), 13217-13220. doi:10.1073/pnas.95.22.13217

Barbey, R., Baudouin-Cornu, P., Lee, T. A., Rouillon, A., Zarzov, P., Tyers, M., & Thomas, D. (2005). Inducible dissociation of SCF(Met30) ubiquitin ligase mediates a rapid transcriptional response to cadmium. *EMBO J, 24*(3), 521-532. doi:10.1038/sj.emboj.7600556

Barlowe, C. K., & Appling, D. R. (1988). *In vitro* evidence for the involvement of mitochondrial folate metabolism in the supply of cytoplasmic one-carbon units. *Biofactors, 1*(2), 171-176.

Baudin, A., Ozier-Kalogeropoulos, O., Denouel, A., Lacroute, F., & Cullin, C. (1993). A simple and efficient method for direct gene deletion in *Saccharomyces cerevisiae*. *Nucleic Acids Res, 21*(14), 3329-3330. doi:10.1093/nar/21.14.3329

Blaiseau, P. L., Isnard, A. D., Surdin-Kerjan, Y., & Thomas, D. (1997). Met31p and Met32p, two related zinc finger proteins, are involved in transcriptional regulation of yeast sulfur amino acid metabolism. *Mol Cell Biol, 17*(7), 3640-3648. doi:10.1128/mcb.17.7.3640

Blaiseau, P. L., & Thomas, D. (1998). Multiple transcriptional activation complexes tether the yeast activator Met4 to DNA. *EMBO J, 17*(21), 6327-6336. doi:10.1093/emboj/17.21.6327

Bligh, E. G., & Dyer, W. J. (1959). A rapid method of total lipid extraction and purification. *Can J Biochem Physiol, 37*(8), 911-917. doi:10.1139/o59-099

Bradford, M. M. (1976). A rapid and sensitive method for the quantitation of microgram quantities of protein utilizing the principle of protein-dye binding. *Anal Biochem, 72*, 248-254. doi:10.1006/abio.1976.9999

Brattstrom, L., Wilcken, D. E., Ohrvik, J., & Brudin, L. (1998). Common methylenetetrahydrofolate reductase gene mutation leads to hyperhomocysteinemia but not to

vascular disease: the result of a meta-analysis. *Circulation, 98*(23), 2520-2526. doi:10.1161/01.cir.98.23.2520

Brustolin, S., Giugliani, R., & Felix, T. M. (2010). Genetics of homocysteine metabolism and associated disorders. *Braz J Med Biol Res, 43*(1), 1-7. doi:10.1590/s0100-879x2009007500021

Burda, P., Schafer, A., Suormala, T., Rummel, T., Burer, C., Heuberger, D., . . . Baumgartner, M. R. (2015). Insights into severe 5,10-methylenetetrahydrofolate reductase deficiency: molecular genetic and enzymatic characterization of 76 patients. *Hum Mutat, 36*(6), 611-621. doi:10.1002/humu.22779

Carrillo, E., Ben-Ari, G., Wildenhain, J., Tyers, M., Grammentz, D., & Lee, T. A. (2012). Characterizing the roles of Met31 and Met32 in coordinating Met4-activated transcription in the absence of Met30. *Mol Biol Cell, 23*(10), 1928-1942. doi:10.1091/mbc.E11-06-0532

Chan, S. Y., & Appling, D. R. (2003). Regulation of S-adenosylmethionine levels in *Saccharomyces cerevisiae*. *J Biol Chem, 278*(44), 43051-43059. doi:10.1074/jbc.M308696200

Chattopadhyay, S., Moran, R. G., & Goldman, I. D. (2007). Pemetrexed: biochemical and cellular pharmacology, mechanisms, and clinical applications. *Mol Cancer Ther, 6*(2), 404-417. doi:10.1158/1535-7163.MCT-06-0343

Christensen, K. E., & MacKenzie, R. E. (2006). Mitochondrial one-carbon metabolism is adapted to the specific needs of yeast, plants and mammals. *Bioessays, 28*(6), 595-605. doi:10.1002/bies.20420

Clare, C. E., Brassington, A. H., Kwong, W. Y., & Sinclair, K. D. (2019). One-Carbon Metabolism: Linking Nutritional Biochemistry to Epigenetic Programming of Long-Term Development. *Annu Rev Anim Biosci, 7*, 263-287. doi:10.1146/annurev-animal-020518-115206

Copp, A. J., Adzick, N. S., Chitty, L. S., Fletcher, J. M., Holmbeck, G. N., & Shaw, G. M. (2015). Spina bifida. *Nat Rev Dis Primers, 1*, 15007. doi:10.1038/nrdp.2015.7

Cowan, J. M., Urbanowski, M. L., Talmi, M., & Stauffer, G. V. (1993). Regulation of the *Salmonella typhimurium metF* gene by the *MetR* protein. *J Bacteriol, 175*(18), 5862-5866. doi:10.1128/jb.175.18.5862-5866.1993

de Luis, D. A., Fernandez, N., Arranz, M. L., Aller, R., Izaola, O., & Romero, E. (2005). Total homocysteine levels relation with chronic complications of diabetes, body composition, and other cardiovascular risk factors in a population of patients with diabetes mellitus type 2. *J Diabetes Complications, 19*(1), 42-46. doi:10.1016/j.jdiacomp.2003.12.003

DeBerardinis, R. J. (2011). Serine metabolism: some tumors take the road less traveled. *Cell Metab, 14*(3), 285-286. doi:10.1016/j.cmet.2011.08.004

Deshpande, A. A., Bhatia, M., Laxman, S., & Bachhawat, A. K. (2017). Thiol trapping and metabolic redistribution of sulfur metabolites enable cells to overcome cysteine overload. *Microb Cell, 4*(4), 112-126. doi:10.15698/mic2017.04.567

Dominguez-Salas, P., Moore, S. E., Baker, M. S., Bergen, A. W., Cox, S. E., Dyer, R. A., . . . Hennig, B. J. (2014). Maternal nutrition at conception modulates DNA methylation of human metastable epialleles. *Nat Commun, 5*, 3746. doi:10.1038/ncomms4746

Ducker, G. S., Chen, L., Morscher, R. J., Ghergurovich, J. M., Esposito, M., Teng, X., . . . Rabinowitz, J. D. (2016). Reversal of Cytosolic One-Carbon Flux Compensates for Loss of the Mitochondrial Folate Pathway. *Cell Metab, 24*(4), 640-641. doi:10.1016/j.cmet.2016.09.011

Ducker, G. S., & Rabinowitz, J. D. (2017). One-Carbon Metabolism in Health and Disease. *Cell Metab, 25*(1), 27-42. doi:10.1016/j.cmet.2016.08.009

Finkelstein, J. D. (1990). Methionine metabolism in mammals. *J Nutr Biochem, 1*(5), 228-237. doi:10.1016/0955-2863(90)90070-2

Finkelstein, J. D., & Martin, J. J. (1986). Methionine metabolism in mammals. Adaptation to methionine excess. *J Biol Chem, 261*(4), 1582-1587.

Fontecave, M., Atta, M., & Mulliez, E. (2004). S-adenosylmethionine: nothing goes to waste. *Trends Biochem Sci, 29*(5), 243-249. doi:10.1016/j.tibs.2004.03.007

Froese, D. S., Kopec, J., Rembeza, E., Bezerra, G. A., Oberholzer, A. E., Suormala, T., . . . Yue, W. W. (2018). Structural basis for the regulation of human 5,10-methylenetetrahydrofolate reductase by phosphorylation and S-adenosylmethionine inhibition. *Nat Commun, 9*(1), 2261. doi:10.1038/s41467-018-04735-2

Frosst, P., Blom, H. J., Milos, R., Goyette, P., Sheppard, C. A., Matthews, R. G., . . . et al. (1995). A candidate genetic risk factor for vascular disease: a common mutation in methylenetetrahydrofolate reductase. *Nat Genet, 10*(1), 111-113. doi:10.1038/ng0595-111

Ganguli, D., Kumar, C., & Bachhawat, A. K. (2007). The alternative pathway of glutathione degradation is mediated by a novel protein complex involving three new genes in *Saccharomyces cerevisiae*. *Genetics, 175*(3), 1137-1151. doi:10.1534/genetics.106.066944

Gao, X., Sanderson, S. M., Dai, Z., Reid, M. A., Cooper, D. E., Lu, M., . . . Locasale, J. W. (2019). Dietary methionine influences therapy in mouse cancer models and alters human metabolism. *Nature, 572*(7769), 397-401. doi:10.1038/s41586-019-1437-3

Gietz, R. D., Schiestl, R. H., Willems, A. R., & Woods, R. A. (1995). Studies on the transformation of intact yeast cells by the LiAc/SS-DNA/PEG procedure. *Yeast, 11*(4), 355-360. doi:10.1002/yea.320110408

Goyette, P., Sumner, J. S., Milos, R., Duncan, A. M., Rosenblatt, D. S., Matthews, R. G., & Rozen, R. (1994). Human methylenetetrahydrofolate reductase: isolation of cDNA mapping and mutation identification. *Nat Genet, 7*(4), 551.

Greene, R. C., Hunter, J. S., & Coch, E. H. (1973). Properties of *metK* mutants of *Escherichia coli* K-12. *J Bacteriol, 115*(1), 57-67. doi:10.1128/JB.115.1.57-67.1973

Greene, R. C., Su, C. H., & Holloway, C. T. (1970). S-Adenosylmethionine synthetase deficient mutants of *Escherichia coli* K-12 with impaired control of methionine biosynthesis. *Biochem Biophys Res Commun, 38*(6), 1120-1126. doi:10.1016/0006-291x(70)90355-4

Guenther, B. D., Sheppard, C. A., Tran, P., Rozen, R., Matthews, R. G., & Ludwig, M. L. (1999). The structure and properties of methylenetetrahydrofolate reductase from *Escherichia coli* suggest how folate ameliorates human hyperhomocysteinemia. *Nat Struct Biol, 6*(4), 359-365. doi:10.1038/7594

Guthrie, C., & Fink, G. R. (1991). Guide to Yeast Genetics and Molecular Biology. *Academic Press, Cambridge, 194*.

Hansen, J., & Johannesen, P. F. (2000). Cysteine is essential for transcriptional regulation of the sulfur assimilation genes in *Saccharomyces cerevisiae*. *Mol Gen Genet, 263*(3), 535-542. doi:10.1007/s004380051199

Hanson, N. Q., Aras, O., Yang, F., & Tsai, M. Y. (2001). C677T and A1298C polymorphisms of the methylenetetrahydrofolate reductase gene: incidence and effect of combined genotypes on plasma fasting and post-methionine load homocysteine in vascular disease. *Clin Chem, 47*(4), 661-666.

Hayakawa, K., Matsuda, F., & Shimizu, H. (2018). (^{13})C-metabolic flux analysis of ethanol-assimilating *Saccharomyces cerevisiae* for S-adenosyl-L-methionine production. *Microb Cell Fact, 17*(1), 82. doi:10.1186/s12934-018-0935-6

Hoffman, R. M., & Erbe, R. W. (1976). High in vivo rates of methionine biosynthesis in transformed human and malignant rat cells auxotrophic for methionine. *Proc Natl Acad Sci U S A, 73*(5), 1523-1527. doi:10.1073/pnas.73.5.1523

Igari, S., Ohtaki, A., Yamanaka, Y., Sato, Y., Yohda, M., Odaka, M., . . . Yamada, K. (2011). Properties and crystal structure of methylenetetrahydrofolate reductase from Thermus thermophilus HB8. *PLoS One, 6*(8), e23716. doi:10.1371/journal.pone.0023716

Jain, M., Nagar, P., Sharma, A., Batth, R., Aggarwal, S., Kumari, S., & Mustafiz, A. (2018). GLYI and D-LDH play key role in methylglyoxal detoxification and abiotic stress tolerance. *Sci Rep, 8*(1), 5451. doi:10.1038/s41598-018-23806-4

Jencks, D. A., & Mathews, R. G. (1987). Allosteric inhibition of methylenetetrahydrofolate reductase by adenosylmethionine. Effects of adenosylmethionine and NADPH on the equilibrium between active and inactive forms of the enzyme and on the kinetics of approach to equilibrium. *J Biol Chem, 262*(6), 2485-2493.

Jyoti, P., Shree, M., Joshi, C., Prakash, T., Ray, S. K., Satapathy, S. S., & Masakapalli, S. K. (2020). The Entner-Doudoroff and Nonoxidative Pentose Phosphate Pathways Bypass Glycolysis and the Oxidative Pentose Phosphate Pathway in *Ralstonia solanacearum*. *mSystems, 5*(2). doi:10.1128/mSystems.00091-20

Kaiser, C., Michaelis, S., & Mitchell, A. . (1994). Yeast genomic DNA isolation. *Methods in yeast genetics*.

Kanarek, N., Keys, H. R., Cantor, J. R., Lewis, C. A., Chan, S. H., Kunchok, T., . . . Sabatini, D. M. (2018). Histidine catabolism is a major determinant of methotrexate sensitivity. *Nature, 559*(7715), 632-636. doi:10.1038/s41586-018-0316-7

Kang, S. S., Zhou, J., Wong, P. W., Kowalisyn, J., & Strokosch, G. (1988). Intermediate homocysteinemia: a thermolabile variant of methylenetetrahydrofolate reductase. *Am J Hum Genet, 43*(4), 414-421.

Kato, M., Yang, Y. S., Sutter, B. M., Wang, Y., McKnight, S. L., & Tu, B. P. (2019). Redox State Controls Phase Separation of the Yeast Ataxin-2 Protein via Reversible Oxidation of Its Methionine-Rich Low-Complexity Domain. *Cell, 177*(3), 711-721 e718. doi:10.1016/j.cell.2019.02.044

Kaur, H., Ganguli, D., & Bachhawat, A. K. (2012). Glutathione degradation by the alternative pathway (DUG pathway) in *Saccharomyces cerevisiae* is initiated by (Dug2p-Dug3p)2 complex, a novel glutamine amidotransferase (GATase) enzyme acting on glutathione. *J Biol Chem, 287*(12), 8920-8931. doi:10.1074/jbc.M111.327411

Kaur, H., Kumar, C., Junot, C., Toledano, M. B., & Bachhawat, A. K. (2009). Dug1p Is a Cys-Gly peptidase of the gamma-glutamyl cycle of *Saccharomyces cerevisiae* and represents a novel family of Cys-Gly peptidases. *J Biol Chem, 284*(21), 14493-14502. doi:10.1074/jbc.M808952200

Kozbial, P. Z., & Mushegian, A. R. (2005). Natural history of S-adenosylmethionine-binding proteins. *BMC Struct Biol, 5*, 19. doi:10.1186/1472-6807-5-19

Krebs, H. A., Hems, R., & Tyler, B. (1976). The regulation of folate and methionine metabolism. *Biochem J, 158*(2), 341-353. doi:10.1042/bj1580341

Kumar, A., Tikoo, S., Maity, S., Sengupta, S., Sengupta, S., Kaur, A., & Bachhawat, A. K. (2012). Mammalian proapoptotic factor ChaC1 and its homologues function as gamma-glutamyl cyclotransferases acting specifically on glutathione. *EMBO Rep, 13*(12), 1095-1101. doi:10.1038/embor.2012.156

Kung, H. F., Spears, C., Greene, R. C., & Weissbach, H. (1972). Regulation of the terminal reactions in methionine biosynthesis by vitamin B 12 and methionine. *Arch Biochem Biophys, 150*(1), 23-31. doi:10.1016/0003-9861(72)90005-7

Kuras, L., Barbey, R., & Thomas, D. (1997). Assembly of a bZIP-bHLH transcription activation complex: formation of the yeast Cbf1-Met4-Met28 complex is regulated through Met28 stimulation of Cbf1 DNA binding. *EMBO J, 16*(9), 2441-2451. doi:10.1093/emboj/16.9.2441

Kuras, L., Rouillon, A., Lee, T., Barbey, R., Tyers, M., & Thomas, D. (2002). Dual regulation of the met4 transcription factor by ubiquitin-dependent degradation and inhibition of promoter recruitment. *Mol Cell, 10*(1), 69-80. doi:10.1016/s1097-2765(02)00561-0

Kutzbach, C., & Stokstad, E. L. (1967). Feedback inhibition of methylene-tetrahydrofolate reductase in rat liver by S-adenosylmethionine. *Biochim Biophys Acta, 139*(1), 217-220. doi:10.1016/0005-2744(67)90140-4

Kutzbach, C., & Stokstad, E. L. (1971). Mammalian methylenetetrahydrofolate reductase. Partial purification, properties, and inhibition by S-adenosylmethionine. *Biochim Biophys Acta, 250*(3), 459-477. doi:10.1016/0005-2744(71)90247-6

Laxman, S., Sutter, B. M., Wu, X., Kumar, S., Guo, X., Trudgian, D. C., . . . Tu, B. P. (2013). Sulfur amino acids regulate translational capacity and metabolic homeostasis through modulation of tRNA thiolation. *Cell, 154*(2), 416-429. doi:10.1016/j.cell.2013.06.043

Lee, M. N., Takawira, D., Nikolova, A. P., Ballou, D. P., Furtado, V. C., Phung, N. L., . . . Trimmer, E. E. (2009). Functional role for the conformationally mobile phenylalanine 223 in the reaction of methylenetetrahydrofolate reductase from *Escherichia coli*. *Biochemistry, 48*(32), 7673-7685. doi:10.1021/bi9007325

Lee, T. A., Jorgensen, P., Bognar, A. L., Peyraud, C., Thomas, D., & Tyers, M. (2010). Dissection of combinatorial control by the Met4 transcriptional complex. *Mol Biol Cell, 21*(3), 456-469. doi:10.1091/mbc.E09-05-0420

Leroy, C., Cormier, L., & Kuras, L. (2006). Independent recruitment of mediator and SAGA by the activator Met4. *Mol Cell Biol, 26*(8), 3149-3163. doi:10.1128/MCB.26.8.3149-3163.2006

Locasale, J. W. (2013). Serine, glycine and one-carbon units: cancer metabolism in full circle. *Nat Rev Cancer, 13*(8), 572-583. doi:10.1038/nrc3557

Loizeau, K., Gambonnet, B., Zhang, G. F., Curien, G., Jabrin, S., Van Der Straeten, D., . . . Ravanel, S. (2007). Regulation of one-carbon metabolism in *Arabidopsis*: the N-terminal regulatory domain of cystathionine gamma-synthase is cleaved in response to folate starvation. *Plant Physiol, 145*(2), 491-503. doi:10.1104/pp.107.105379

Lopez-Lopez, E., Martin-Guerrero, I., Ballesteros, J., & Garcia-Orad, A. (2013). A systematic review and meta-analysis of MTHFR polymorphisms in methotrexate toxicity prediction in pediatric acute lymphoblastic leukemia. *Pharmacogenomics J, 13*(6), 498-506. doi:10.1038/tpj.2012.44

Luka, Z., Mudd, S. H., & Wagner, C. (2009). Glycine N-methyltransferase and regulation of S-adenosylmethionine levels. *J Biol Chem, 284*(34), 22507-22511. doi:10.1074/jbc.R109.019273

Marini, N. J., Gin, J., Ziegle, J., Keho, K. H., Ginzinger, D., Gilbert, D. A., & Rine, J. (2008). The prevalence of folate-remedial MTHFR enzyme variants in humans. *Proc Natl Acad Sci U S A, 105*(23), 8055-8060. doi:10.1073/pnas.0802813105

Martin, Y. N., Salavaggione, O. E., Eckloff, B. W., Wieben, E. D., Schaid, D. J., & Weinshilboum, R. M. (2006). Human methylenetetrahydrofolate reductase pharmacogenomics: gene resequencing and functional genomics. *Pharmacogenet Genomics, 16*(4), 265-277. doi:10.1097/01.fpc.0000194423.20393.08

Masakapalli, S. K., Bryant, F. M., Kruger, N. J., & Ratcliffe, R. G. (2014). The metabolic flux phenotype of heterotrophic *Arabidopsis* cells reveals a flexible balance between the cytosolic and plastidic contributions to carbohydrate oxidation in response to phosphate limitation. *Plant J, 78*(6), 964-977. doi:10.1111/tpj.12522

Matthews, R. G., & Baugh, C. M. (1980). Interactions of pig liver methylenetetrahydrofolate reductase with methylenetetrahydropteroylpolyglutamate substrates and with dihydropteroylpolyglutamate inhibitors. *Biochemistry, 19*(10), 2040-2045. doi:10.1021/bi00551a005

Matthews, R. G., & Daubner, S. C. (1982). Modulation of methylenetetrahydrofolate reductase activity by S-adenosylmethionine and by dihydrofolate and its polyglutamate analogues. *Adv Enzyme Regul, 20*, 123-131. doi:10.1016/0065-2571(82)90012-7

Matthews, R. G., & Haywood, B. J. (1979). Inhibition of pig liver methylenetetrahydrofolate reductase by dihydrofolate: some mechanistic and regulatory implications. *Biochemistry, 18*(22), 4845-4851. doi:10.1021/bi00589a012

Matthews, R. G., Sheppard, C., & Goulding, C. (1998). Methylenetetrahydrofolate reductase and methionine synthase: biochemistry and molecular biology. *Eur J Pediatr, 157 Suppl 2*, S54-59. doi:10.1007/pl00014305

Matthews, R. G., Vanoni, M. A., Hainfeld, J. F., & Wall, J. (1984). Methylenetetrahydrofolate reductase. Evidence for spatially distinct subunit domains obtained by scanning transmission electron microscopy and limited proteolysis. *J Biol Chem, 259*(19), 11647-11650.

McCaddon, A., Davies, G., Hudson, P., Tandy, S., & Cattell, H. (1998). Total serum homocysteine in senile dementia of Alzheimer type. *Int J Geriatr Psychiatry, 13*(4), 235-239. doi:10.1002/(sici)1099-1166(199804)13:4<235::aid-gps761>3.0.co;2-8

McKenzie, K. Q., & Jones, E. W. (1977). Mutants of formyltetrahydrofolate interconversion pathway of *Saccharomyces cerevisiae*. *Genetics, 86*(1), 85-102.

McNeil, J. B., Zhang, F., Taylor, B. V., Sinclair, D. A., Pearlman, R. E., & Bognar, A. L. (1997). Cloning, and molecular characterization of the GCV1 gene encoding the glycine cleavage T-protein from *Saccharomyces cerevisiae*. *Gene, 186*(1), 13-20. doi:10.1016/s0378-1119(96)00670-1

Mentch, S. J., Mehrmohamadi, M., Huang, L., Liu, X., Gupta, D., Mattocks, D., . . . Locasale, J. W. (2015). Histone Methylation Dynamics and Gene Regulation Occur through the Sensing of One-Carbon Metabolism. *Cell Metab, 22*(5), 861-873. doi:10.1016/j.cmet.2015.08.024

Millard, P., Letisse, F., Sokol, S., & Portais, J. C. (2012). IsoCor: correcting MS data in isotope labeling experiments. *Bioinformatics, 28*(9), 1294-1296. doi:10.1093/bioinformatics/bts127

Mills, J. L., McPartlin, J. M., Kirke, P. N., Lee, Y. J., Conley, M. R., Weir, D. G., & Scott, J. M. (1995). Homocysteine metabolism in pregnancies complicated by neural-tube defects. *Lancet, 345*(8943), 149-151. doi:10.1016/s0140-6736(95)90165-5

Mudd, S. H., Uhlendorf, B. W., Freeman, J. M., Finkelstein, J. D., & Shih, V. E. (1972). Homocystinuria associated with decreased methylenetetrahydrofolate reductase activity. *Biochem Biophys Res Commun, 46*(2), 905-912. doi:10.1016/s0006-291x(72)80227-4

Murin, R., Vidomanova, E., Kowtharapu, B. S., Hatok, J., & Dobrota, D. (2017). Role of S-adenosylmethionine cycle in carcinogenesis. *Gen Physiol Biophys, 36*(5), 513-520. doi:10.4149/gpb_2017031

Nagarajan, L., & Storms, R. K. (1997). Molecular characterization of GCV3, the *Saccharomyces cerevisiae* gene coding for the glycine cleavage system hydrogen carrier protein. *J Biol Chem, 272*(7), 4444-4450. doi:10.1074/jbc.272.7.4444

Newman, A. C., & Maddocks, O. D. K. (2017). One-carbon metabolism in cancer. *Br J Cancer, 116*(12), 1499-1504. doi:10.1038/bjc.2017.118

Ogur, M., Liu, T. N., Cheung, I., Paulavicius, I., Wales, W., Mehnert, D., & Blaise, D. (1977). "Active" one-carbon generation in *Saccharomyces cerevisiae*. *J Bacteriol, 129*(2), 926-933. doi:10.1128/JB.129.2.926-933.1977

Ouni, I., Flick, K., & Kaiser, P. (2010). A transcriptional activator is part of an SCF ubiquitin ligase to control degradation of its cofactors. *Mol Cell, 40*(6), 954-964. doi:10.1016/j.molcel.2010.11.018

Pasternack, L. B., Laude, D. A., Jr., & Appling, D. R. (1994). ^{13}C NMR analysis of intercompartmental flow of one-carbon units into choline and purines in *Saccharomyces cerevisiae*. *Biochemistry, 33*(1), 74-82. doi:10.1021/bi00167a010

Pavlikova, M., Sokolova, J., Janosikova, B., Melenovska, P., Krupkova, L., Zvarova, J., & Kozich, V. (2012). Rare allelic variants determine folate status in an unsupplemented European population. *J Nutr, 142*(8), 1403-1409. doi:10.3945/jn.112.160549

Pejchal, R., Sargeant, R., & Ludwig, M. L. (2005). Structures of NADH and CH_3-H_4folate complexes of *Escherichia coli* methylenetetrahydrofolate reductase reveal a spartan strategy for a ping-pong reaction. *Biochemistry, 44*(34), 11447-11457. doi:10.1021/bi050533q

Piper, M. D., Hong, S. P., Ball, G. E., & Dawes, I. W. (2000). Regulation of the balance of one-carbon metabolism in *Saccharomyces cerevisiae*. *J Biol Chem, 275*(40), 30987-30995. doi:10.1074/jbc.M004248200

Pirkov, I., Norbeck, J., Gustafsson, L., & Albers, E. (2008). A complete inventory of all enzymes in the eukaryotic methionine salvage pathway. *FEBS J, 275*(16), 4111-4120. doi:10.1111/j.1742-4658.2008.06552.x

Raymond, R. K., Kastanos, E. K., & Appling, D. R. (1999). *Saccharomyces cerevisiae* expresses two genes encoding isozymes of methylenetetrahydrofolate reductase. *Arch Biochem Biophys, 372*(2), 300-308. doi:10.1006/abbi.1999.1498

Rebora, K., Desmoucelles, C., Borne, F., Pinson, B., & Daignan-Fornier, B. (2001). Yeast AMP pathway genes respond to adenine through regulated synthesis of a metabolic intermediate. *Mol Cell Biol, 21*(23), 7901-7912. doi:10.1128/MCB.21.23.7901-7912.2001

Roje, S., Chan, S. Y., Kaplan, F., Raymond, R. K., Horne, D. W., Appling, D. R., & Hanson, A. D. (2002). Metabolic engineering in yeast demonstrates that S-adenosylmethionine controls flux through the methylenetetrahydrofolate reductase reaction *in vivo*. *J Biol Chem, 277*(6), 4056-4061. doi:10.1074/jbc.M110651200

Roje, S., Wang, H., McNeil, S. D., Raymond, R. K., Appling, D. R., Shachar-Hill, Y., . . . Hanson, A. D. (1999). Isolation, characterization, and functional expression of cDNAs encoding NADH-dependent methylenetetrahydrofolate reductase from higher plants. *J Biol Chem, 274*(51), 36089-36096. doi:10.1074/jbc.274.51.36089

Rosenblatt, D. S. (1995). Inherited disorders of folate transport and metabolism. In: C.R. Scriver, A.L. Beaudet, W.S. Sly, D. Valle (Eds.). *The Metabolic and Molecular Bases of Inherited Disease, 7th ed, New York, McGraw-Hill Book Co*, 3111-3128.

Rummel, T., Suormala, T., Haberle, J., Koch, H. G., Berning, C., Perrett, D., & Fowler, B. (2007). Intermediate hyperhomocysteinaemia and compound heterozygosity for the common variant c.677C>T and a MTHFR gene mutation. *J Inherit Metab Dis, 30*(3), 401. doi:10.1007/s10545-007-0445-x

Sambrook, J., Fritsch, E. F., & Maniatis, T. (1989). Molecular cloning: a laboratory manual, 2nd ed. *Cold Spring Harbor Laboratory, Cold Spring Harbor, N.Y.*

Schiff, M., Benoist, J. F., Tilea, B., Royer, N., Giraudier, S., & Ogier de Baulny, H. (2011). Isolated remethylation disorders: do our treatments benefit patients? *J Inherit Metab Dis, 34*(1), 137-145. doi:10.1007/s10545-010-9120-8

Schirch, L. V. (1984). Folates in glycine and serine metabolism. *In Folates and Pterins, Vol. 1. Chemistry and Biochemistry of folates, 1*, 399-431. Wiley, New York.

Selhub, J., & Miller, J. W. (1992). The pathogenesis of homocysteinemia: interruption of the coordinate regulation by S-adenosylmethionine of the remethylation and transsulfuration of homocysteine. *Am J Clin Nutr, 55*(1), 131-138. doi:10.1093/ajcn/55.1.131

Sheppard, C. A., Trimmer, E. E., & Matthews, R. G. (1999). Purification and properties of NADH-dependent 5, 10-methylenetetrahydrofolate reductase (MetF) from *Escherichia coli*. *J Bacteriol, 181*(3), 718-725. doi:10.1128/JB.181.3.718-725.1999

Shoeman, R., Redfield, B., Coleman, T., Greene, R. C., Smith, A. A., Brot, N., & Weissbach, H. (1985). Regulation of methionine synthesis in *Escherichia coli*: Effect of *metJ* gene product and S-adenosylmethionine on the expression of the *metF* gene. *Proc Natl Acad Sci U S A, 82*(11), 3601-3605. doi:10.1073/pnas.82.11.3601

Shree, M., & S, K. M. (2018). Intracellular Fate of Universally Labelled (^{13})C Isotopic Tracers of Glucose and Xylose in Central Metabolic Pathways of *Xanthomonas oryzae*. *Metabolites, 8*(4). doi:10.3390/metabo8040066

Sinclair, D. A., Hong, S. P., & Dawes, I. W. (1996). Specific induction by glycine of the gene for the P-subunit of glycine decarboxylase from *Saccharomyces cerevisiae*. *Mol Microbiol, 19*(3), 611-623. doi:10.1046/j.1365-2958.1996.419947.x

Sinclair, K. D., Allegrucci, C., Singh, R., Gardner, D. S., Sebastian, S., Bispham, J., . . . Young, L. E. (2007). DNA methylation, insulin resistance, and blood pressure in offspring determined by maternal periconceptional B vitamin and methionine status. *Proc Natl Acad Sci U S A, 104*(49), 19351-19356. doi:10.1073/pnas.0707258104

Steegborn, C., Clausen, T., Sondermann, P., Jacob, U., Worbs, M., Marinkovic, S., . . . Wahl, M. C. (1999). Kinetics and inhibition of recombinant human cystathionine gamma-lyase. Toward the rational control of transsulfuration. *J Biol Chem, 274*(18), 12675-12684. doi:10.1074/jbc.274.18.12675

Sumner, J., Jencks, D. A., Khani, S., & Matthews, R. G. (1986). Photoaffinity labeling of methylenetetrahydrofolate reductase with 8-azido-S-adenosylmethionine. *J Biol Chem, 261*(17), 7697-7700.

Thomas, D., Cherest, H., & Surdin-Kerjan, Y. (1989). Elements involved in S-adenosylmethionine-mediated regulation of the *Saccharomyces cerevisiae* MET25 gene. *Mol Cell Biol, 9*(8), 3292-3298. doi:10.1128/mcb.9.8.3292

Thomas, D., Cherest, H., & Surdin-Kerjan, Y. (1991). Identification of the structural gene for glucose-6-phosphate dehydrogenase in yeast. Inactivation leads to a nutritional requirement for organic sulfur. *EMBO J, 10*(3), 547-553.

Thomas, D., & Surdin-Kerjan, Y. (1997). Metabolism of sulfur amino acids in *Saccharomyces cerevisiae*. *Microbiol Mol Biol Rev, 61*(4), 503-532.

Tibbetts, A. S., & Appling, D. R. (2010). Compartmentalization of Mammalian folate-mediated one-carbon metabolism. *Annu Rev Nutr, 30*, 57-81. doi:10.1146/annurev.nutr.012809.104810

Trimmer, E. E. (2013). Methylenetetrahydrofolate reductase: biochemical characterization and medical significance. *Curr Pharm Des, 19*(14), 2574-2593. doi:10.2174/1381612811319140008

Trimmer, E. E., Ballou, D. P., Ludwig, M. L., & Matthews, R. G. (2001). Folate activation and catalysis in methylenetetrahydrofolate reductase from *Escherichia coli*: roles for aspartate 120 and glutamate 28. *Biochemistry, 40*(21), 6216-6226. doi:10.1021/bi002790v

van Guldener, C., & Stehouwer, C. D. (2003). Homocysteine metabolism in renal disease. *Clin Chem Lab Med, 41*(11), 1412-1417. doi:10.1515/CCLM.2003.217

Walvekar, A., Rashida, Z., Maddali, H., & Laxman, S. (2018). A versatile LC-MS/MS approach for comprehensive, quantitative analysis of central metabolic pathways. *Wellcome Open Res, 3*, 122. doi:10.12688/wellcomeopenres.14832.1

Wang, H. L., Sun, L., Zhou, S., & Wang, F. (2018). Association between 5,10-methylenetetrahydrofolate, gene polymorphism and congenital heart disease. *J Biol Regul Homeost Agents, 32*(5), 1255-1260.

Waterland, R. A., Kellermayer, R., Laritsky, E., Rayco-Solon, P., Harris, R. A., Travisano, M., . . . Prentice, A. M. (2010). Season of conception in rural gambia affects DNA methylation at

putative human metastable epialleles. *PLoS Genet, 6*(12), e1001252. doi:10.1371/journal.pgen.1001252

Watkins, D., & Rosenblatt, D. S. (2012). Update and new concepts in vitamin responsive disorders of folate transport and metabolism. *J Inherit Metab Dis, 35*(4), 665-670. doi:10.1007/s10545-011-9418-1

White, W. H., Gunyuzlu, P. L., & Toyn, J. H. (2001). *Saccharomyces cerevisiae* is capable of de Novo pantothenic acid biosynthesis involving a novel pathway of beta-alanine production from spermine. *J Biol Chem, 276*(14), 10794-10800. doi:10.1074/jbc.M009804200

Winkelmayer, W. C., Sunder-Plassmann, G., Huber, A., & Fodinger, M. (2004). Patterns of co-occurrence of three single nucleotide polymorphisms of the 5,10-methylenetetrahydrofolate reductase gene in kidney transplant recipients. *Eur J Clin Invest, 34*(9), 613-618. doi:10.1111/j.1365-2362.2004.01394.x

Wu, S., Zhang, J., Li, F., Du, W., Zhou, X., Wan, M., . . . Zhou, Y. (2019). One-Carbon Metabolism Links Nutrition Intake to Embryonic Development via Epigenetic Mechanisms. *Stem Cells Int, 2019*, 3894101. doi:10.1155/2019/3894101

Yadav, S., Mody, T. A., Sharma, A., & Bachhawat, A. K. (2020). A Genetic Screen To Identify Genes Influencing the Secondary Redox Couple NADPH/NADP(+) in the Yeast *Saccharomyces cerevisiae*. *G3 (Bethesda), 10*(1), 371-378. doi:10.1534/g3.119.400606

Yamada, K., Strahler, J. R., Andrews, P. C., & Matthews, R. G. (2005). Regulation of human methylenetetrahydrofolate reductase by phosphorylation. *Proc Natl Acad Sci U S A, 102*(30), 10454-10459. doi:10.1073/pnas.0504786102

Yang, M., & Vousden, K. H. (2016). Serine and one-carbon metabolism in cancer. *Nat Rev Cancer, 16*(10), 650-662. doi:10.1038/nrc.2016.81

Ye, C., Sutter, B. M., Wang, Y., Kuang, Z., & Tu, B. P. (2017). A Metabolic Function for Phospholipid and Histone Methylation. *Mol Cell, 66*(2), 180-193 e188. doi:10.1016/j.molcel.2017.02.026

Zheng, Y., Ramsamooj, S., Li, Q., Johnson, J. L., Yaron, T. M., Sharra, K., & Cantley, L. C. (2019). Regulation of folate and methionine metabolism by multisite phosphorylation of human methylenetetrahydrofolate reductase. *Sci Rep, 9*(1), 4190. doi:10.1038/s41598-019-40950-7

Appendix

Comparison of MID [M-57] in yeast cells bearing WT (W) or mutant (M) Met13p, fed with ^{12}C, $^{13}C_1$ and $^{13}C_U$ substrates

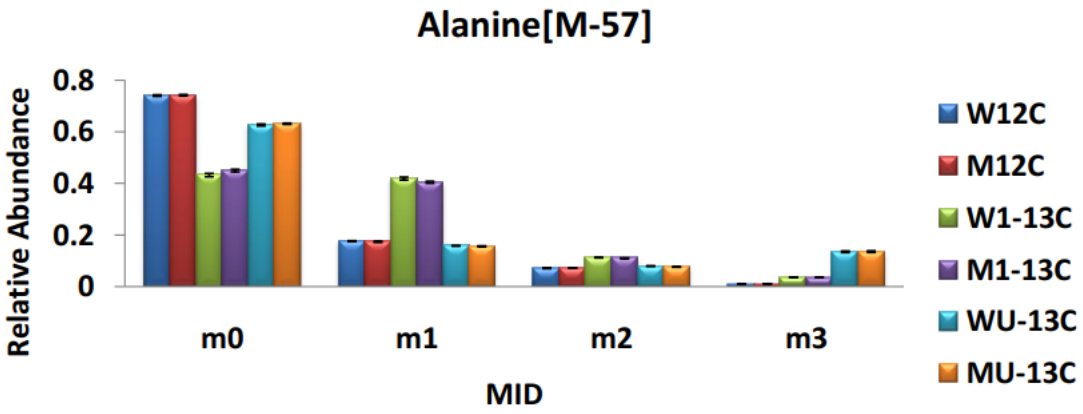

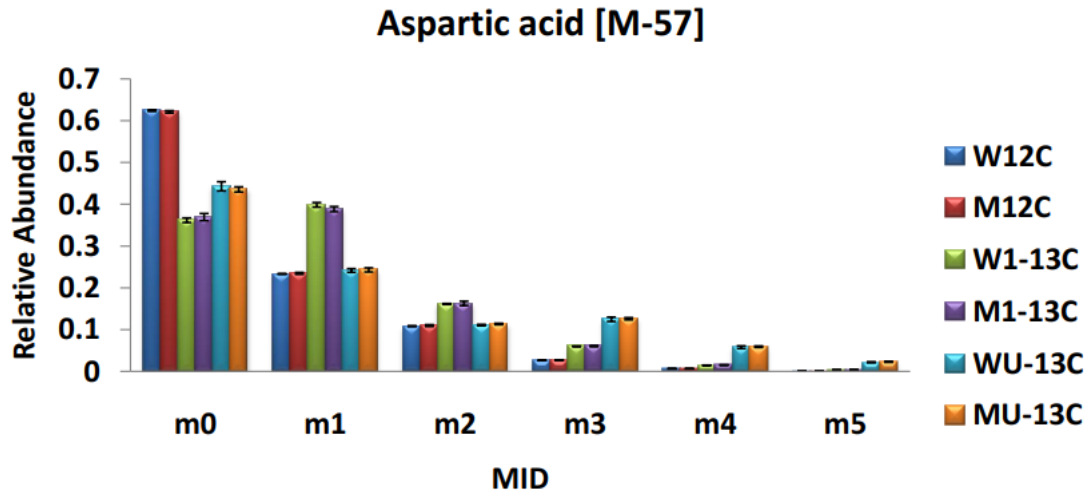

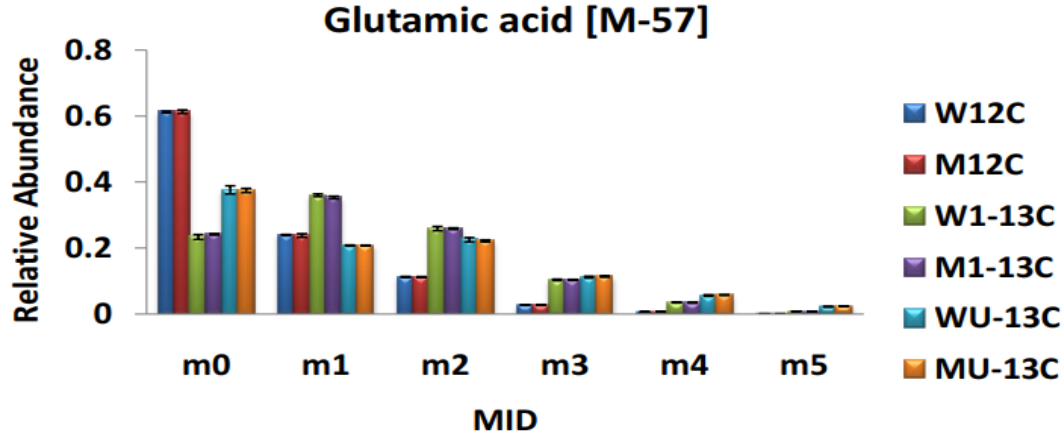

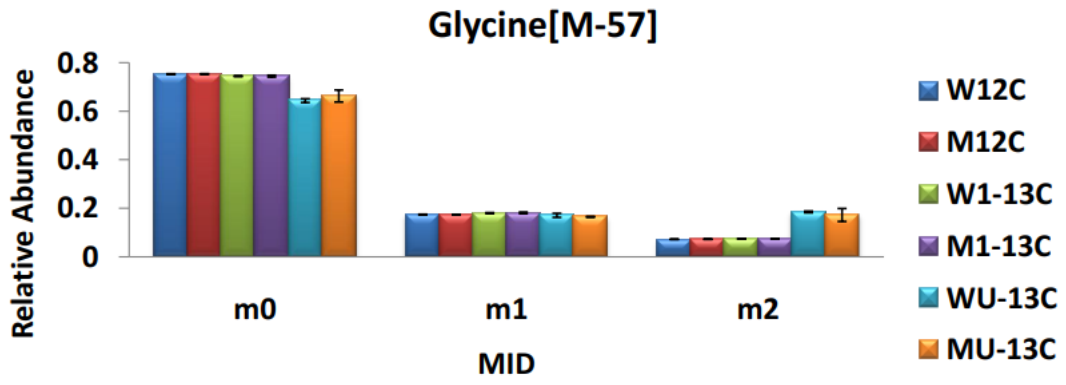
Glycine[M-57]
Relative Abundance
0.8
0.6
0.4
0.2
0
m0
m1
m2
MID
W12C
M12C
W1-13C
M1-13C
WU-13C
MU-13C

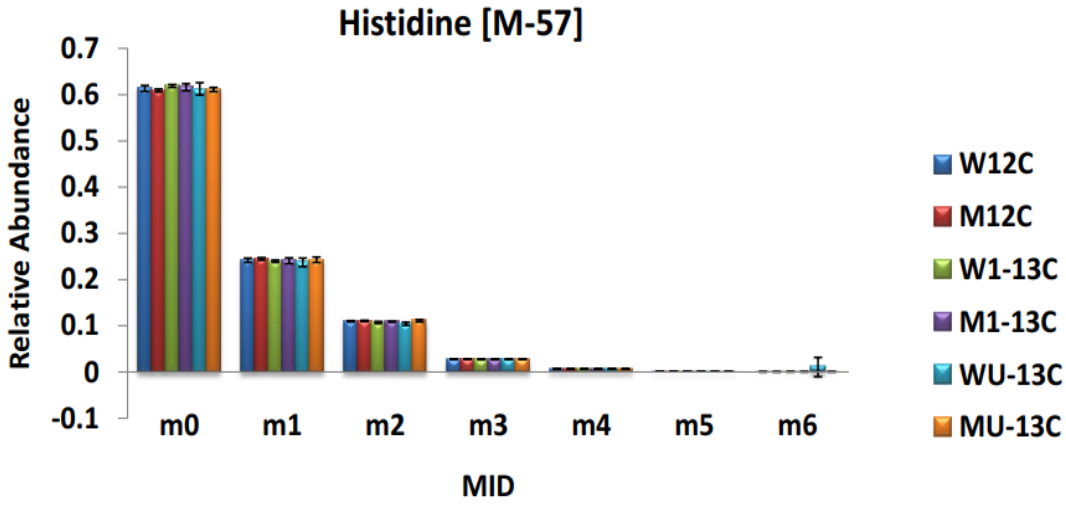
Histidine [M-57]
Relative Abundance
0.7
0.6
0.5
0.4
0.3
0.2
0.1
0
-0.1
m0
m1
m2
m3
m4
m5
m6
MID
W12C
M12C
W1-13C
M1-13C
WU-13C
MU-13C

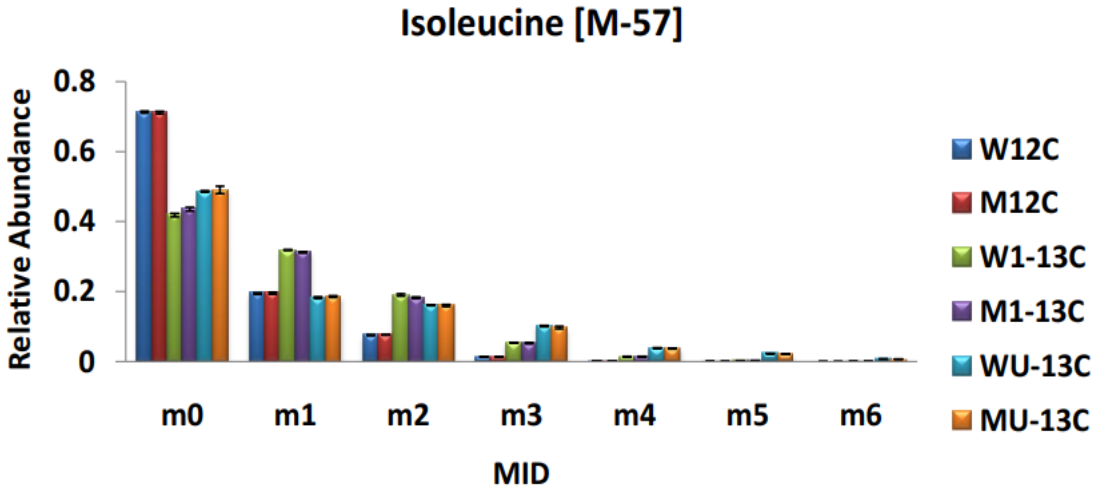
Isoleucine [M-57]
Relative Abundance
0.8
0.6
0.4
0.2
0
m0
m1
m2
m3
m4
m5
m6
MID
W12C
M12C
W1-13C
M1-13C
WU-13C
MU-13C

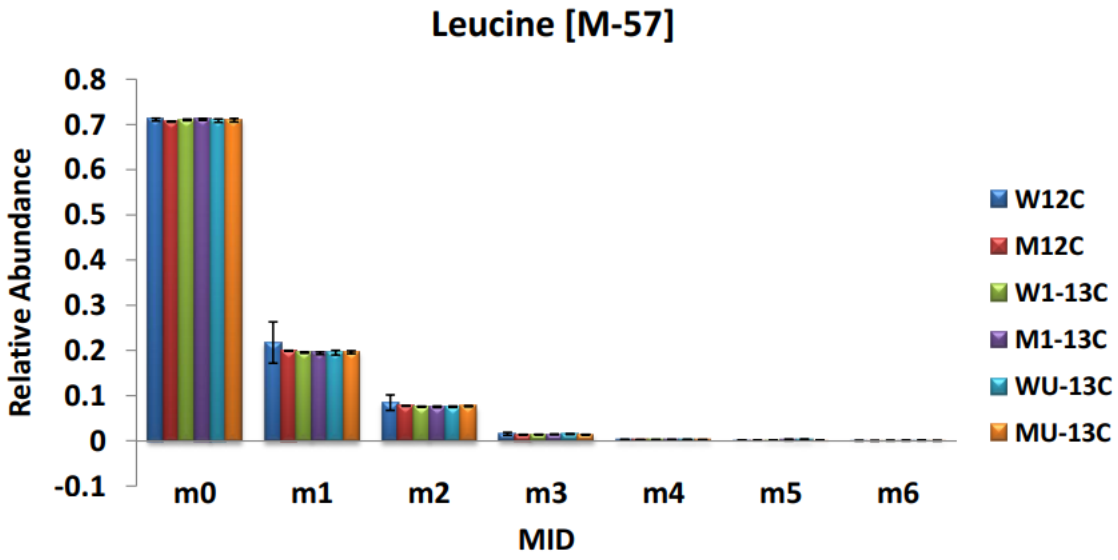
Leucine [M-57]
Relative Abundance
0.8
0.7
0.6
0.5
0.4
0.3
0.2
0.1
0
-0.1
m0
m1
m2
m3
m4
m5
m6
MID
W12C
M12C
W1-13C
M1-13C
WU-13C
MU-13C

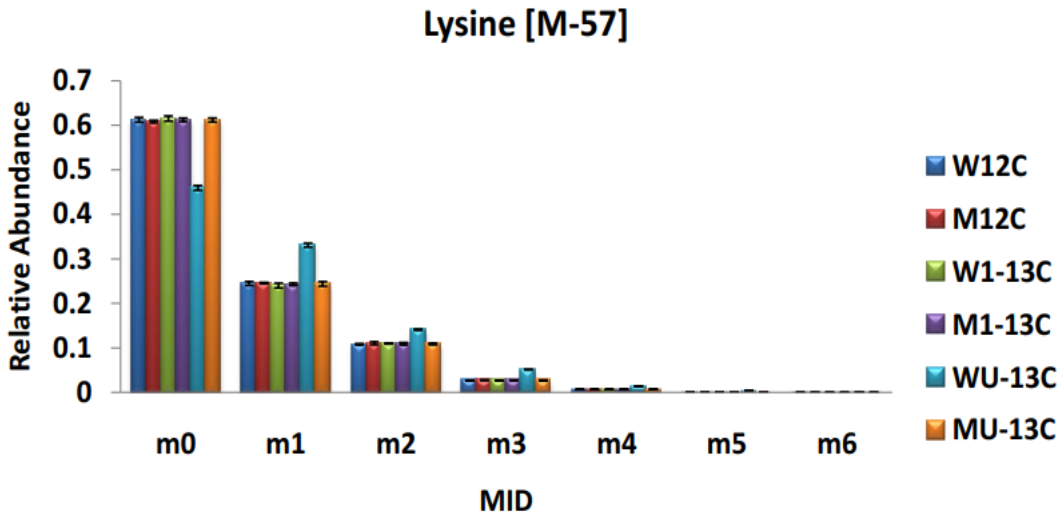
Lysine [M-57]
Relative Abundance
0.7
0.6
0.5
0.4
0.3
0.2
0.1
0
m0
m1
m2
m3
m4
m5
m6
MID
W12C
M12C
W1-13C
M1-13C
WU-13C
MU-13C

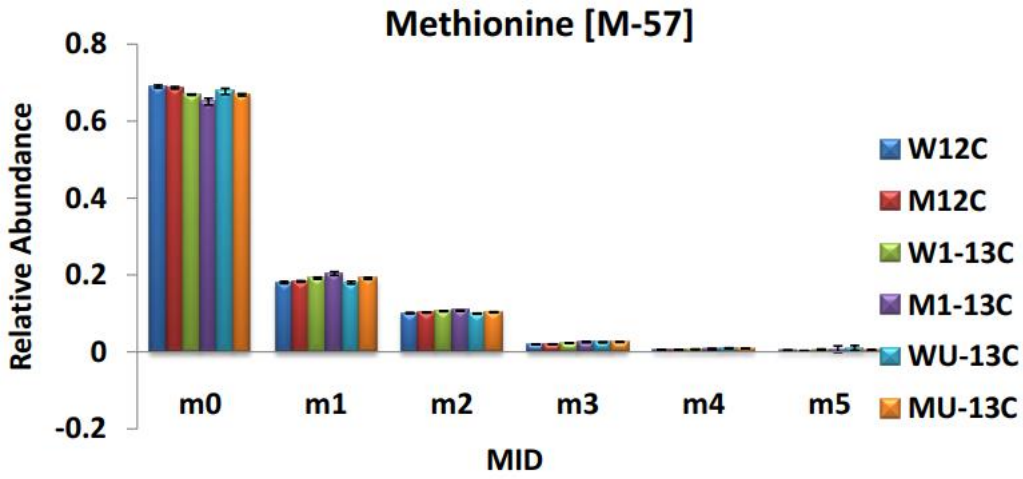
Methionine [M-57]
Relative Abundance
0.8
0.6
0.4
0.2
0
-0.2
m0
m1
m2
m3
m4
m5
MID
W12C
M12C
W1-13C
M1-13C
WU-13C
MU-13C

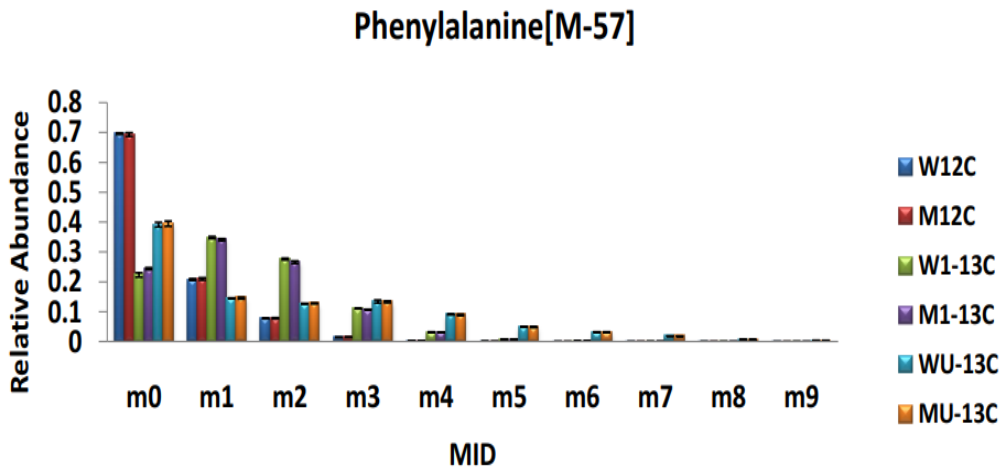
Phenylalanine[M-57]
Relative Abundance
0.8
0.7
0.6
0.5
0.4
0.3
0.2
0.1
0
m0
m1
m2
m3
m4
m5
m6
m7
m8
m9
MID
W12C
M12C
W1-13C
M1-13C
WU-13C
MU-13C

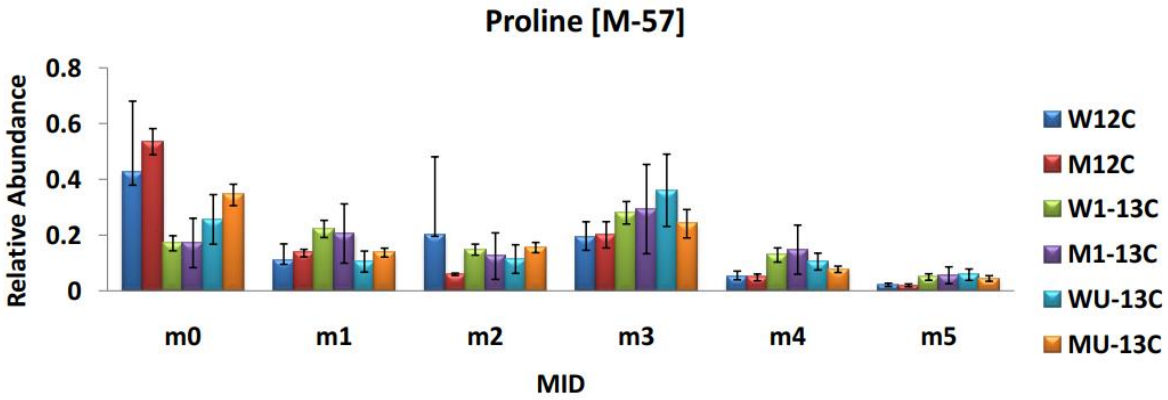
Proline [M-57]
Relative Abundance
0.8
0.6
0.4
0.2
0
m0
m1
m2
m3
m4
m5
MID
W12C
M12C
W1-13C
M1-13C
WU-13C
MU-13C

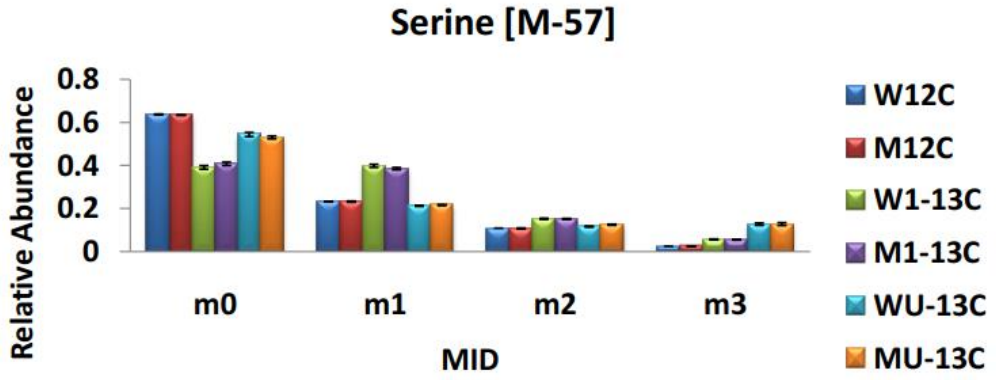
Serine [M-57]
Relative Abundance
0.8
0.6
0.4
0.2
0
m0
m1
m2
m3
MID
W12C
M12C
W1-13C
M1-13C
WU-13C
MU-13C

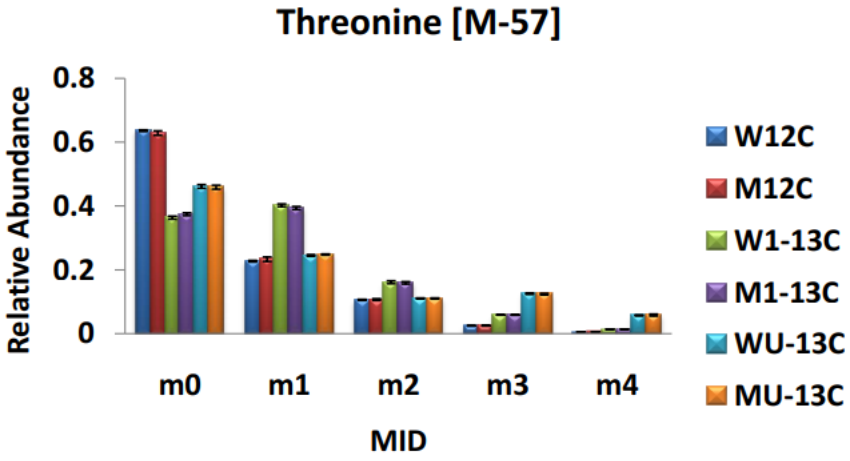
Threonine [M-57]
Relative Abundance
0.8
0.6
0.4
0.2
0
m0
m1
m2
m3
m4
MID
W12C
M12C
W1-13C
M1-13C
WU-13C
MU-13C

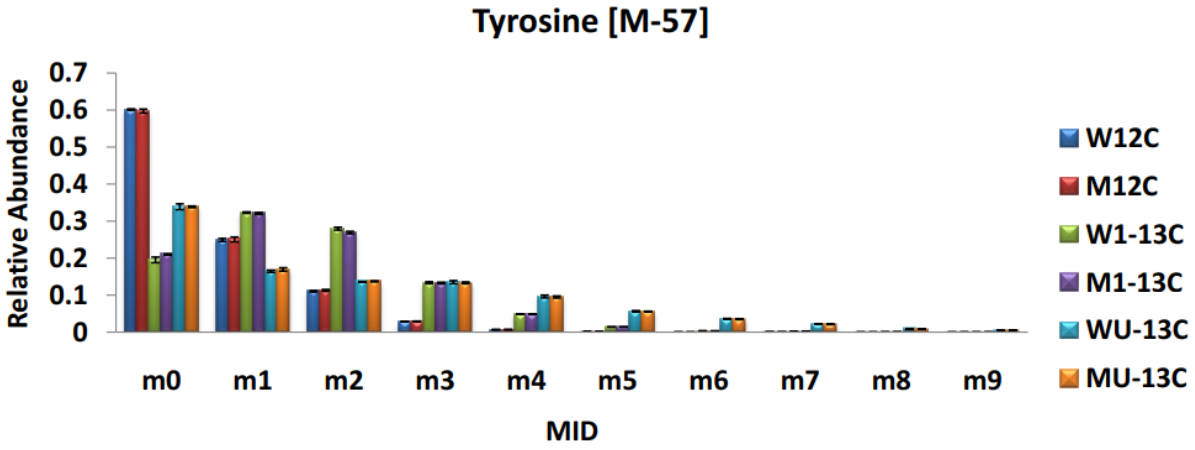
Tyrosine [M-57]
Relative Abundance
0.7
0.6
0.5
0.4
0.3
0.2
0.1
0
m0
m1
m2
m3
m4
m5
m6
m7
m8
m9
MID
W12C
M12C
W1-13C
M1-13C
WU-13C
MU-13C

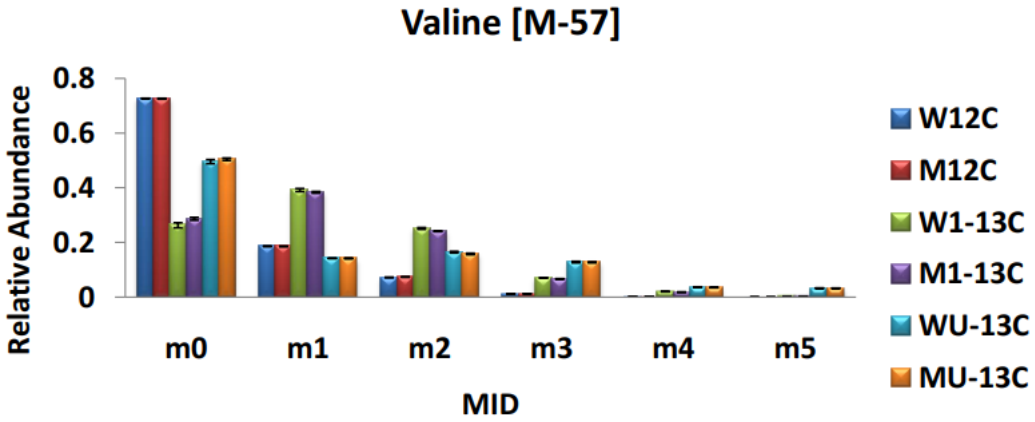
Valine [M-57]
Relative Abundance
0.8
0.6
0.4
0.2
0
m0
m1
m2
m3
m4
m5
MID
W12C
M12C
W1-13C
M1-13C
WU-13C
MU-13C